THE FLYING FISH, AN UNTETHERED OCEANOGRAPHIC SENSOR PLATFORM WITH ACOUSTIC HOMING CAPABILITY.

by

Joshua King Hoyt

S.B., Massachusetts Institute of Technology (1980)

S.M., Massachusetts Institute of Technology (1982)

SUBMITTED IN PARTIAL FULFILLMENT OF THE
REQUIREMENTS FOR THE DEGREE OF
DOCTOR OF PHILOSOPHY

at the

MASSACHUSETTS INSTITUTE OF TECHNOLOGY

and the

WOODS HOLE OCEANOGRAPHIC INSTITUTION

May, 1986

© Joshua K. Hoyt 1986

The author hereby grants to M.I.T. and W.H.O.I. permission to reproduce and to distribute copies of this thesis document either in whole or in part.

Signature of
Author _____
Department of Mechanical Engineering, Massachusetts Institute of Technology and the Joint Program in Oceanographic Engineering, Massachusetts Institute of Technology/Woods Hole Oceanographic Institution, May, 1986.

Certified
by _____
Thesis Supervisor.

Accepted
by _____
Chairman, Joint Committee for Oceanographic Engineering, Massachusetts Institute of Technology/Woods Hole Oceanographic Institution.

THE FLYING FISH, A PROTOTYPE OCEANOGRAPHIC SENSOR PLATFORM

WITH ACOUSTIC HOMING CAPABILITY.

by

Joshua K. Hoyt

Submitted to the Department of Mechnical Engineering and to
the Joint Committee for Oceanographic Engineering,
Massachusetts Institute of Technology and
Woods Hole Oceanographic Institution, May 1986,
in Partial Fulfillment of the Requirements for
the Degree of Doctor of Philosophy

ABSTRACT

The Flying Fish is an autonomous, streamlined, gravity driven underwater vehicle of high speed (15 knots) vertical excursions to depths of 6000 meters. This prototype uses short baseline acoustic interferometry to guide itself to a monochromatic acoustic beacon at the surface. Phase difference measurements made on two orthogonal axes are used to deduce the relative bearing to the beacon. An autopilot uses this information to actuate control surfaces and correct vehicle attitude. This thesis describes the oceanographic context in which the vehicle will be used, translates the scientific mission into a set of coherent engineering specifications, describes a prototype design that meets these specifications, and demonstrates proof-of-concept with a series of sea trials. Some recommendations are made for future refinements.

Thesis Supervisor: Dr. Albert Bradley, Research Specialist
Department of Ocean Engineering
Woods Hole Oceanographic Intitution

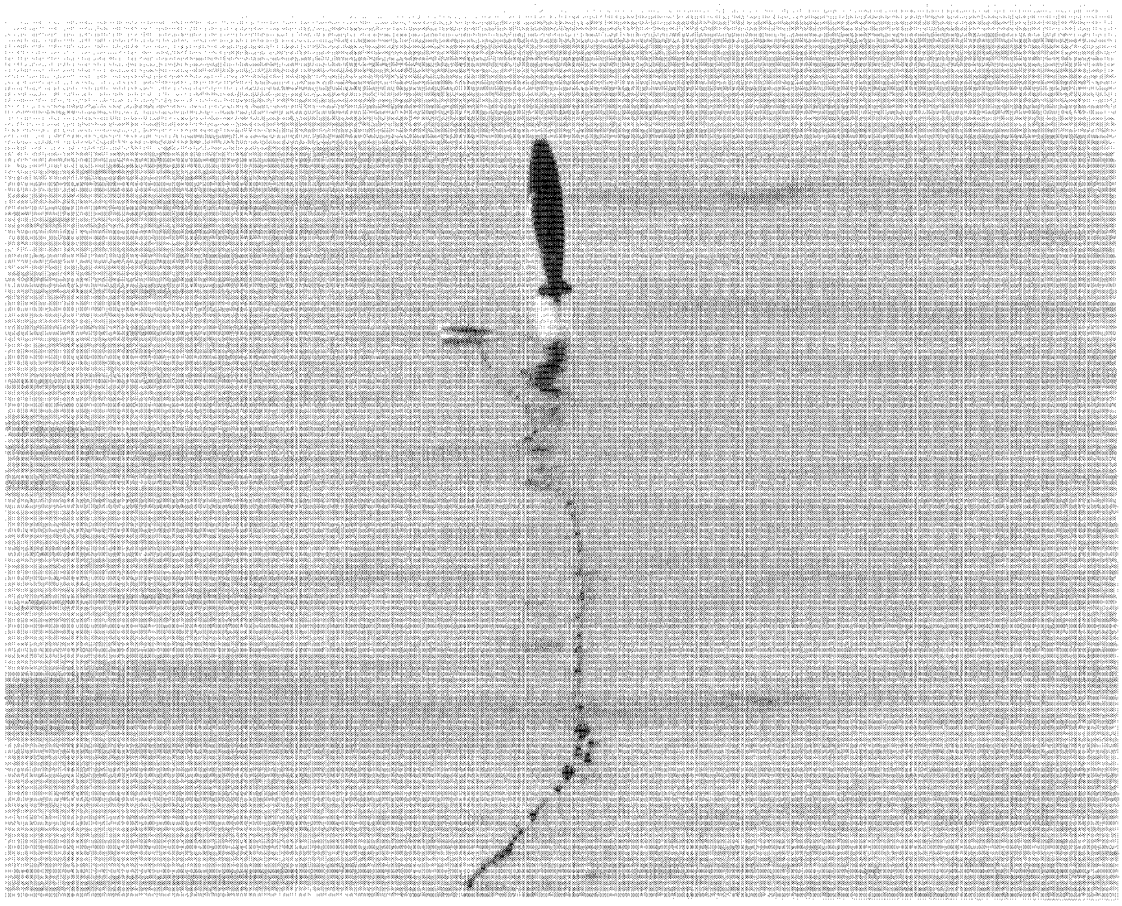

The Flying Fish Successfully Homing on a 15 KHz Monochromatic Sound Source

ACKNOWLEDGEMENTS

I would like to thank my advisor, Al Bradley, for his patience, direction, and encouragement. The acoustic tracking techniques used in this thesis were first shown to be feasible in the Pop-Up Profiler, a prototype current meter developed by Dr. Bradley. His experiences with the Pop-Up proved invaluable in the development of the Flying Fish. I would like to thank Doug Webb who originally outlined the possibility of using short baseline acoustic interferometry to steer a sensor platform more than fifteen years ago. Doug is the one who approached me in January of 1981 with the idea that the Flying Fish would be a viable thesis. His experience and guidance have been extremely helpful throughout the past five years and I expect our friendship to continue. I would like to thank Sandy Williams who gave me the most practical piece of advise during my years as a graduate student ("Don't buy a wooden boat."). His wealth of experience helped me to plan for and deal with the unforseen obstacles that are a part of the instrument development business.

Many others provided support throughout the past years. Dr. Spindel allocated Pew Foundation funds for a trip to see Bruce Carmichael in California prior to the acceptance of a proposal by the National Science Foundation. Mr. Carmichael provided many insights into the hydrodynamics of streamlined bodies and was able to trim the vast literature down to a manageable number of pertinent papers and books.

I would like to thank the engineers, machinists, and technicians in the Ocean Engineering Department at W.H.O.I. who were extremely helpful

in translating drawings to finished parts, often on extremely short notice. Their years of experience contributed greatly to my education.

Lastly, I must thank my thesis committee who were very supportive of this effort. Their helpful suggestions for improving the clarity of the text and the ideas is greatly appreciated.

This research was conducted under NSF contract number OCE-8310168

TABLE OF CONTENTS

LIST OF FIGURES

4.5 BLOCK DIAGRAM OF THE SOFTWARE STRUCTURE OF THE PHASE COMPARATOR

4.6 PHASE DIFFERENCE I/O RELATIONSHIP FOR EACH OF THE TWO COMPARATORS (AT 15.05 KHZ.

4.7 THE EFFECTS OF TEMPERATURE AND FREQUENCY ON PHASE SHIFTS IN THE RECEIVERS AS SOURCES OF ERROR IN PHASE COMPARISON.

4.8 A BLOCK DIAGRAM OF THE MOTOR CONTROLLER SUB-ASSEMBLY

4.9 LINEAR MODEL OF MOTOR DYNAMICS (AFTER OGATA)

4.10 ROOT LOCUS OF MOTOR USED IN THE FAST PROFILER

4.11 BLOCK DIAGRAM OF MOTOR CONTROLLER ALGORITHM

4.12 PHOTO OF AUTOPILOT HARDWARE

4.13 BLOCK DIAGRAM OF AUTOPILOT ALGORITHM

5.1 LAMB'S COEFFICIENTS FOR PROLATE SPHEROIDS OF VARIOUS L/D

5.2 BLOCK DIAGRAM OF THE CONTROL LOOP

5.3 OVERALL SYSTEM ROOT LOCUS

5.4 ROLL CONTROL AS A SOURCE OF DIFFERENTIAL INPUT

6.1 PHOTO OF SHALLOW WATER TESTING OF THE FLYING FISH

6.2 BLOCK DIAGRAM OF THE DEPLOYMENT PROGRAM USED IN THE FIELD TESTS

6.3 THE PRESSURE RECORD FROM DIVE 6.

6.4 THE ACCELOROMETER RECORD DURING THE TURN AROUND TRANSIENT JUST AFTER THE BALLAST WEIGHT WAS DROPPED (DIVE 2).

6.5 THE RECONSTRUCTED TRAJECTORY FROM THE ACCELOROMETER RECORD OF DIVE 6.

6.6 AN ATTEMPT TO CORRELATE MOTOR SET POINT WITH THE ACCELOROMETER RECORD TO DEDUCE THE VEHICLE RESPONSE TIME.

6.7 THE RATE GYRO RECORD FROM DIVES 4 AND 6.

LIST OF TABLES

1 TRANSLATING THE SCIENTIFIC MISSION INTO A CONSISTENT SET OF ENGINEERING SPECIFICATIONS.

1.1 INTRODUCTION.

The Flying Fish is an autonomous, streamlined, gravity driven oceanographic instrument platform capable of (1) high speed vertical excursions from the surface to depths of 6000 meters and (2) guiding itself back to an acoustic beacon at the surface. Phase difference measurements made at four hydrophones mounted in the nose of this axisymmetric body are used to actuate control surfaces to correct vehicle attitude. The initial oceanographic sensor package is intended to measure conductivity and temperature as a function of depth. These parameters are used both as water mass tracers and, in the equation of state of seawater, to calculate the density field and thus the total transport of large scale circulation patterns.

This chapter begins with a description of the scientific mission. These requirements are then translated into a set of engineering specifications. Subsequent chapters use these specifications to define the mechanical and electronic system requirements and their implementation. The resulting design is described not only in the context of a single prototype but also as a test bed for the automated test procedures which will be required if this concept is to be used operationally. Further, standard interfaces and modular subsystems are used so that any suitable payload may be integrated with a minimum of

change to the existing design.

1.2 THE SCIENTIFIC RATIONALE FOR THE DEVELOPMENT OF THE FLYING FISH.

1.2.1 Background: A Short Primer of Hydrographic Surveys.

One of the fundamental limitations of present meteorological and atmospheric models used for weather prediction is the unknown boundary condition imposed by the world ocean (U.S. WOCE Planning Report #3). Despite advances in understanding the basic physics of the ocean, there is a dearth of field data covering the spatial and temporal scales required by computer models of the ocean. A complete study of an entire oceanic basin was undertaken only once, and the time scale spread over two years (1957-58) using discrete water samples (Fuglister, 1970). Large scale monitoring programs to study the global atmospheric weather patterns have, at present, no counterpart within the oceanographic community.

There are three general approaches in physical oceanography to measuring the circulation patterns of the world oceans. One approach uses direct measurements of fluid velocity and direction at discrete points. This Eulerian approach is best exemplified by the use of moored current meters. These instruments have a limited on site endurance (12-18 months) and have difficulty measuring low frequency seasonal and interannual variability. Drifters, a second class of instruments, make Lagrangian measurements. These instruments cover a broad range, from postcards to SOFAR (Sound Fixing And Ranging) floats. When used in large numbers and studied statistically they give good estimates of local fluid velocity and trajectory but not of total transport. They are

excellent for flow visualization studies. The last method for calculating circulation patterns is based on measurements of salinity and temperature as functions of depth. From these quantities, one can calculate the density field. Geostrophy (the study of potential flow fields on a rotating reference frame) exploits knowledge of the density field to determine the dynamic head driving large scale circulation. The primary contributors to density field variability are salinity and temperature. Historically these quantities have been measured from water samples taken at discrete locations. More recently, the density field has been measured in situ from conductivity, temperature, and pressure sensors appended to data loggers. This wire lowered CTD (conductivity and temperature as a function of depth) sensor is the backbone of large scale circulation and global heat budget studies.

In addition to the cable lowered CTD, several profiling instruments have been designed to address specific process oriented scientific questions. The nature of these questions requires only a few instruments which have no widespread application. As such, they are not commercially viable products. Table 1.1 summarizes the capabilities of these instruments and contrasts them with the attributes of the Flying Fish.

1.2.2 An Outline of the Potential Benefits of the Flying Fish.

Despite many advances in sensor technology, most sections of the world ocean are still undersampled. This undersampling is directly attributable to the high cost of mounting large scale ocean monitoring programs using present day technology. The Flying Fish was designed to help break this cost bottleneck by increasing deployment speeds by a

PROFILER NAME	MEASUREMENT TYPE	DEPLOYMENT TIME	COMMENTS
XBT	TEMPERATURE	5 min	Expendable, limited depth (1000m), limited temperature and spatial resolution
XCTD	CTD	5 min	Same as above
WHITE HORSE	CTD & CURRENTS	4 hours	Requires transponder net
PEGASUS	CTD & CURRENTS	4 hours	Requires transponder net
POP-UP	CURRENTS	Autonomous	No CTD capability
MICRO-PROFILER	CTD & CURRENTS	5 hours	Large and complex (one of a kind)
FLYING FISH	CTD	30 min	Fast, full ocean depth, high resolution, acoustic homing, potential for current measurement, commercially exploitable

Table 1.1 Some present day profilers and their capabilities

factor of between 3 and 6 (depending on station density and ship speed; see Figure 1.1). The development of a small, fast, streamlined free-fall sensor platform with acoustic homing capability has several tangible benefits:

-Faster deployment times shorten the time between first and last profiles of a trans-oceanic section to dramatically improve the synopticity of the observation.

-Faster deployment times reduce ship operating costs.

-Decoupling the ship motion from the sensor platform improves the flow around the sensors.

-Elimination of the winch and the electromechanical cable increases the number of ships capable of collecting data.

1.2.3 The Flying Fish: Its Specifications and its Mission.

The fish is designed to make, at a minimum, 10 meter averages of conductivity, temperature, and depth. The scientific merit of this goal is beyond the scope of this thesis. However, the finite response characteristics of the sensors, combined with a spatial resolution of 10 meters, puts a practical upper limit (of order 10 meters/second) on the desired terminal velocity of the fish. Other scientific considerations which are incorporated in the design of the fish are:

-less than one hour turn around between stations

-easy to use in the field (the complexity of the electronics should be transparent to the user).

-portable (including all support equipment needed for data archiving and sensor calibration)

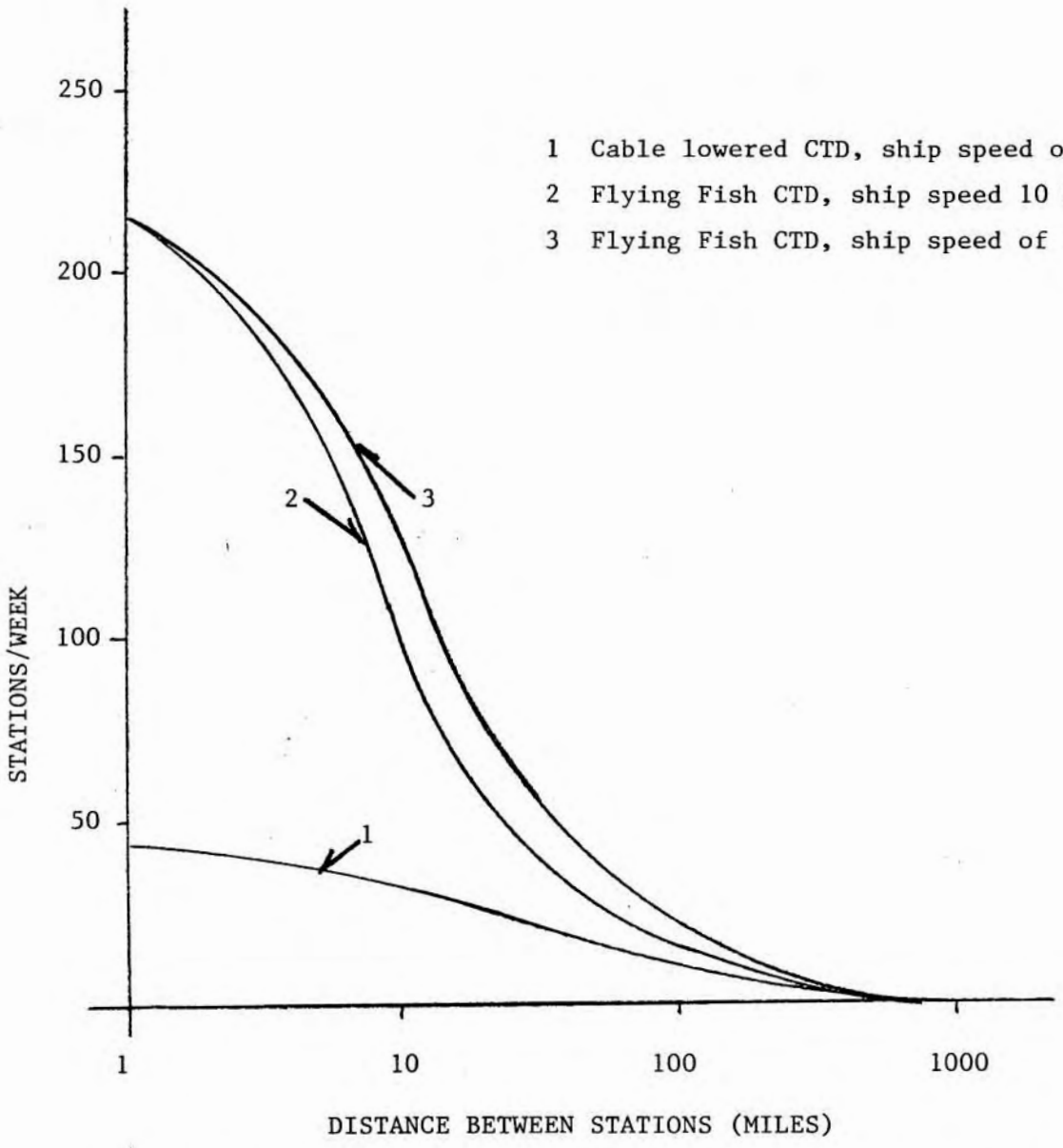

Figure 1.1. Intercomparison of Flying Fish and cable lowered CTD. Performance based on 40 minute and 4 hour deployments to full ocean depth.

-automated testing and sensor calibration to assist in the quality control of data.

This last consideration goes beyond the design of the fish itself, but is included here because the mechanical and electronic interfaces must be able to incorporate such capabilities.

1.3 ENGINEERING SYSTEM SPECIFICATIONS.

This thesis describes the development of a manueverable free-fall vehicle as a platform for a suite of hydrographic sensors. The instrument's principal attributes, portability and speed, are based on scientific need. In this section, these requirements are translated into a set of consistent engineering specifications.

As stated above, speed is a desirable goal. The lower bound of acceptable performance is obviously given by the speed of present day deployments (roughly one to two meters per second). The upper bound is a function of both the response characteristics of the sensors and of the spatial resolution desired in the measured quantities. For the study of general circulation, this translates into sensor fall rates of 5 to 10 m/s through the water column. Once the size and shape of the fish have been outlined, the rest of the hydrodynamic envelope can be defined based on maneuverability requirements.

1.3.1 Determining Vehicle Size.

Given that speed is the primary performance criterion, the first step is to define the size of the fish. The lower bound in fish size is given by the payload requirements. These include:

-propulsion mechanism

-vehicle guidance and control sub-assembly

-data aquisition and storage electronics

Assume that the following crude relationships are valid:

(1)the drag force (and hence the terminal velocity) is independent of Reynolds Number and is proportional to (volume)$^{2/3}$.

(2) the propulsive force (regardless of the propulsion system) is proportional to displacement (eg. the size of the energy reservoir).

If these relationships hold, then the speed of the fish can be increased without limit by just making it bigger. Thus, the upper bound of the vehicle size, if based on speed as the only criterion, is infinite.

In practice, there is a penalty proportional to size. A bigger fish requires more sophisticated handling equipment (see Figure 1.2 for a schematic representation) and is generally more expensive to build. This cost benefit relationship is derived in Appendix A. This derivation shows that if cost is an important parameter in the design of the fish, there exists a strong argument for a small fish.

1.3.2 The Optimum Shape.

One of the primary motives behind building the Flying Fish is to speed up data collection. Given a fixed payload and driving force, the speed is strictly a function of the drag characteristics of the fish. Thus, streamlining to reduce drag and provide smooth flow over the control surfaces is essential.

In the size and speed range of the Flying Fish, two general classes of streamlined bodies exist: laminar and turbulent profiles. This

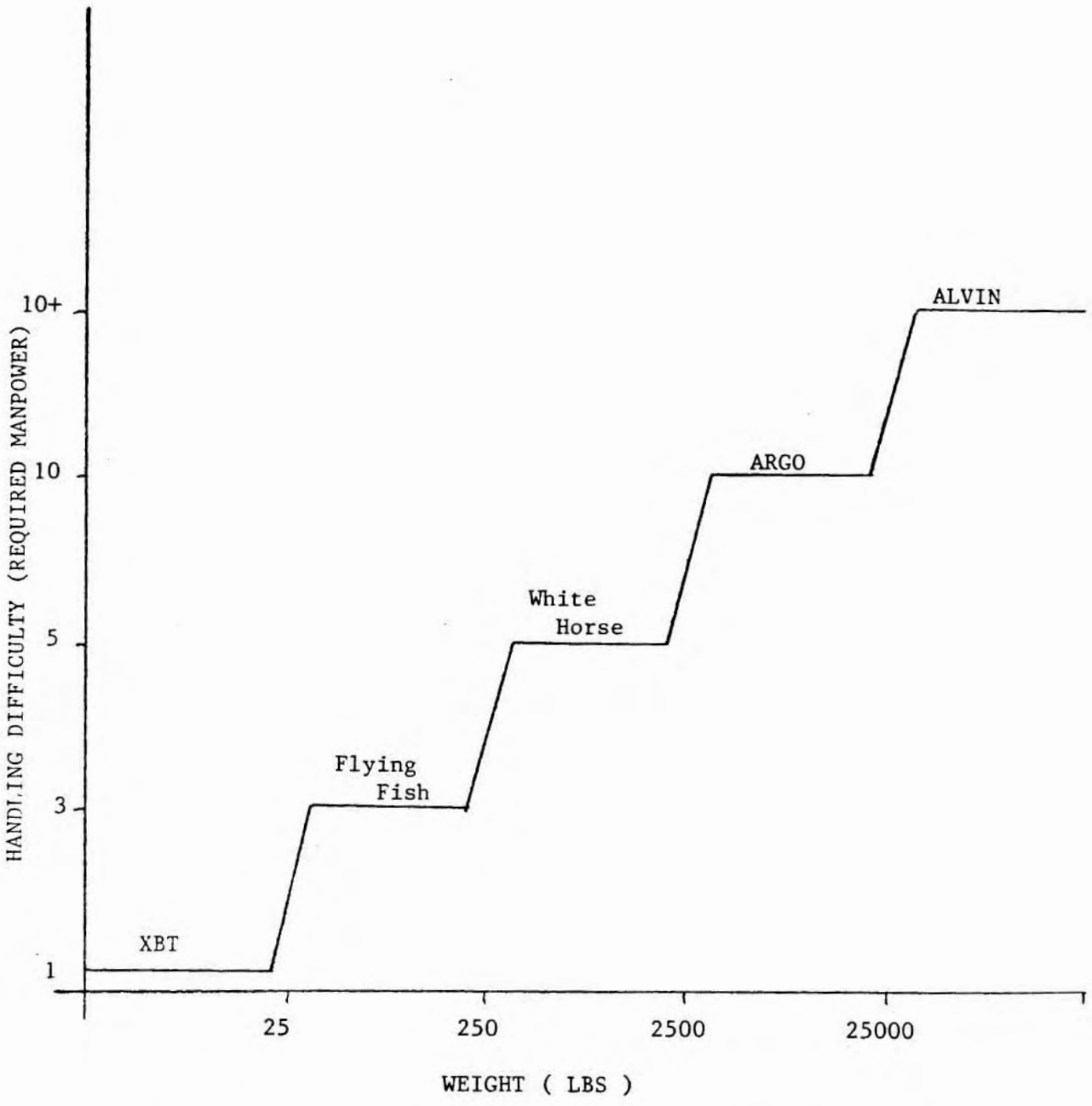

Figure 1.2. Handling Difficulty and Manpower Requirements for Several Oceanographic Instrument Systems.

classification refers qualitatively to the characteristics of the fluid boundary layer surrounding the body. Laminar bodies can have drag forces of as little as 30% of the drag of a conventional body of the same displacement (Parsons and Goodson,). This incredible performance is unfortunately offset by several inherent drawbacks which limit their practicality:

-laminar profiles are very susceptible to surface imperfections and to the presence of suspended matter in the water column. Typically the surface finish must be optically smooth. Should a turbulent boundary layer be tripped prematurely by a surface scratch the drag penalty is substantial.

-a paucity of technical data in the open literature on maneuverability and stability of these low drag bodies.

With these practical limitations in mind, a more conservative approach was chosen. The conventional profiles of the SERIES 58 bodies of revolution derived and tested at the David Taylor Model Basin were chosen for study. The potential performance of these shapes is discussed in Chapter 2.

1.3.3 The Propulsion Mechanism

Because of the unique mission of the fish, to vertically profile the ocean, active propulsion was discarded in favor of exploiting the gravitational potential of an expendable slug of dense material which is dropped on each dive. A hundred pound slug of steel is roughly equivalent to a 4 HP motor driving the fish at 15 knots. This approach does away with both the large drive motor and its attendant energy

storage requirements. The smaller fish is not only easier to handle in a seaway but is simpler and less expensive to build.

1.3.4 The Need for Acoustic Homing.

The need for acoustic homing is based on the fact that the speed advantage of a streamlined body is lost if recovery time is excessive. Typically, when recovering an oceanographic instrument at sea, the ship is maneuvered to within a few meters of the instrument, where it is then hooked and brought aboard. This procedure takes a minimum of half an hour and often more than an hour. By having a maneuverable instrument and steering it toward a recovery fixture, the recovery time can be minimized and the short deployment time preserved. Figure 1.3 is a schematic of this operational scenario.

1.3.5 The Performance Envelope.

The performance envelope describes the maximum glide angle that the fish is designed for. This is related to the station keeping ability of the surface ship once it has deployed the fish. For a dive to full ocean depth (6000 meters) the surface support vessel should be able to stay within a 1000 meter radius of the deployment area. This translates into a glide envelope of about 10 degrees. This envelope is used to define the size and shape of the control surface (Section 2.3.2), to define the sensitivity of the actuator (Section 3.5.4), and to bound the control loop characteristics (Section 5.4.3).

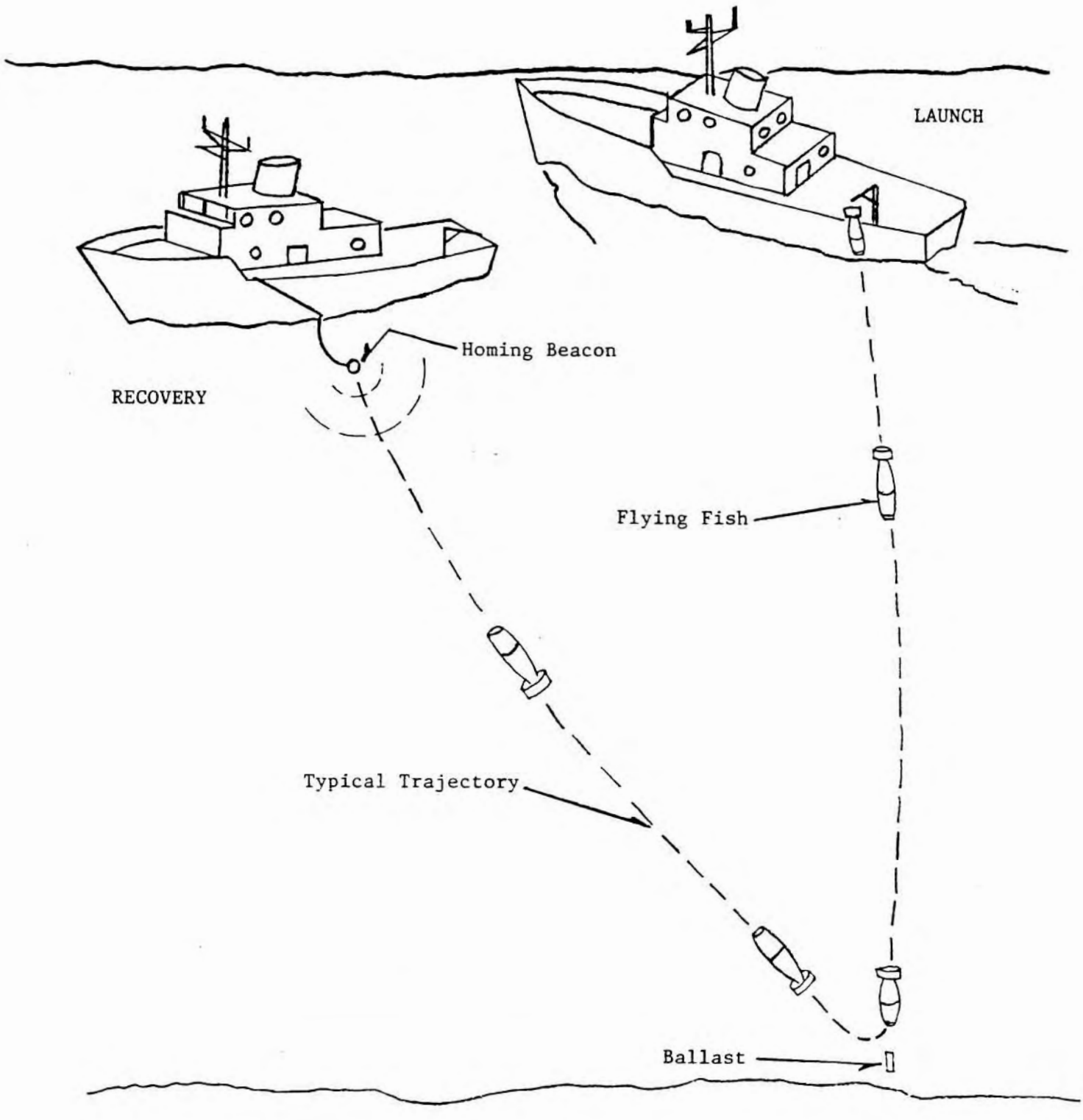

Figure 1.3 Schematic of the Operational Senario.
(after Albert Bradley)

1.3.6 Turn Around Time Between Deployments.

On present day hydrographic surveys, the typical distance between CTD stations is roughly 50 nautical miles, though in densly sampled areas it can be as little as 5 to 10 nautical miles. With ship speeds averaging between 10 and 15 knots, time between stations is of order 1 to 3 hours. In this time interval the fish must recuperate from the last dive and be ready for the next one. This tight schedule precludes the possibility of opening the pressure housing as part of the operational sequence. Thus, provision must be made in the design for data discharge and battery recharge through an external connection. Typical data volumes can be used to define the data rates through this connection. For the moment, it is sufficient to state that a 20 milliampere SAIL (Serial ASCII Instrument Loop) at 9600 Baud will handle the expected data transfer in half an hour and operational battery recharge should take also about half an hour.

1.4 Summary.

The important performance criterion are:

-speed; as fast as practical within the limits of sensor measurement capabilities (of order 5 to 10 m/s)

-size; the smallest vehicle that can accomodate the payload with a L/D ratio no smaller than 5.

-acoustic homing to a recovery fixture.

-low operational maintenance: 1 hour to transfer data and recharge/replace batteries.

2. VEHICLE HYDRODYNAMICS

2.1 BACKGROUND

In the previous chapter, the scientific mission requirements were used to outline the engineering specifications. Of these specifications, the speed and performance envelope impact (1)the shape of the body and the size of the control surfaces, (2)the size, propulsion, and operating depth affect the mechanical design, and (3) the time between stations affects the electrical interface. In this chapter, the primary consideration of speed and vehicle drag is followed by a discussion of the total stabilizing fin and control surface area as defined by the stability requirements. The maneuverability requirements are used to design the control surface actuator (both fin size and actuator torque/speed characteristics). Lastly, a sensitivity analysis of the vehicle hydrodynamics is exploited to estimate homing errors due to perturbations in the control loop and errors made in measuring the desired vehicle trajectory.

A comprehensive theory for flow about an elongated body moving through a viscous fluid which agrees with experimental results and which accurately predicts forces and moments is still not available. Nevertheless, some empirically derived principles have been established for making usable estimates of these quantities. For the Flying Fish, the major hydrodynamic considerations are: (1) drag; (2)static stability; (3)glide angle; (4)homing error; and (5) vehicle dynamics and control. The vehicle is assumed to be axisymmetric, which reduces the equations of motion (see Section 5.4.1) to a single second order differential equation

which can be solved analytically. The pitch and yaw dynamics are assumed to be decoupled and physically identical, a tremendous simplification in the control algorithm.

2.2 THE EFFECT OF BODY SHAPE ON SPEED AND DISPLACEMENT.

2.2.1 Axisymmetric Bodies in the Laminar Flow Regime.

Laminar boundary layers impart a lower shear stress at an interface than turbulent boundary layers. The boundary layer type (laminar or turbulent) is a function of the Reynolds Number, and is generally fixed. The operating Reynolds Numbers of the Flying Fish is in the transition region between laminar and turbulent boundary layers (see Figure 2.1). With care, the Reynolds Numbers characterized by a laminar boundary layer can be extended. The resulting difference in drag coefficient on a streamlined body of revolution can be as much as a factor of four. For a given payload and driving force, this means a laminar boundary layer will result in twice the terminal velocity. Since speed is a primary consideration, there is a strong incentive to pursue this line of investigation.

There are two ways to hamper the growth of a turbulent boundary layer: (1)induce a favourable pressure gradient in the direction of the flow; this can be accomplished in a purely geometrical fashion by increasing the body girth at a specified rate (Parsons and Goodson; Carmichael, personal communication); (2) induce a density gradient orthogonal to the flow; several attempts to achieve this by exhausting heat and long polymer chains through the bow of submarines and torpedoes have been marginally successful (Carmichael, personal communication;

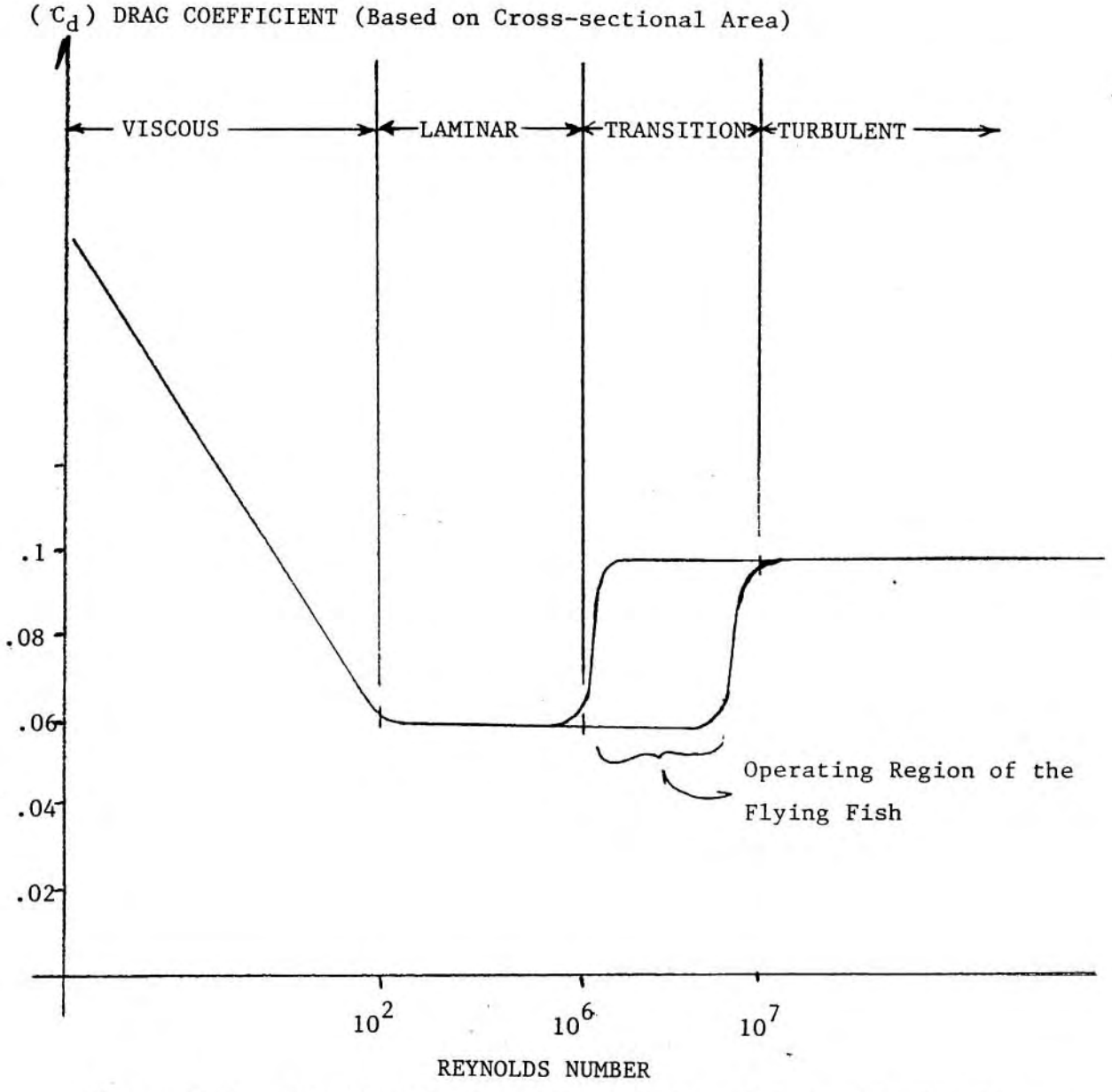

Figure 2.1 Idealized Drag Characteristics of Streamlined Bodies of Revolution for Various Flow Regimes.

Leehey, personal communication).

The first approach to maintaining a laminar boundary layer was found to be susceptible to the surface finish (optically smooth) and to the presence of particulates suspended in the water column. The penalty for premature formation of a turbulent boundary layer was a dramatic increase in the drag coefficient (Carmichael, Leehey, personal communication) which resulted in large scatter in the terminal velocity of the body when measured under realistic conditions. The second approach to suppressing the growth of a turbulent boundary layer was deemed impractical in this application and not pursued. For the Flying Fish, where deployments from the deck of working vessels will be routine, laminar profiles were abandoned in favour of conventional streamlined bodies.

2.2.2 SERIES 58 Bodies of Revolution.

The two non-dimensional quantites of interest in this section are the drag coefficient and the displacement coefficient. For free-fall vehicles, the drag coefficient is used to relate the propulsive force to the terminal velocity. The displacement coefficient is an indicator of the payload capacity of the body. The sensitivity of these quantities to changes in vehicle shape was used to define the final hydrodynamic outline of the bare hull of the fish.

Though several theories exist to predict drag forces analytically, it is essentially a non-linear phenomenon that is best studied empirically. In an unbounded fluid, the Reynolds number becomes the only significant non-dimensional parameter necessary to describe drag forces. By limiting the study of drag forces to those on streamlined bodies of

revolution, one finds substantial operating regions where the drag coefficients are independent of the Reynolds Number (see Figure 2.1).

A study of the model tank tests of the SERIES 58 bodies of revolution initially conducted by the David Taylor Model Basin leads to the following broad conclusions:

-The optimum L/D based on drag characteristics alone is 7. For L/D less than 7, the form drag is the major contributor; for L/D greater than 7, the skin friction becomes substantial.

-The sensitivity of drag force to L/D for L/D as low as 5 is only 4%.(see Figure 2.2).

-The displacement coefficient is very sensitive to L/D (see Figure 2.3).

-since drag is proportional to the square of the velocity, the most effective use of ballast (ie the minimum deployment time for a given potential energy) is to design a vehicle with an ascent rate equal to the rate of decent.

-the addition of control surfaces typically adds 15% to the drag coefficient, a 4% reduction in the terminal velocity (Abkowitz, 1969).

For the prototype fish the SERIES 58 profile 4175 (see Table 2.1) with a length to diameter ratio of 5 was chosen. The reasons are two-fold: (1)the penalty for a non-optimum drag coefficient is small (of order 5%); (2)the large displacement coefficient results in a relatively large payload in a small vehicle. The smallest vehicle with an acceptable drag penalty that could accomodate the payload (including floatation materials that could withstand an operating environment of 10,000 psi.) was a 2 meter long prototype displacing 0.17 cubic meters.

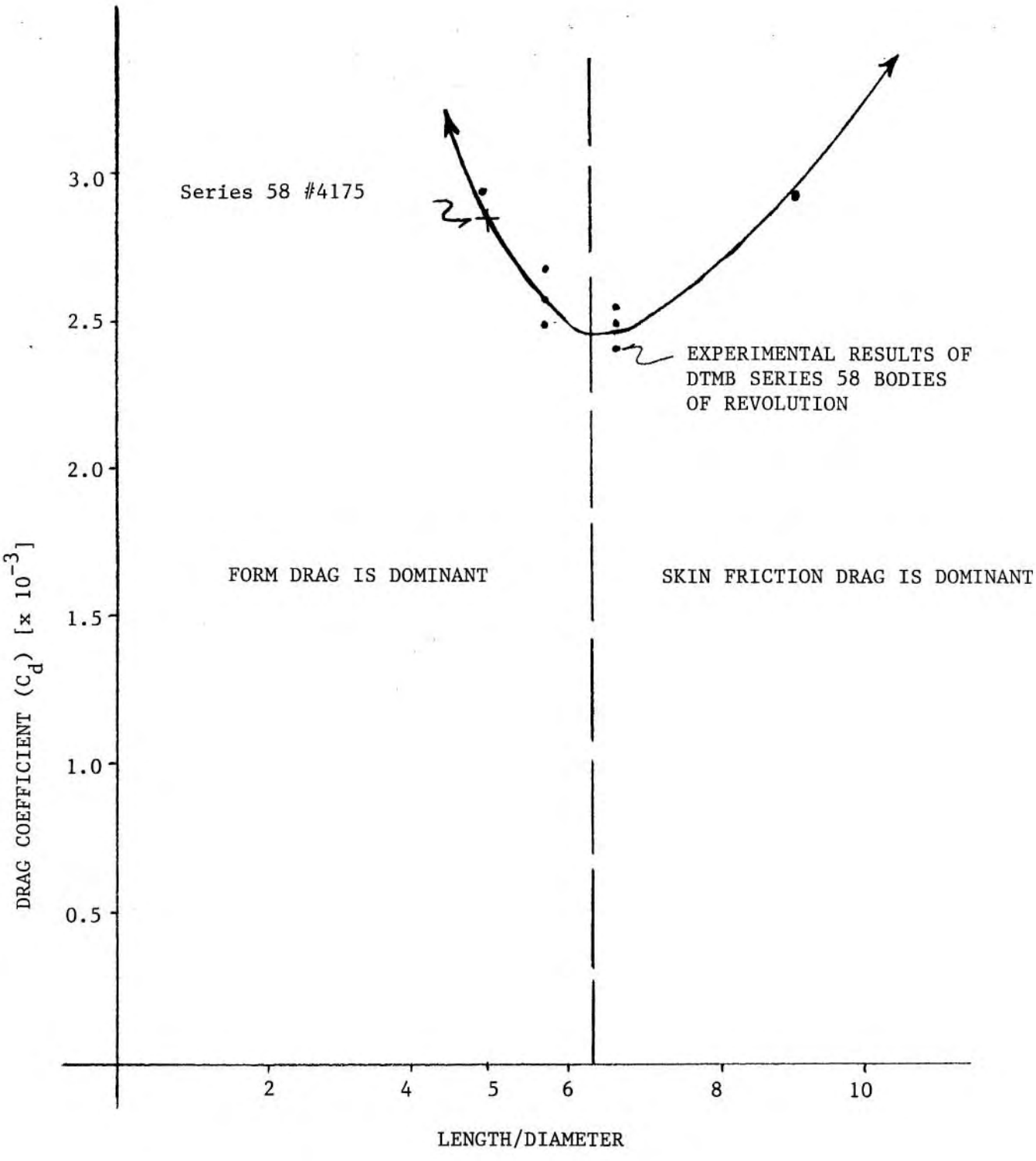

Figure 2.2. The Effect of L/D on Drag Coefficient (after Hoerner) With Data from the David Taylor Model Basin.

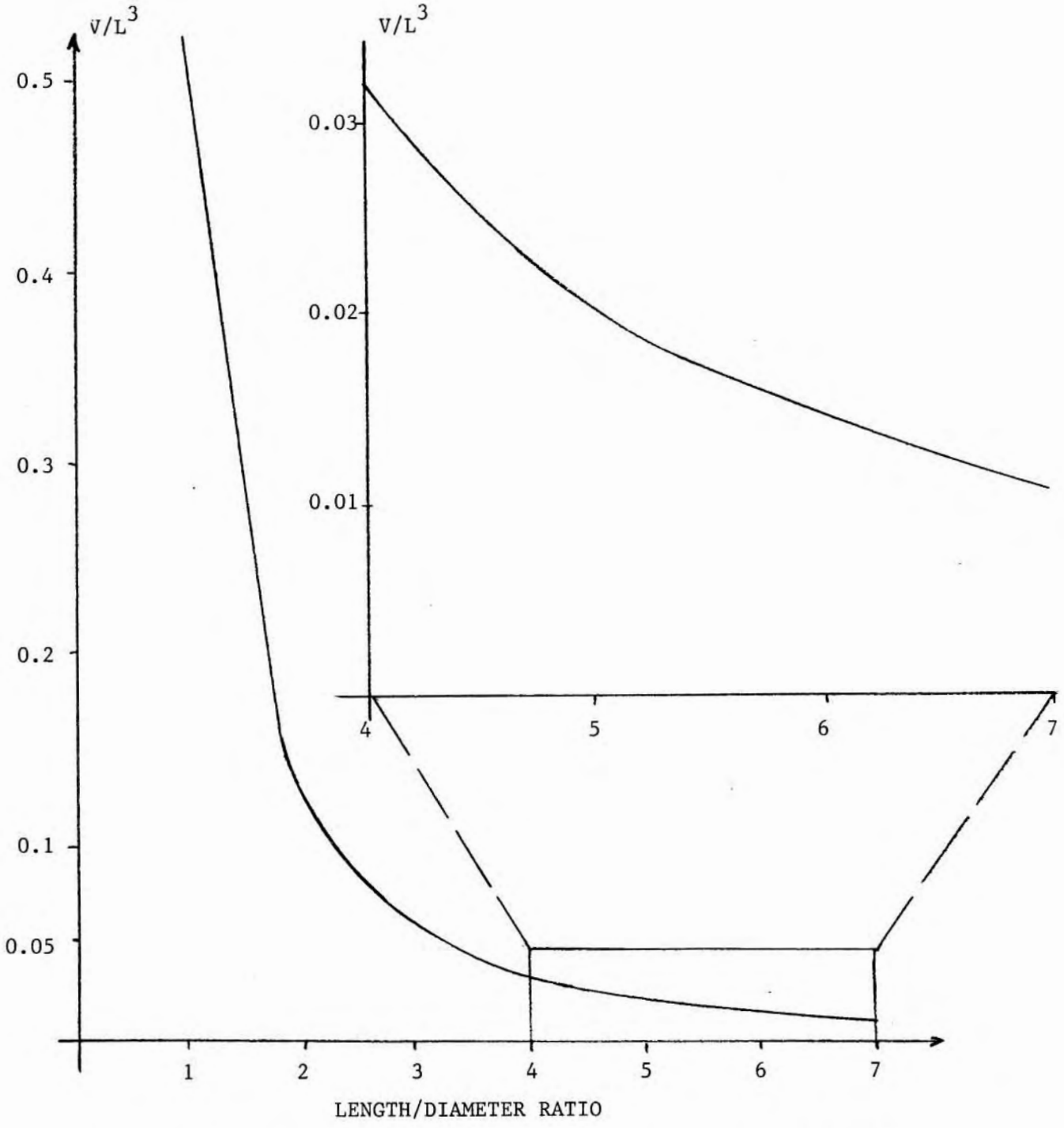

Figure 2.3 The Effect of Lenth to Diameter Ratio on Payload Capacity for a Prolate Spheroid.

Polynomial for the 2 dimensional profile of the Series 58 model 4175:

$$y^2 = a_1x + a_2x^2 + a_3x^3 + a_4x^4 + a_5x^5 + a_6x^6$$

where $a_1 = 1.000000$
$a_2 = 0.837153$
$a_3 = -8.585996$
$a_4 = +14.075954$
$a_5 = -10.542535$
$a_6 = 3.215422$

Wetted Surface Coefficient = $\frac{S}{L\ D} = 0.7426$

Longitudinal Center of Buoyancy = $\frac{X}{L} = 0.4484$

Model length: 9 ft. L/D = 5
volume: 13.74 ft^3
Wetted surface: 37.79 ft^2

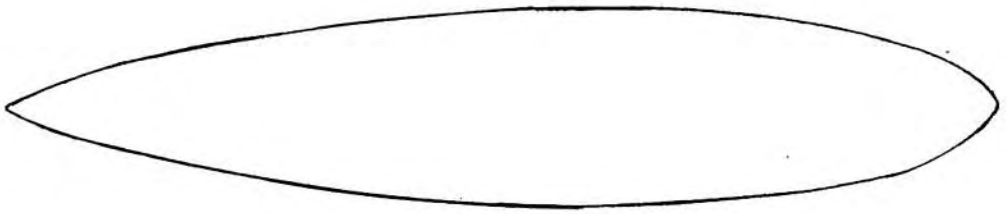

Table 2.1 Physical Dimensions of the Series 58 Model 4175 Bare Hull Used for the Flying Fish (L/D = 5).

The unballasted fish is 23 Kg. buoyant and, from the empirical results compiled by the David Taylor Model Basin, has a terminal velocity of 6 1/2 meters per second (see Figure 2.4).

2.3 STATIC STABILITY AND THE DESIGN OF STABILIZING FINS

For a body acted on only by hydrodynamic forces in an infinite fluid, an equilbrium state is one in which the moments and forces sum to zero. For an axisymmetric body, straight ahead motion at constant velocity is the equilibrium state used for stability studies. A stable body is one which returns to equilibrium when perturbed. Static stability describes only the initial tendency of the body to return to equilibrium and does not guarantee ultimate stability.

The coordinate system chosen to sum moments and forces (see Figure 2.5) agrees with the SNAME standard (SNAME, 1950). The origin is at the center of gravity (CG), both X-Y and X-Z form planes of symmetry, and X, Y, and Z are principal axes of inertia. These conditions greatly simplify the equations of motion (Abkowitz, 1969). The equations of motion, derived in Section 5.4.1, show that only the pitching moment coefficient affects static stability. The yawing moment, by symmetry, is a decoupled system described by the same equation.

The primary purpose of stability studies is to see if a passive vehicle will maintain straight line motion in the presence of perturbations. Several empirical methods for deriving the stability of a streamlined body have been developed for torpedoes, airplane fuselages, missiles, and dirigibles. The method used here is based on empirical calculations (derived at Rockwell for airplane fuselages) of the

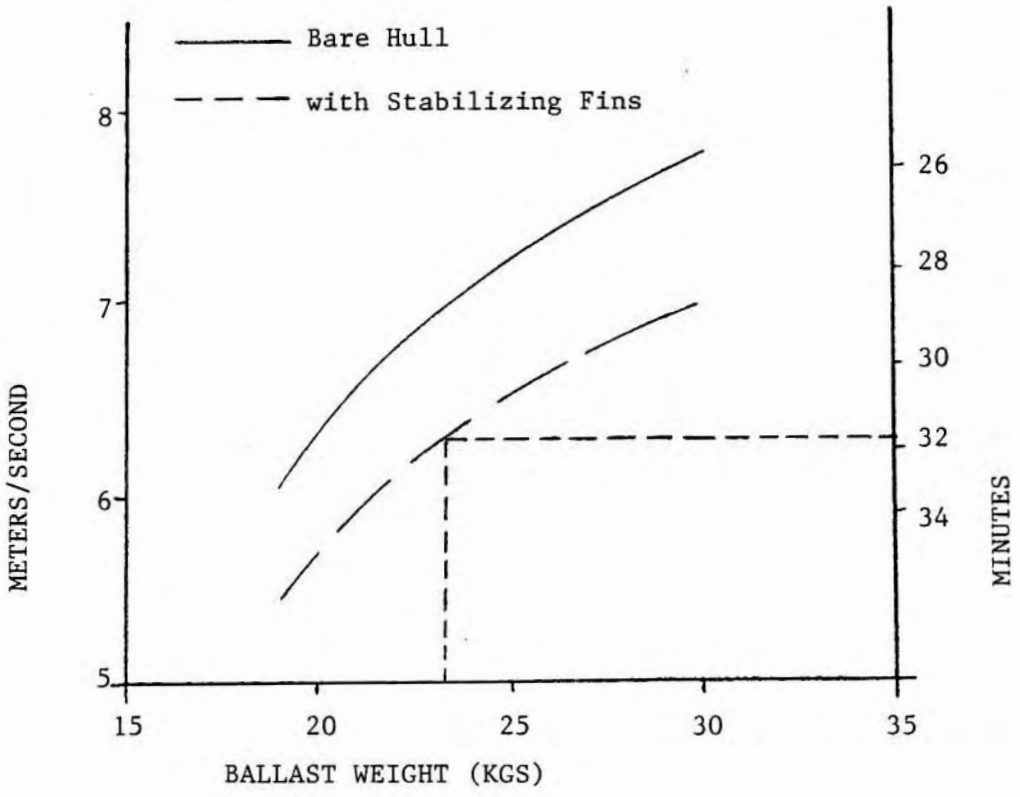

Figure 2.4 Round Trip Deployment Time for the Flying Fish Based on Series 58 Model 4175 and a Water Depth of 6000 meters.

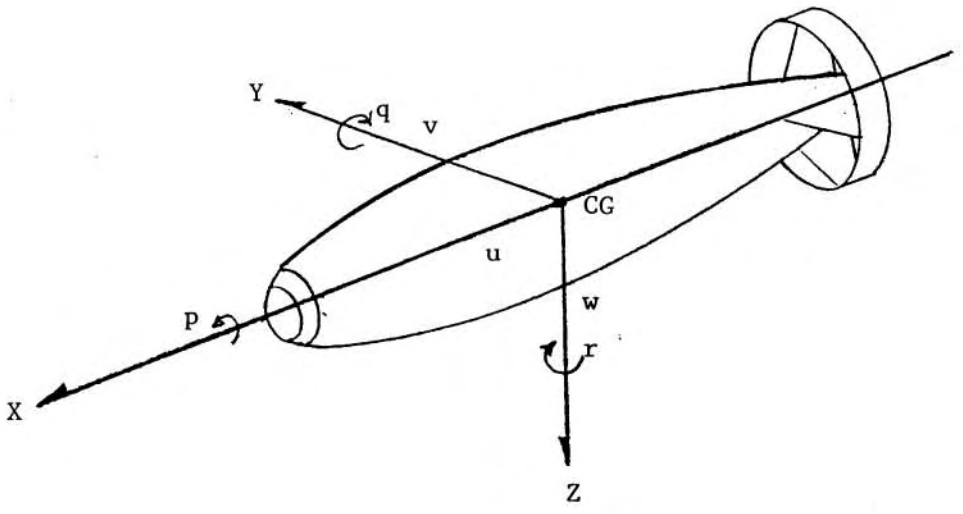

Figure 2.5 Definition of the Coordinate System Used to Derive the Equations of Motion.

upsetting moment induced on the bare hull by the fluid. Stabilizing fins were then designed to provide a righting moment 25% greater than the upsetting moment (Carmichael, personal communication). The effects of finite aspect ratio fins, hull interference, and wake turbulence, based on several references, were included in the calculation of fin size (see Section 2.3.2). If the stabilizing fins are too large, then the vehicle will be so stable as to not respond to rudder comands. Thus, the size of the stabilizing fins is a measure of the sensitivity of the vehicle attitude to rudder commands. This relationship of vehicle attitude to rudder angle is derived for the quasi-steady case in Section 2.4.2. This analysis is helpful in designing the size of the control surfaces. The effect of time varying rudder control on vehicle dynamics is discussed in Section 5.4.3 in relation to the control loop constants used in the autopilot model.

2.3.1 The Upsetting Moment.

2.3.1.1 History.

While the invicid fluid assumption is a poor one for estimating drag forces, it is reasonable for predicting lift forces and pitching moments on a streamlined body. In 1923 Munk derived an empirical formula to predict the pitching moment of slender bodies with constant density distribution. This work formed the basis of stability predictions used in the design of dirigibles but did not take into account the effect of variable center of gravity on stability.

2.3.1.2 The Effect of the Center of Gravity on Stability, the Rockwell Formula.

In order to include the effects of an uneven distribution of mass, Rockwell developed an empirical method for calculating the upsetting moment as a function of vehicle geometry and center of gravity (Perkins and Hage, 1949). This work was originally done to aid in the design of airplane fuselages. Equation 2.1 is the dimensionalized form of the Rockwell formula. The parameter K_B is taken from Figure 2.6 (after Perkins and Hage, 1949).

$$\frac{dM}{d\alpha} = \frac{.96K_B}{57.3}(S_s.L_F).\left(\frac{h_1}{h_2}\right)^{1/2} \cdot \left(\frac{w_2}{w_1}\right)^{1/3} \cdot \frac{1}{2}\rho U^2 \qquad 2.1$$

where M is the pitching moment
α is the angle of attack
L_f is the fuselage length
S_s is the projected side area of the hull
h_1, h_2, w_1, and w_2 are geometric parameters given by Figure 2.7
K_B is given by Figure 2.6 as a function of L/D and CG position.

For the Flying Fish:

$\rho = 1\,000\ Kg/m^3$
$U = 7\ m/s$
$S_s = .37\ m^2$
$L_f = 2\ m$

$$\left(\frac{h_1}{h_2}\right)^{1/2} = 1.14$$

$$\left(\frac{w_2}{w_1}\right)^{1/3} = .92$$

Equation 2.1 Dimensionalized pitching moment and static stability equation as developed by North American Aviation Inc. (Rockwell International); after Perkins and Hage, 1949.

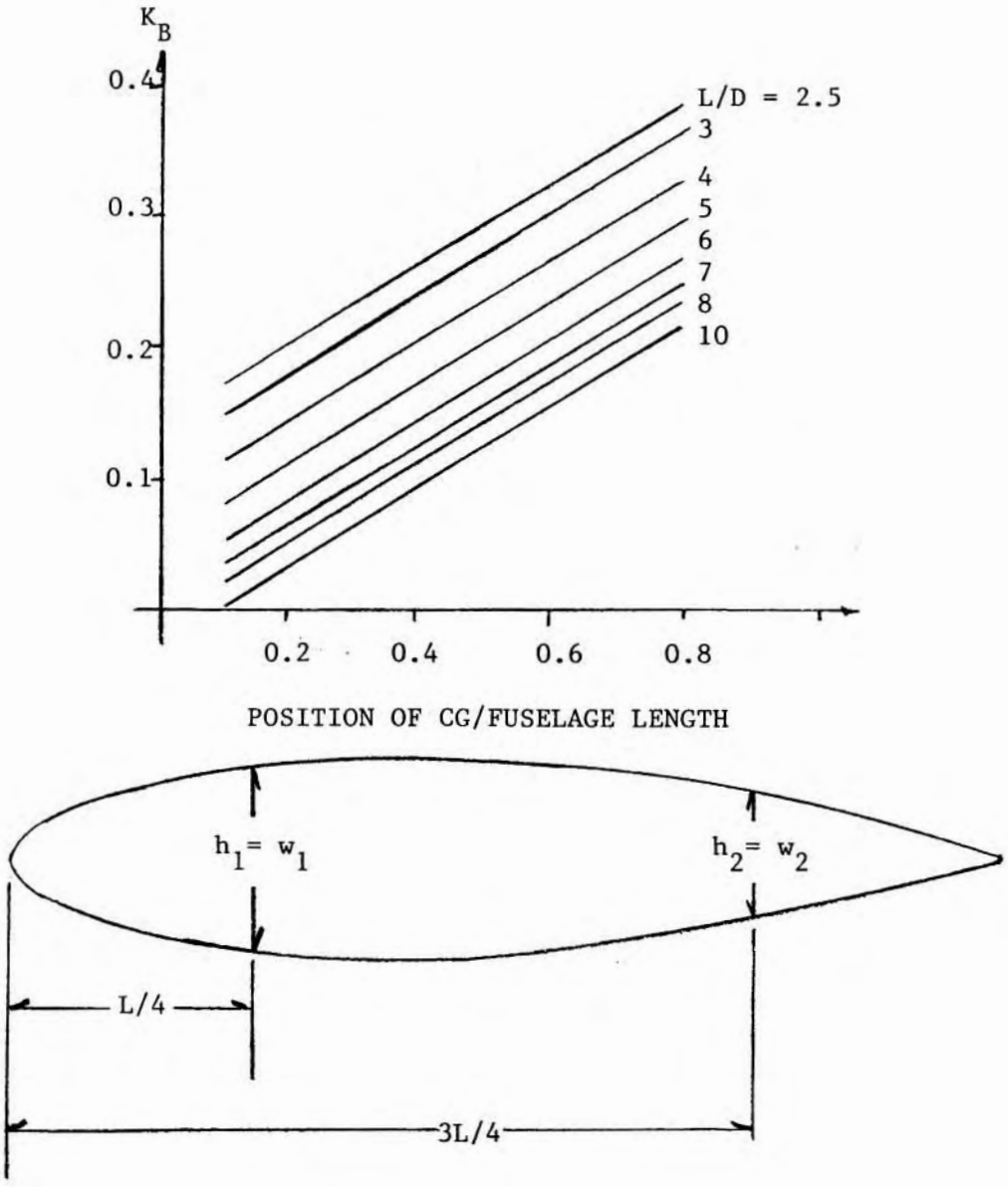

Figure 2.6 Empirically Determined Fuselage Directional Stability Coefficient (K_B). Originally from North American Aviation Inc.; (after Perkins and Hage, 1949). Note that for an axisymmetric body, $h_1 = w_1$ and $h_2 = w_2$.

2.3.1.3 Calculating the Bare Hull Upsetting Moment for the Series 58 Profile #4175 Using the Rockwell Formula.

The geometric characteristics of the body and the values used to calculate the upsetting moment are given in Table 2.1. The results are plotted as a function of CG in Figure 2.7. Since maneuverability is only an issue during ascent when the vehicle is homing in on the acoustic beacon, the center of buoyancy, rather than the center of gravity, becomes the governing independent variable in calculating the upsetting moment. Though the final weight distribution (which is a function of the details of the payload distribution) has yet to be stated, the predicted upsetting moment is of order 60 Nm/degree.

2.3.2 The Stabilizing Moment.

Equation 2.2 was used to calculate the correcting moment for undeflected control surfaces given the 2 dimensional foil characteristics (Figure 2.8) and the foil geometry (Figure 2.9).

$$\frac{dM}{d\alpha} = \left(\frac{dL}{d\alpha}\right)_{fin} \cdot X_1 \, \eta_1 \, \eta_1 \, \eta_1 \, \eta_1 + \left(\frac{dL}{d\alpha}\right)_{annulus} \cdot X_1 + B(CB-CG) \qquad 2.2$$

where X_1 = distance between the CG and the 1/4 chord of the tail fin
η_1 = correction for low aspect ratio
η_2 = correction for hull interference
η_3 = correction for wake losses
η_4 = correction for end plate effect
B = the righting moment of the Buoyancy

and $\frac{dL}{d\alpha} = \frac{dC_l}{d\alpha} \cdot \frac{1}{2} \rho U^2 \bar{c} \, b$ (this is the 2-D lift curve slope; see Figure 2.8)

c and b are geometric parameters given by Figure 2.10

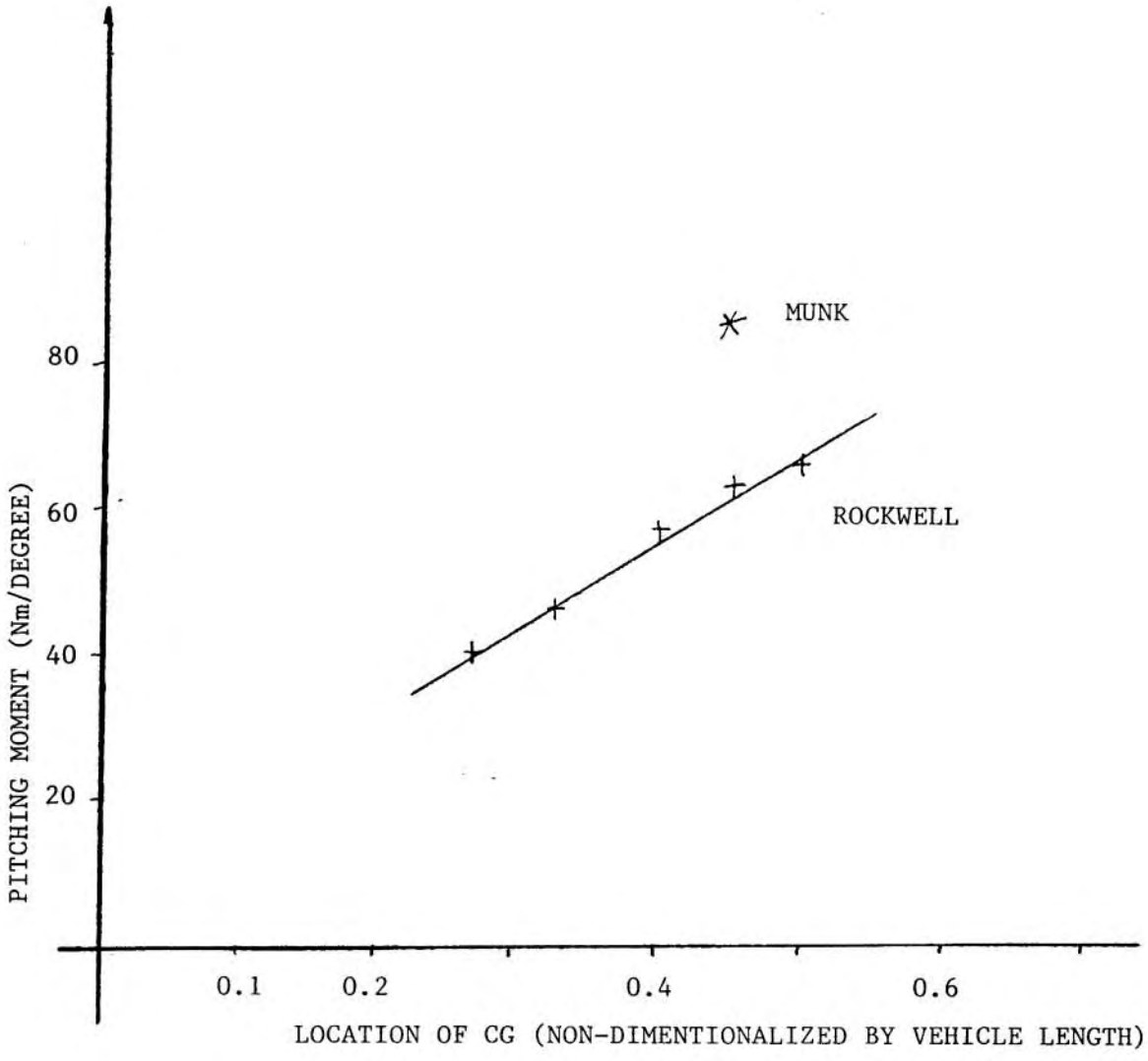

Figure 2.7 Predicted Pitching Moment as a Function of the Center of Gravity of the Flying Fish Bare Hull (measured from Leading Edge of the Hull).

To first order, η_1 and η_4 negate each other. For the Flying Fish, the following values were derived from Abkowitz:

η_2 = .8 to .9

η_3 = .8

This equation reveals that the stability can be increased by:

-moving the stabilizing fins farther aft (increasing x)

-increasing the wing area (S)

-moving the center of buoyancy forward.

-increasing the aspect ratio of the fins (bigger nl)

-increasing the lift curve slope (a characteristic of each airfoil; generally difficult to do)

2.3.3 The Fin Configuration.

The 2-Dimensional NACA 0012 foil (see Figure 2.8 after Abbott and von Doenhoff, 1959) was chosen for its combination of high lift, low drag, and benign stall characteristics . The sweep of the fins has more to do with the ability to shed lines and seaweed than with hydrodynamic performance. An annular wing was chosen to increase the effective fin area without increasing the fragility of the fins. This structure also provided some protection for the sensor elements. To support this structure, a rigid leading edge with movable flaps was chosen despite the better performance of the all-movable flaps. For reasons of simplicity in actuator design, an unbalanced aileron was chosen. A simple projection of the annular fin area on the X-Y and X-Z planes is a very good approximation of its contribution to stability (Fletcher, 1957). In addition, the annular wing is minimally affected by the

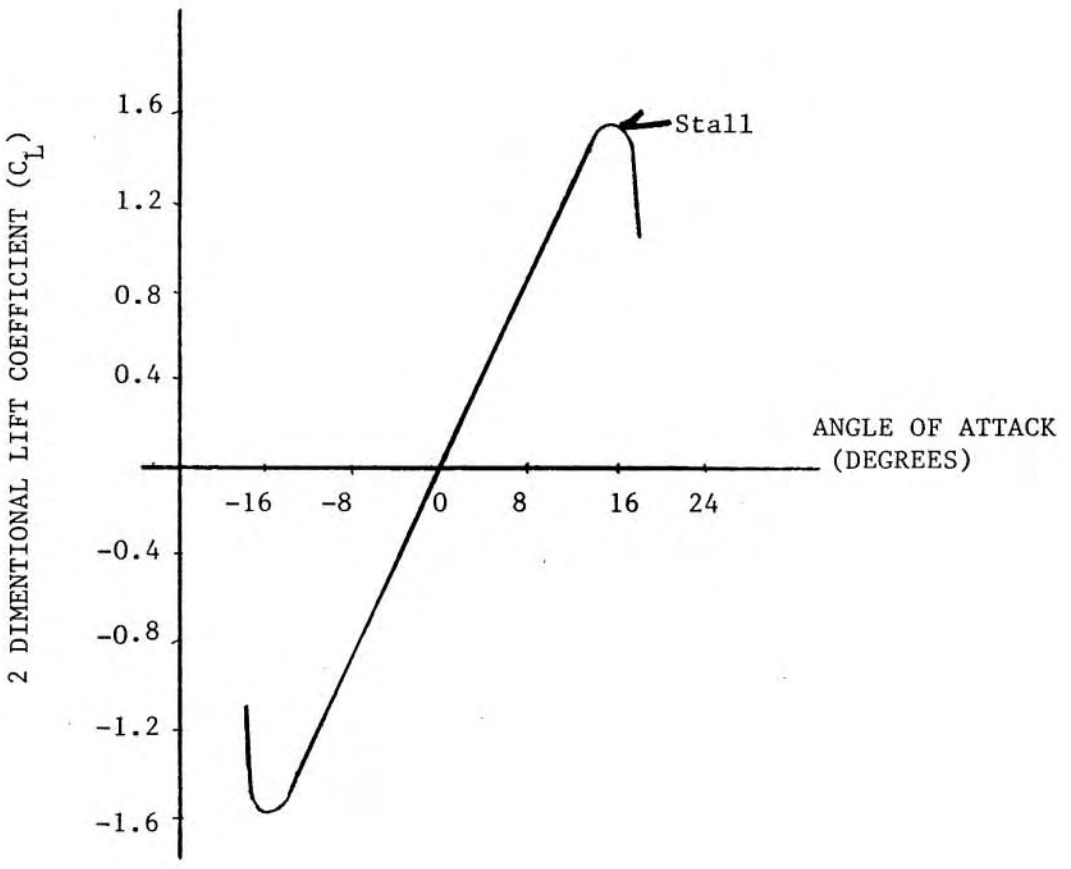

Figure 2.8 Section Lift Coefficient as a Function of Angle of Attack for NACA 0012 Two Dimensional Wing Section (after Abbott and von Doenhoff).

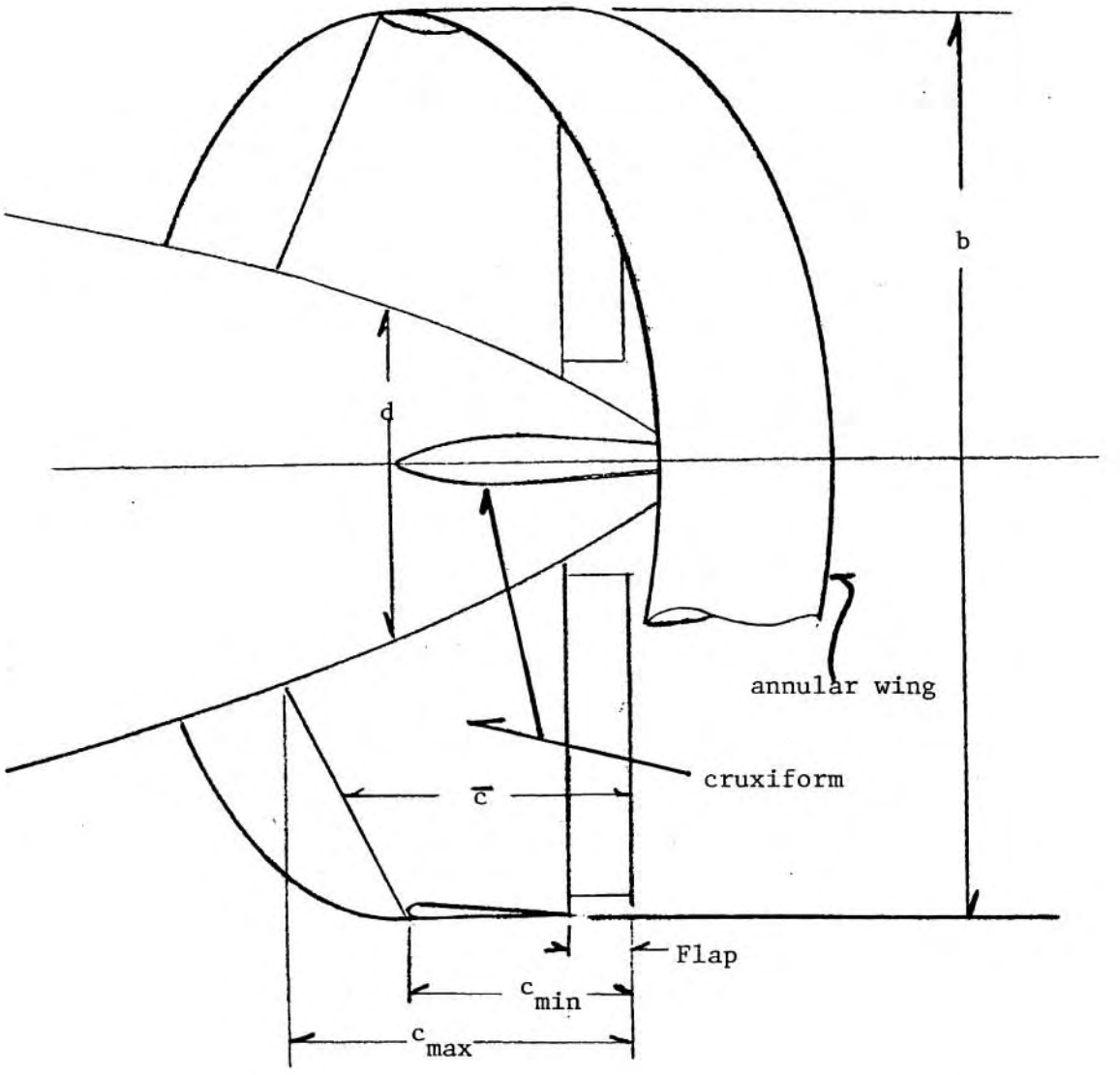

Figure 2.9. Schematic of the Stabilizing Fin and Control Surface Geometry of the Flying Fish.

hull or wake. The effects of hull interferance, finite aspect ratio, wake, and endplate effects on fin size are summarized in Equation 2.2. The resulting design gives the desired correcting moment of 125% of the upsetting moment. The ratio of the correcting to upsetting moment affects the location of the poles that describe the vehicle dynamics (as described in Section 5.4.3).

2.4 THE GLIDE ANGLE

The static equilibrium relationship between vehicle glide angle and control flap deflection of inherently stable vehicles is an indicator of vehicle maneuverability and is best characterized by two ratios: (1)the ratio of flap deflection to vehicle angle of attack and (2) the ratio of angle of attack to glide path. Figure 2.10 is a free-body diagram that defines the rudder deflection angle, the vehicle angle of attack, and the glide angle.

2.4.1 The Angle of Attack to Glide Angle Ratio.

A streamlined axisymmetric body has finite body lift (it is essentially a wing with an aspect ratio of D/L) which can be predicted with reasonable accuracy from slender body theory (Equation 2.3).

$$C_{N_\alpha} = \frac{K \pi AR}{2} \qquad 2.3$$

where C_{N_α} = lift curve slope

AR = the aspect ratio of the body (D/L)
K = a constant of proportionality

The result of this body lift is a finite angle of attack (α) when static equilibrium has been established on a given glide angle (θ). If one accepts the linear approximation, the ratio of angle of attack to glide angle is a

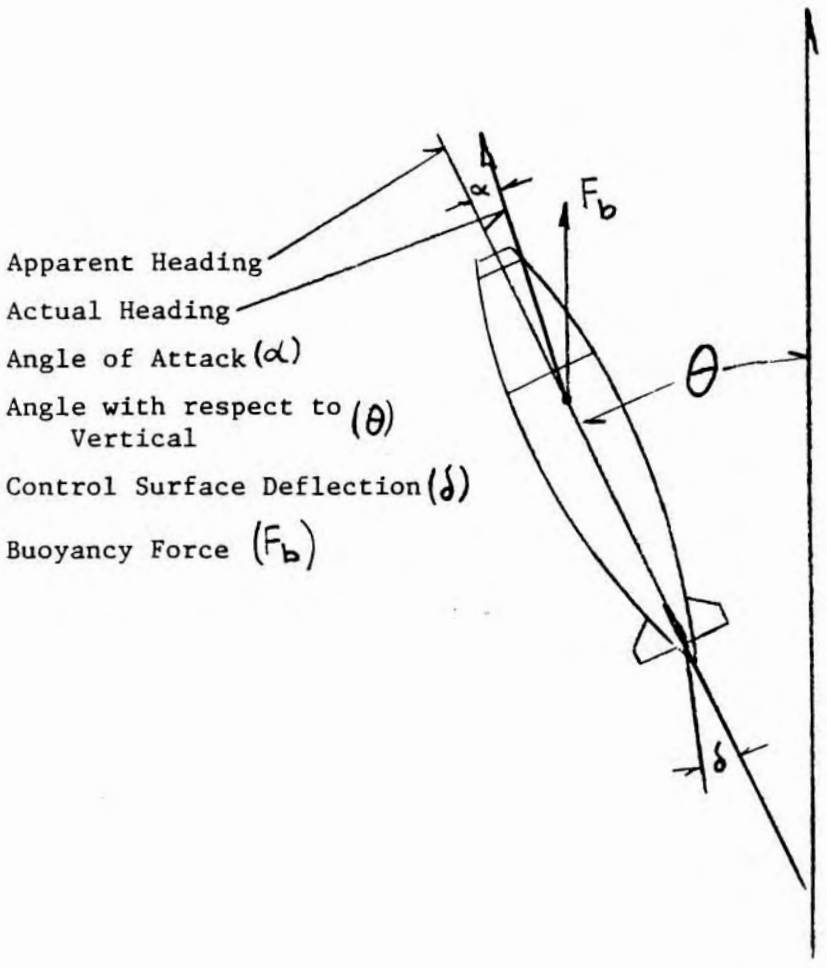

Figure 2.10 Free-body Diagram of the Flying Fish During Homing.

constant. For the Flying Fish, this constant (refered to as the Body Lift Factor) is about 0.08. This finite angle of attack gives rise to a homing error which is discussed below.

2.4.2 The Ratio of Rudder Deflection to Angle of Attack.

Both the upsetting and righting moments are to a first approximation linear functions of the angle of attack. Further, flap deflections can be modelled as equivalent changes in the angle of attack of the entire tail fin assembly (see Figure 2.11). Thus the ratio δ/α, for small angle maneuvers, is a constant. This constant is an indicator of the sensitivity of the vehicle attitude to control flap deflection (ie. the maneuverability) and to the magnitude of the required control effort once the maneuverability requirements have been established.

This measure of maneuverability is calculated in three steps:

-Translate elevator deflections (δ) to an equivalent full flap deflection (δ') using Figure 2.11 to determine the elevator effectiveness ($\eta\delta$).

-from the previous section, calculate the righting moment (including the contributions of the bare hull, the buoyancy, and the annular wing but not the contribution of the cruxiform control surfaces (see Figure 2.9 for clarification of geometry).

-calculate the flap deflection required to maintain static stability.

-if the vehicle is not sufficiently maneuverable, reduce fin size. Conversely, if the vehicle is not stable enough, increase the fin size.

For the Flying Fish the ratios of full flap and partial flap deflections to angle of attack are:

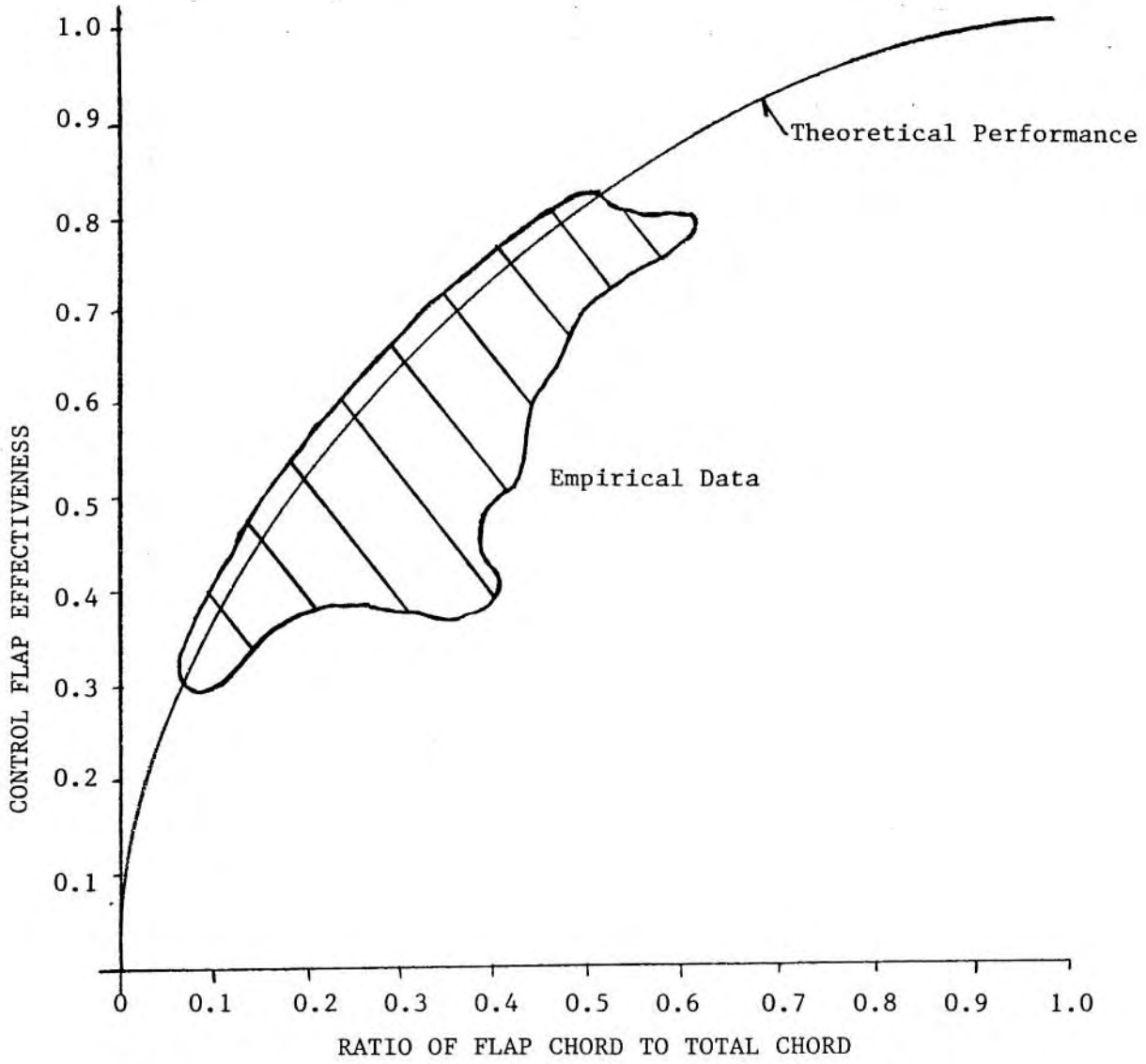

Figure 2.11 The Effectiveness of Flaps as a Function of Total Stabilizing Fin Chord (after Felhner, 1951).

$\delta'/\alpha = 1$ $\delta/\alpha = 1.5$

where δ is the control flap deflection
δ' is the effective full flap deflection
α is the angle of attack

2.5 CONTROL LOOP SOPHISTICATION.

As described briefly in the introduction, the Fast Profiler is designed to home acoustically on a beacon at the surface. The surface beacon emits a continuous monochromatic tone. In the far-field approximation, the acoustic wave can be modelled as a plane wave.

The sophistication of the homing hardware and algorithm can vary over a wide spectrum of viable alternatives. This sophistication reflects the precision with which the vehicle must home in on the acoustic beacon. On one end of the spectrum, no control effort is exerted and the vehicle simply drifts upwards. The homing error in this trivial case depends only on the relative drift between the ship and the fish. On the other end of the spectrum, a full 6 dimensional (linear + angular motion in each axis) inertial guidance system can be implemented. Such a system can fix both the position of the fish and the relative position of the beacon and proceed along some optimum path between the two. Several intermediate levels of homing sophistication are also viable:

(1) A phase difference measured between two hydrophones on a vehicle with constant spin; here the vehicle spirals toward the beacon, constantly correcting its attitude. The flaw with this approach is that there is a finite time between actuator fin deflection and attitude change which can result in an unstable trajectory.

(2) A phase difference measured between each of two orthogonal sets of

hydrophones (2 hydrophones in each set). Here, the two axes are controlled separately and vehicle symmetry is exploited since the hydrodynamic model of the two axes are identical. The potential flaw with this approach is that if the vehicle attitude is servoed to zero phase difference between all four hydrophones, this guarantees that the vehicle is pointed directly at the surface beacon, but this does not say anything about the actual trajectory of the fish. Because of the finite body lift of the fish, the actual trajectory is a logarithmic spiral toward the surface beacon (see Figure 2.12). Near the end of the deployment, the steady state error may accrue to the point where, even if the mean trajectory is within the performance envelope of the fish, the instantaneous trajectory may be extreme and the fish may stall.

(3) An enhanced version of the above scheme includes a vertical reference so that a phase offset may be added such that the actual and desired trajectories are identical.

Both methods 2 and 3 were implemented in the fish. The detailed implementation of this autopilot control system is discussed in Section 4.9. The results of field trials are discussed in Chapter 6.

2.6 HOMING CAPABILITY

2.6.1 The Contributions of Geometry, Desired Trajectory, and Sampling Speed.

Practical limitations to the performance envelope of the fish exist on several levels: (1)beyond 10 degrees off the vertical, increased body lift is required; (2)beyond 40 degrees, the pitch and yaw axes are no longer symmetrical because of the gravitational contribution; and (3) beyond a glide angle of 5:1, some form of propulsion is required. For the prototype, the smallest performance envelope that satisfied the scientific mission was

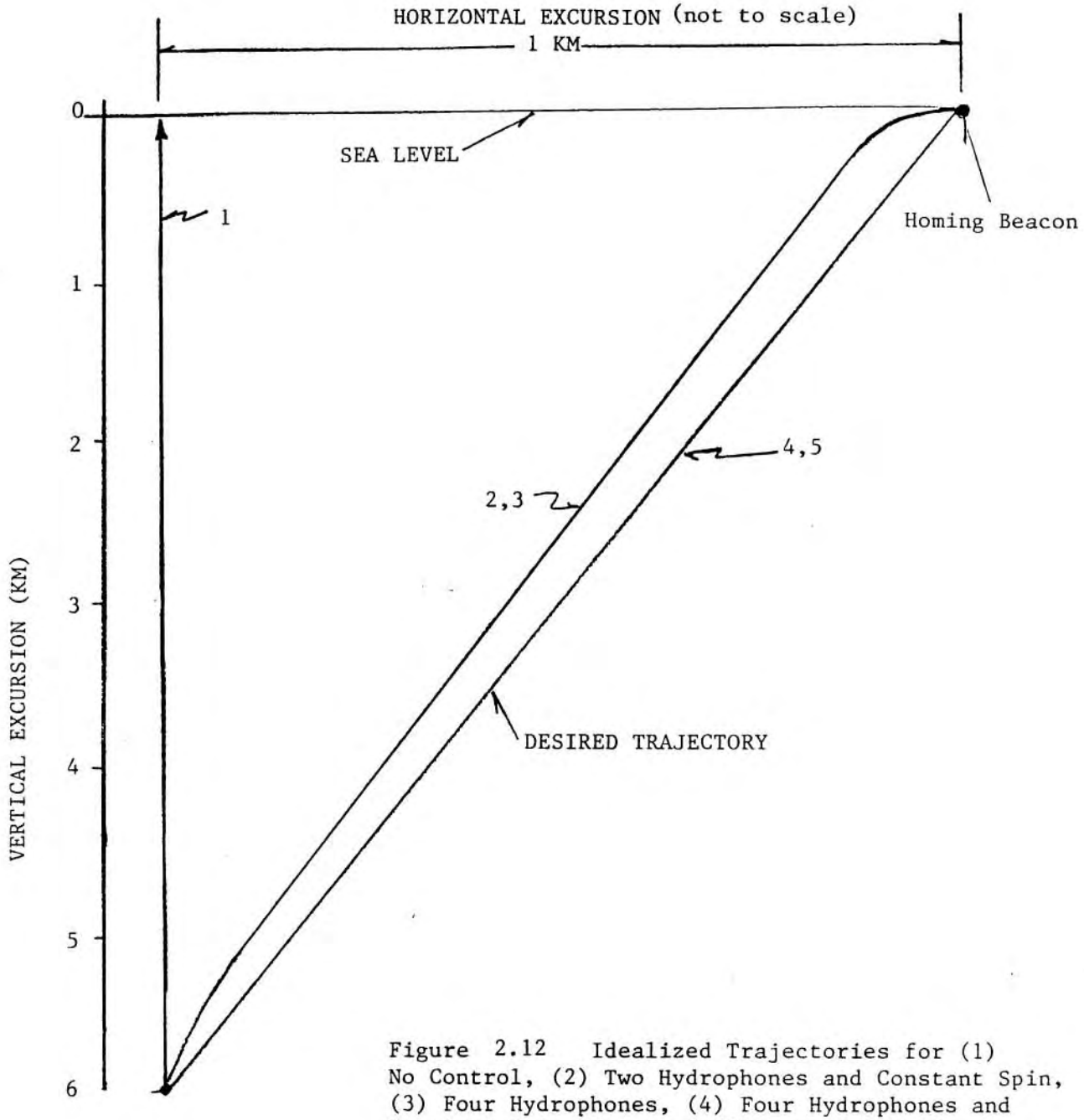

Figure 2.12 Idealized Trajectories for (1) No Control, (2) Two Hydrophones and Constant Spin, (3) Four Hydrophones, (4) Four Hydrophones and Vertical Reference, and (5) Inertial Guidance.

chosen. The limited maneuvering required by the fish simplified the control algorithm and eliminated the need for active propulsion.

The hydrophone array on the fish consists of two orthogonal sets of hydrophones. The distance separating the hydrophones forms the baseline for an interferometric calculation of the bearing to the surface beacon. Two bearings, one for each independent axis, are calculated. If the vehicle attitude is servoed to zero phase difference between all hydrophones, the vehicle is aimed directly at the surface beacon. For now, only the impact of this scheme on the hydrodynamic performance is of interest. Specifically, the sources of homing error are outlined (as defined by the distance between the vehicle and the surface beacon once the fish is on the surface), and the sensitivity of this error to changes in the hydrodynamic envelope.

In light of the analysis in Section 2.4, it is evident that for a finite glide angle, if the vehicle attitude is servoed to zero phase difference between all hydrophones, the actual vehicle trajectory is not a straight line for the beacon (see Figure 2.12). Instead, the trajectory is a logarithmic spiral which may cause the fish to exceed its operating envelope and result in large homing errors.

This section attempts to quantify the homing error as a function of the body lift, glide angle, sampling interval, and errors made in measuring the bearing to the homing beacon. This last contribution to homing error gives some indication of the phase resolution required by the acoustic tracking array/receiver circuitry (see Section 4.6). A simple quasi-static model was developed to predict the homing error. From this model, the sensitivity of homing error to hydrodynamic and engineering constraints could be explicitly determined. Figures 2.13 through 2.15 summarize the results of this study.

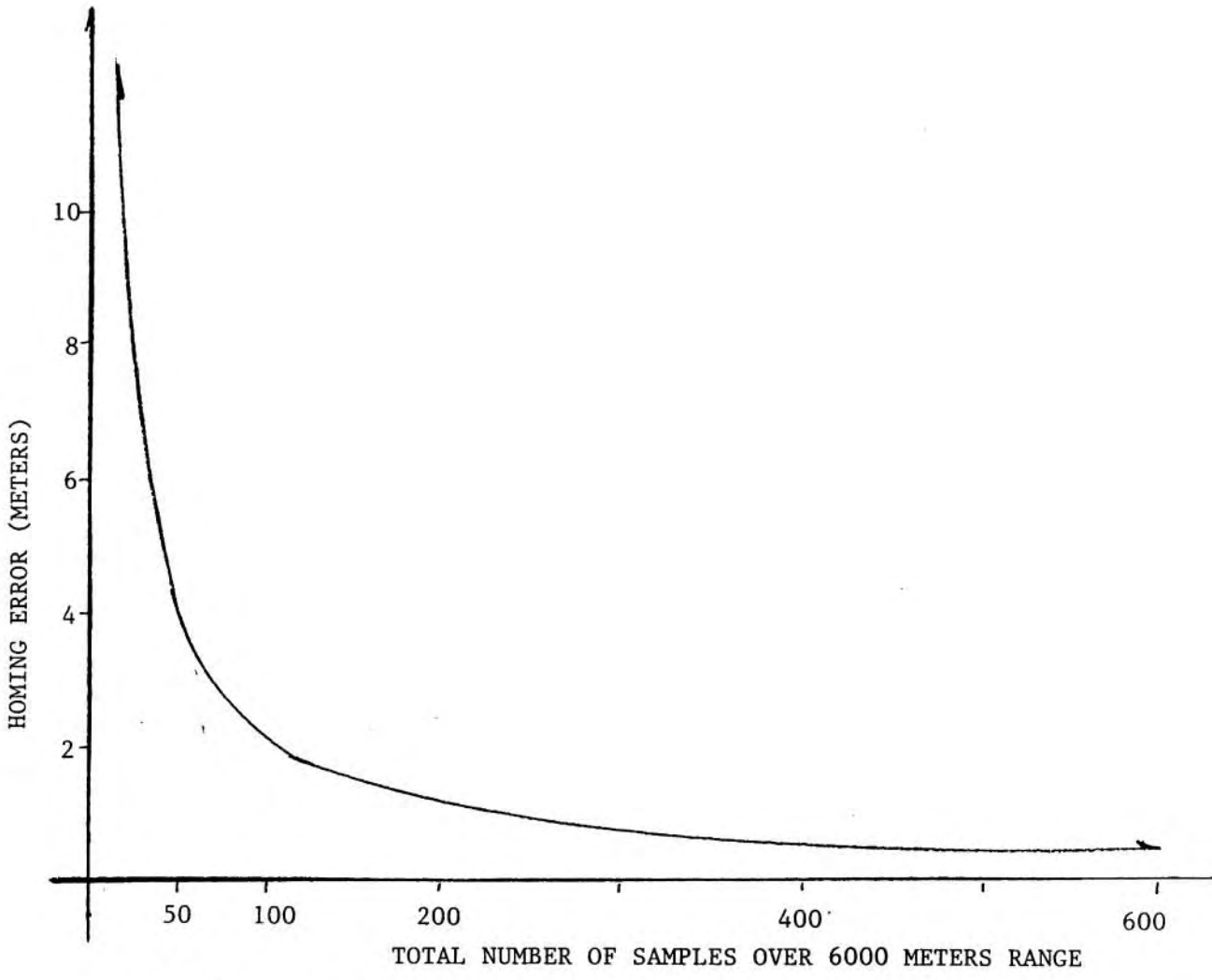

Figure 2.13 Calculated Homing Error as a Function of Number of Times that the Bearing to the Homing Beacon is Sampled during a typical ascent from 6000 meters. Samples are assumed to be evenly spaced in time and space (ie. 600 samples corresponds to one sample every 10 meters).

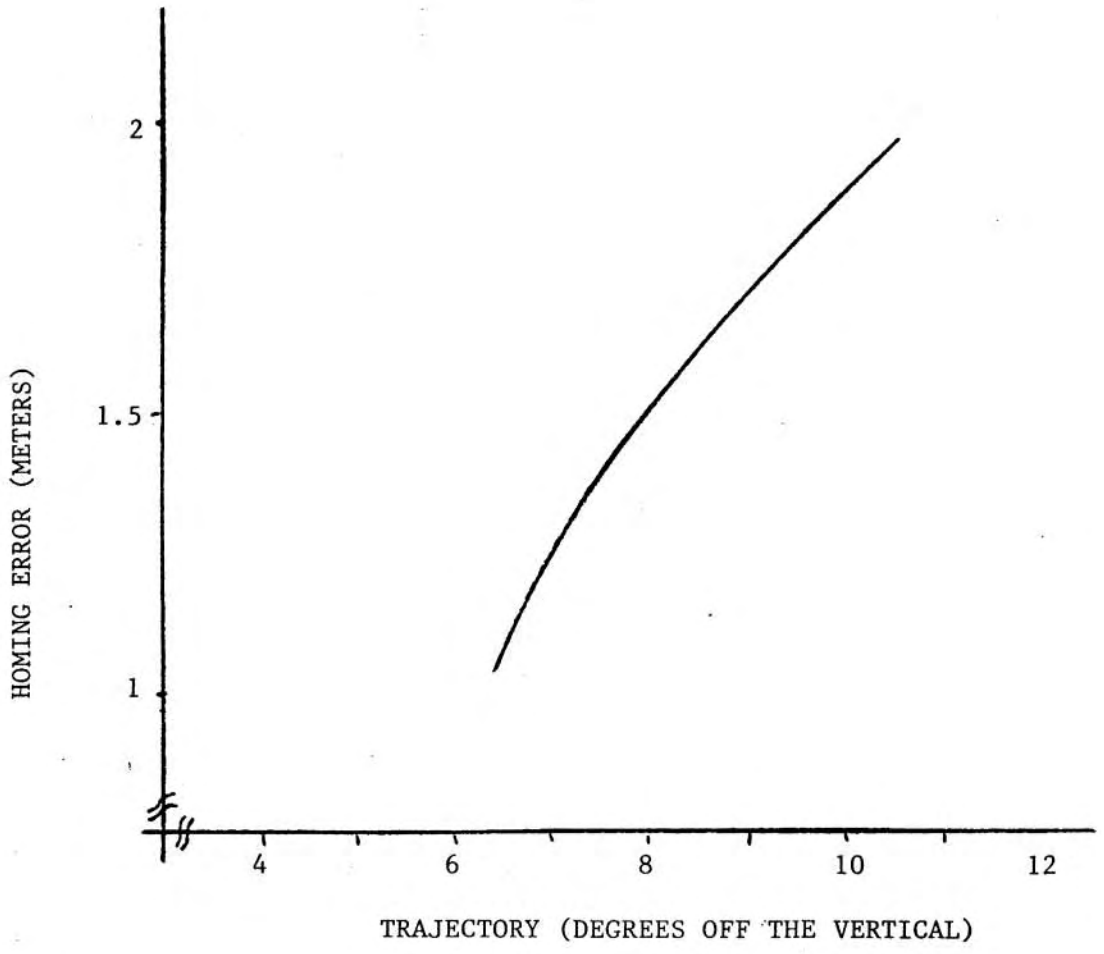

Figure 2.14 Calculated Homing Error as a Function of Trajectory.

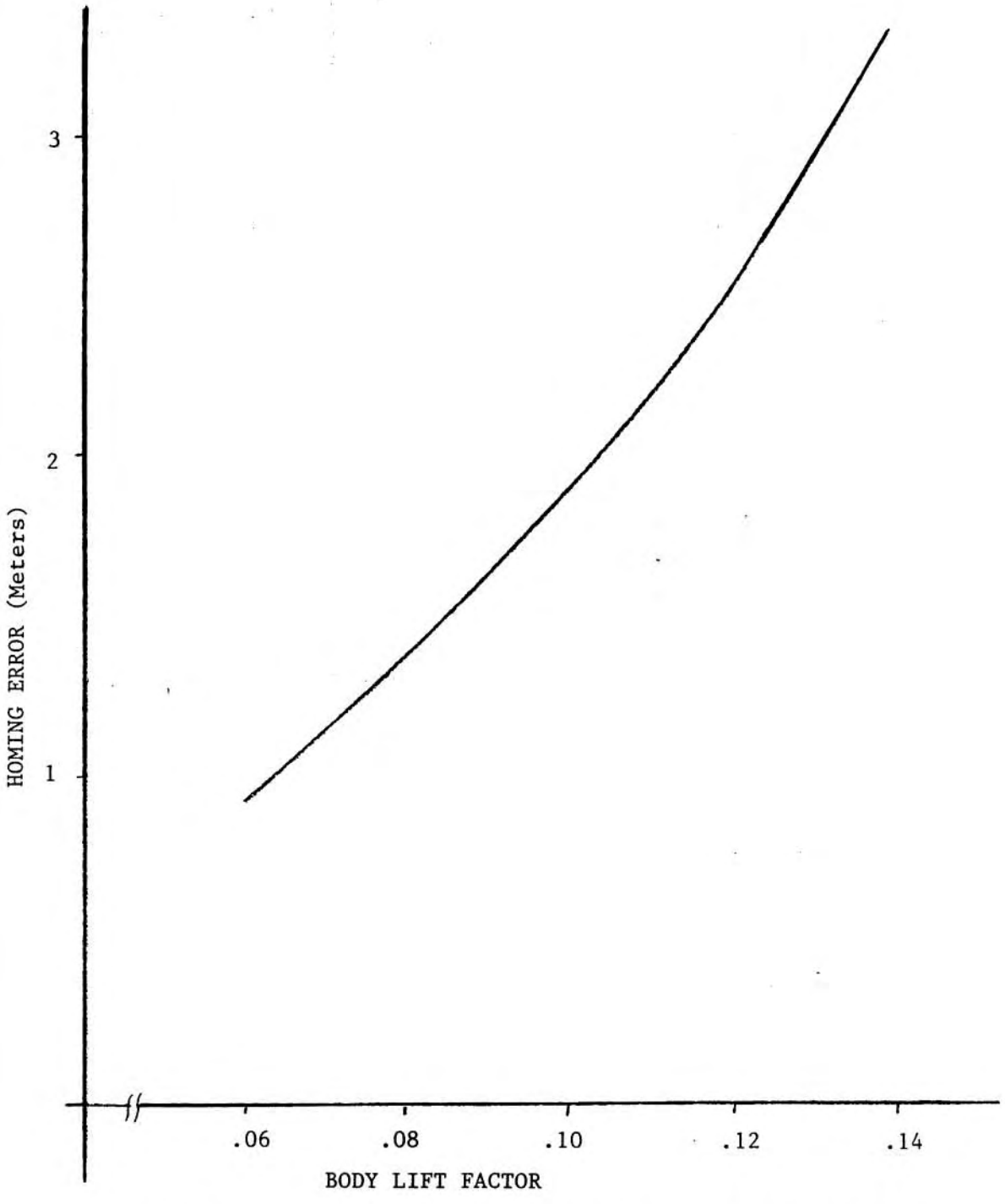

Figure 2.15 Calculated Homing Error as a Function of Body Lift for a Trajectory 10 Degrees Off the Vertical.

From these figures, the following conclusions can be made:

-Any sampling speed faster than 1 Hz is virtually indistiguishable from a continuous measurement of bearing.

-The maximum contribution to homing error due to glide angle is at the limit of the design performance envelope (10 degrees) and is of order 2 meters. This could be eliminated as a source of error if the fish were programmed to offset its trajectory as a function of the glide angle. To do this, two additional inputs to the control algorithm must be added: (1) a vertical reference, and (2) confidence in the ratio a/θ (which would determine the phase offset).

2.6.2 The Contribution of Phase Measurement Error to Homing Capability.

In Figures 2.13 to 2.15 the effects of sampling interval, body lift, and desired trajectory on homing capability have all assumed the ability of the control loop to measure the phase differences at the hydrophones with infinite resolution and no offset error. This analysis is important not only in calculating the contribution of an error in bearing to the final homing error but also in determining the relationship between hydrophone spacing and the frequency of the homing beacon.

In this analysis, the acoustic signal is modelled as a plane wave of constant frequency. The phase difference measured at the hydrophones described by Equation 2.4 is defined graphically in Figure 2.16.

$$\Delta\Phi = 2 \sin \theta(L_H/\lambda) \qquad 2.4$$

From this relation, it is evident that a higher homing frequency or larger

hydrophone baseline will improve the phase resolving capability of the fish. Such steps are not implemented without cost. Specifically, one must address the following issues:

-the baseline cannot be enlarged beyond the practical limits imposed by the physical size of the fish.

-higher frequencies attenuate more quickly in the ocean and, for a given S/N measured at the hydrophones, more acoustic power must be put in the water (possible but not desirable).

-if the baseline is greater than the wavelength of the acoustic signal, a single phase difference corresponds to a multiplicity of headings. Such an ambiguity cannot be easily resolved by the fish and may result in the fish attempting to home on an acoustic image.

The sensitivity of the homing error to offset errors in measured phase difference between two hydrophones as a function of the non-dimensional ratio L_h/λ is shown in Figure 2.16. It is evident from this analysis that precise phase differences (of order 1-2 degrees) are necessary if homing errors due to phase offset are to be of the same order as the other contributors to homing error. This requirement can be translated into a system specification that directly affects the hydrophone spacing, the source frequency, the source strength, the gain of the receiver/pre-amplifier, and the number of samples averaged. The relationship of these quantities is discussed below.

2.7 CALCULATING THE REQUIRED SIGNAL TO NOISE RATIO.

The following discussion assumes an operating frequency for the homing beacon of 15 KHz with a hydrophone baseline of 15 cm. The wavelength at this

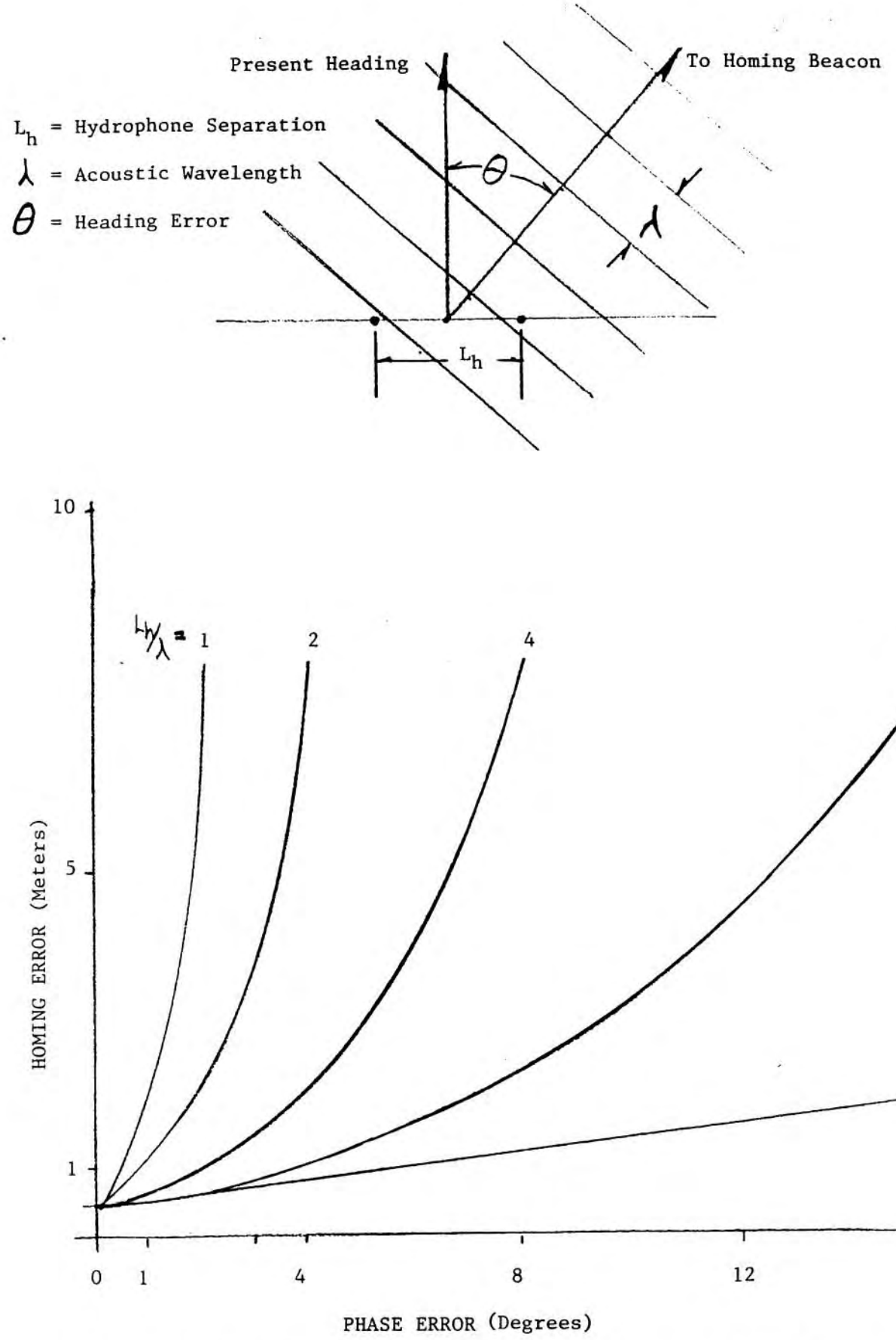

Figure 2.16 Calculated Homing Error as a Function of (1) Phase Error and (2) the Ratio of Hydrophone Separation to Wavelength of the Acoustic Signal Generated by the Homing Beacon.

frequency is 10 cm. Because L_h/λ is greater than 1, there is some potential for ambiguity in that more than one acoustic image exists. Within the +/-10 degree operating envelope of the fish, however, only one acoustic image is possible. This phase/heading relationship is given by Figure 2.17.

To achieve the desired 1 degree phase resolution, a signal to noise ratio of 57 is required at the receiver. For a relatively narrow receiver operating range (100 Hz centered at 15 KHz), the ambient noise spectrum is assumed white and the sound pressure level is -60db//ubar/Hz (Wenz, 1962). Additional calculations for attenuation and spreading losses (Marsh, 1969) result in a source strength requirement as a function of receiver bandwidth (see Table 2.2). The implementation of a narrow (10 Hz) Phase-Lock Loop filter is discussed in Section 4.6.

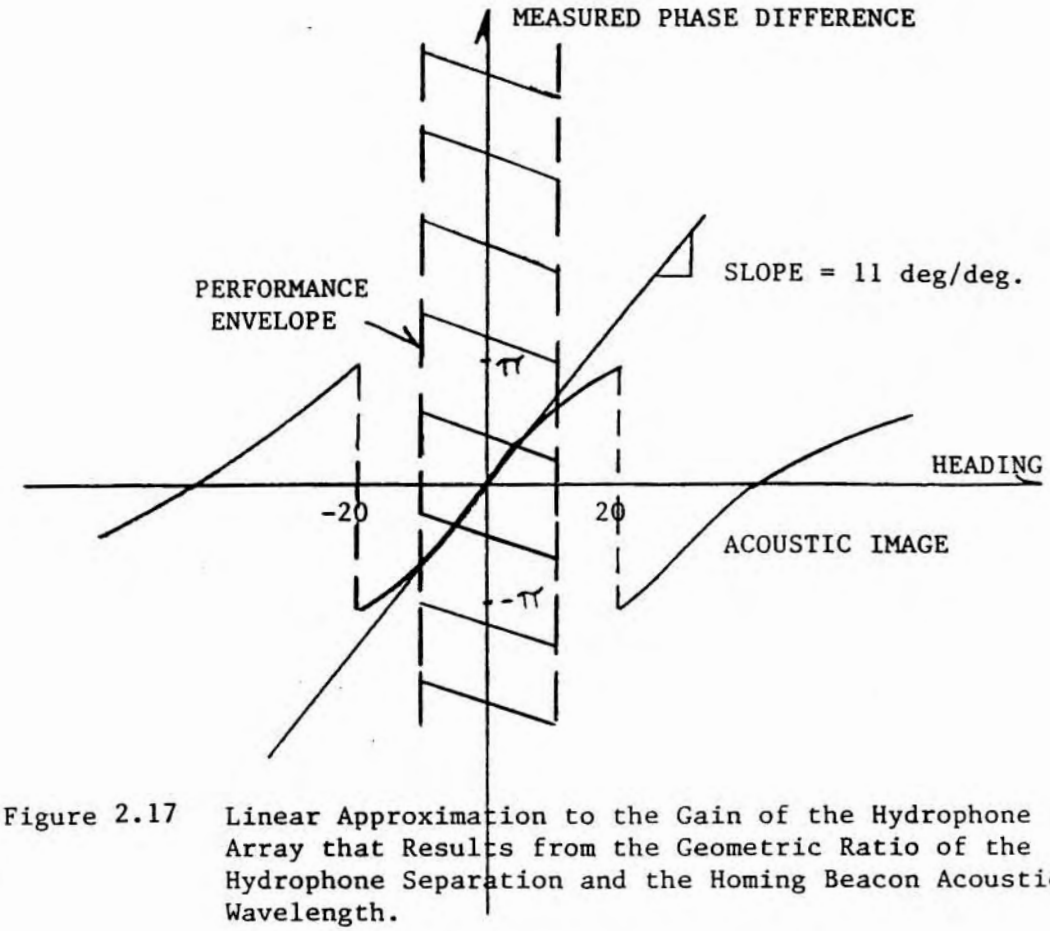

Figure 2.17 Linear Approximation to the Gain of the Hydrophone Array that Results from the Geometric Ratio of the Hydrophone Separation and the Homing Beacon Acoustic Wavelength.

I Required Signal/Noise (S/N) as specified by Phase Resolution Requirements: 57 = 35 dB

II Signal Strength:

1) Source Level:	72 dB/Watt (re 1 ubar)
2) Spreading Losses over 6 Km:	-75 dB
3) Attenuation at 15 KHz	- 9 dB
4) Signal Strength at Receiver:	-12 dB/Watt (re 1 ubar)

III Noise Strength for Sea State 3 (after Wenz): -60 dB/Hz (re 1 ubar)

IV Required Source Strength as a Function of Receiver Bandwidth:

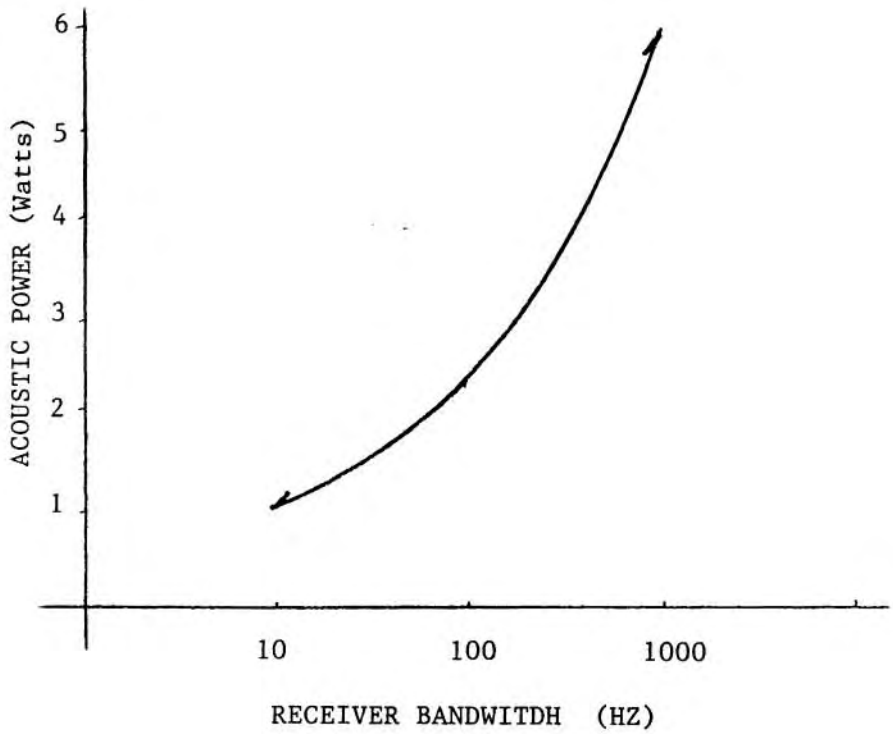

Table 2.2 Signal and Noise Estimates Used to Design the Homing Receivers.

3 THE MECHANICAL ARCHITECTURE OF THE VEHICLE

Figure 3.1 is a cut-away view of the fish that highlights the major mechanical sub-assemblies. These include the hydrophone array, the release mechanism, the main pressure housing, the floatation material, the control surface actuators, and the recovery aids. This chapter describes the principal attributes of these components, compares various competetive approaches to the design of each component and summarizes the advantages and disadvantages of the final design.

3.1 THE HYDROPHONE ARRAY

3.1.1 Geometry.

As discussed in Section 2.5, the hydrophone array consists of four elements made up of two orthogonal sets (two hydrophones for each axis). The hydrophone baseline is the distance separating the two elements in a set. The sensitivity analysis of the homing error outlined in Section 2.6 shows that an increase in the homing beacon frequency or the hydrophone baseline (ie. an increase in the non-dimensional quantity (L_h/λ) will give the most significant reduction in the homing error. Three reasons why these approaches should not be taken too far are:

-the fish cannot physically accomodate a large baseline

-a baseline greater than one wavelength results in false acoustic images. In short, a phase comparator measures phase modulo 360 degrees and cannot tell the difference between 5 degrees and 365 degrees. If these images are outside the operating envelope of the fish (10 degrees off the vertical), then there is an effective gain in the ability to

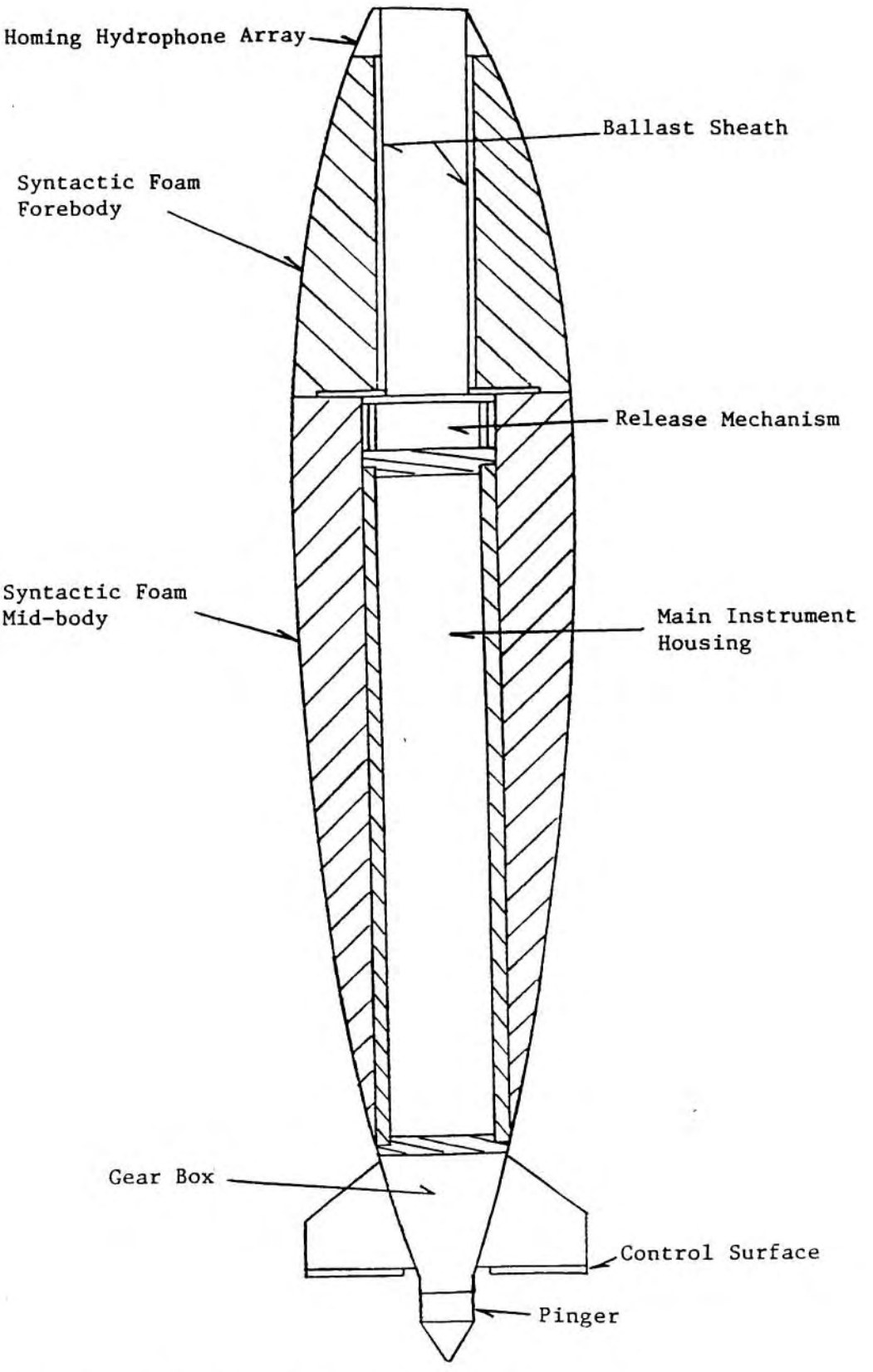

Figure 3.1a Cut-away View of the Flying Fish

Figure 3.1b A disassembled view of the Flying Fish showing 1) the syntactic foam shell (two parts) and 2) the main housing (with gear box attached).

resolve the bearing from the fish to the surface beacon.

-higher frequencies attenuate more quickly in water; thus, for a given signal to noise ratio at the receiver, more acoustic power must be radiated into the water.

The four hydrophones are potted in acoustically transparent urethane in the nose of the fish where flow noise is minimal. The homing beacon is a single tone CW signal at 15 KHz. A printed circuit board molded into the urethane distributes power to the preamplifiers and connects the hydrophone signals to standard high pressure underwater electrical connectors. Flash tubes and trigger transformers are also molded into the piece (see Sections 3.7 and 4.10 for discussion of recovery aids).

The hydrophone baseline is 14.5 cm. This results in a false acoustic image at +/-20 degrees, well outside the operating envelope of the fish and sets the expected phase error (without any averaging) at 1 degree. With this arrangement, both sources of error (hydrodynamics and phase error) should contribute equally to the total homing error, each contribution being of order 1 meter. Figure 3.2 shows the hydrophone array.

3.1.2 Phase Offsets Due to Alignment Problems and Hydrophone Variability.

The hydrophones are cylindrical piezoelectric devices which output a voltage proportional to the ambient AC pressure field. The preamplifier may have some inherent phase shifts which will vary from unit to unit. As long as the phase shift is independent of pressure, temperature, and

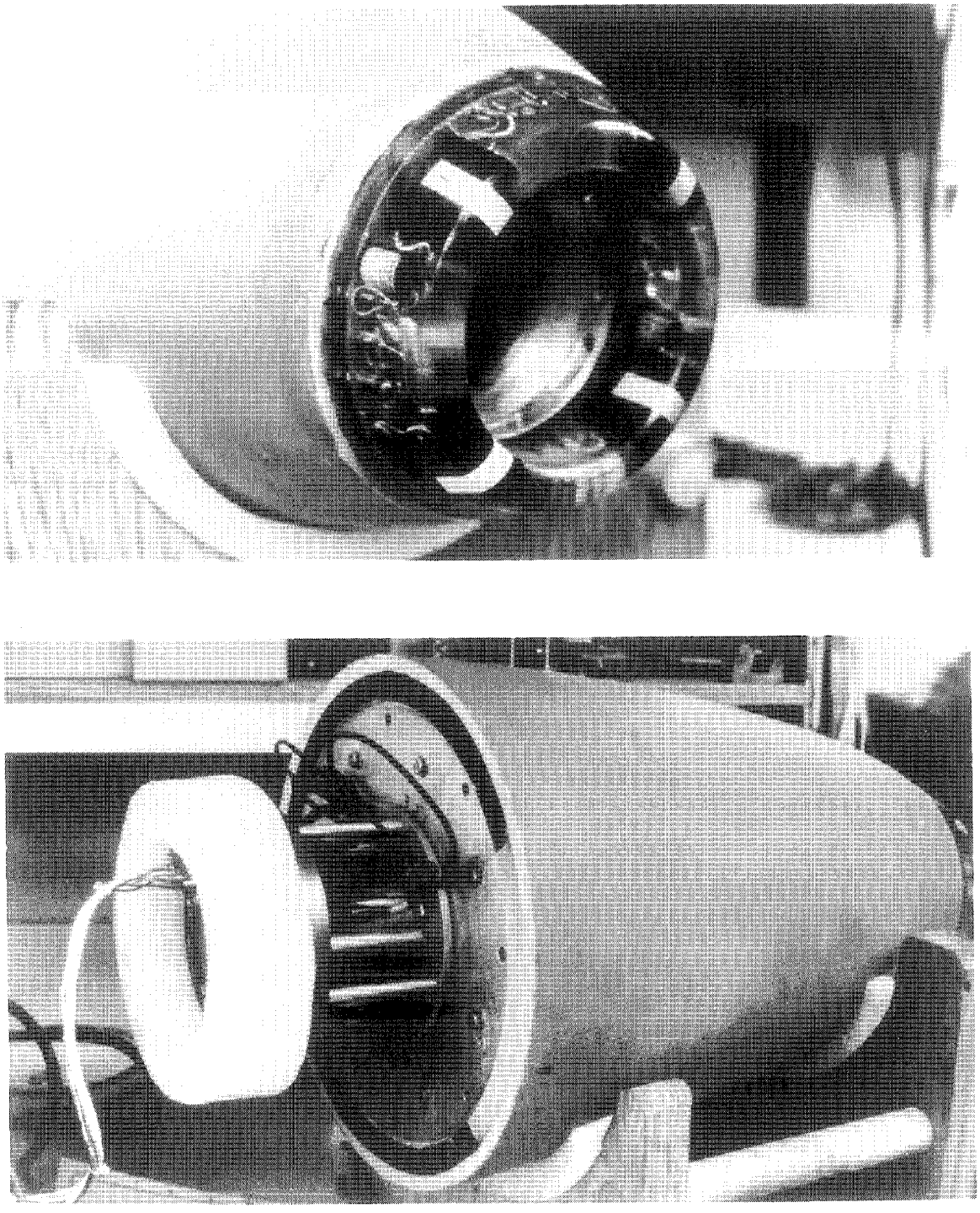

Figure 3.2 Close-up of hydrophone array and Flying Fish forebody.

frequency, a simple additive constant will offset any differences in phase shifts between each hydrophone/pre-amplifier. The phase input to phase output of the hydrophone/pre-amplifier/receiver network must be measured and any offset included in the control algorithm. This phase input/output relationship is discussed in greater detail in Section 4.7 which describes the receiver circuitry.

Simple mechanical alignment is not sufficient to guarantee the phase resolution specified by the hydrodynamic analysis done in Section 2.6. A 0.001 meter misalignment of the hydrophones in the X axis will result in a 5 degree phase error (equivalent to a 0.6 degree heading error). This source of error can be eliminated using the same additive constant that offsets differences in phase shift between hydrophones. There is no simple mechanism to eliminate errors that result from crosscoupling of the Y and Z axes if there is any misalignment in the orthogonality of the two hydrophone axes.

3.2 THE RELEASE MECHANISM

3.2.1 Specifications.

For a gravity driven vehicle, a simple and reliable ballast drop mechanism is essential. The principal attributes of such a mechanism must be:

-The time lag between actuation and drop should not exceed a few seconds. Because of the high speed of the vehicle, imprecise knowledge of the actuation time lag could result in catastrophe. Thus, corroding links and burn wires (typical actuation times of minutes to days) are unacceptable.

-precise control over drop depth; for mid-ocean deployments, depth control should be of order 1 to 10 meters. This precludes the use of rupture disks, relief valves, and other pressure activated devices that have typical tolerances of 5% (in water depths of 6000 meters, this corresponds to a depth control of 300 meters). Because of the simplicity of these devices, they have been used in series with the principal release mechanism as a backup during preliminary testing of the prototype when water depth exceeds the depth of the tests. In hydrographic surveys, a near bottom approach may be desirable and such a backup is impractical.

-easy and safe to re-load. Time between deployments should be kept to a maintenance free minimum. This eliminates explosive bolts which require rebuilding of their seals and are unreliable at depth (in addition, their transport and storage are subject to restrictive regulation).

-failsafe capability. In the event of a malfunction (eg. low battery voltage or a leak in the main pressure housing) the release should have the capability to be over-ridden by backup circuitry and/or mechanism.

A secondary set of considerations includes the ballast geometry (eg. slug, pellets, washer punchings) and the material (lead, mercury, steel). These considerations, though important to the ease of operation and the cost per deployment, were not the governing parameters; the cost of most ballast, when compared with the cost of running a ship, is small regardless of the material and geometry.

3.2.2 The Design of an Electromagnetic Release.

Appendix A.1 describes several viable release mechanisms and a detailed description of the electromagnet that was built into the fish. The major advantage of the electromagnet is its simplicity. With no moving parts, failsafe capability is enhanced. Its major drawback is its power consumption. For the short deployments that are expected (one-way trips to full ocean depth take 15 minutes) this power consumption is acceptable. The magnet was designed to handle the large dynamic loading that occurs during deployment. A pulse-width-modulated drive to the magnet allows the current to be reduced (for energy savings) once the vehicle is below the wave field (approx 100 meters below the surface). An electrical "or" circuit allows any of a number of external signals to override the release command and drop the weight. Under normal operation, a pressure sensor registers a predetermined depth for ballast release. Sub-system failures and a backup timer will result in the controlled abort of a dive (ie. the pinger will change its ping rate and the fish will attempt to home if a beacon is present). An uncontrolled abort will result in the event of power loss. The details of how subsystem failures are recognized and how the backup timer is implemented are discussed in Section 4.2. Because the surface finish of the electromagnet affects its holding power, small polished steel disks that attach to the steel ballast weights are kept in an oily rag until required.

3.3 THE MAIN PRESSURE HOUSING.

The main housing contains the sensor electronics, the hydrophone

receivers, the data logger, the controller, the actuator driver, and the battery/power distribution network (see Chapter 4 for a discussion of the electronic architecture). These electronic assemblies, which occupy 0.02 cubic meters, must be protected from seawater at pressures up to 10,000 psi. Since the size of the vehicle is so closely tied to the weight budget, the main criterion for selecting a housing material and geometry is the strength to weight ratio. Secondary considerations include the number of interconnects required and ease of assembly and disassembly. To keep the number of interconnects small, use of a single housing was desirable.

3.3.1 Conventional Approaches to Deep Ocean Pressure Housings

3.3.1.1 Geometry. Conventional geometries consist almost wholly of spheres and cylinders. Because of their symmetry, spheres provide the best strength to weight configuration. They are in general more difficult to manufacture and it is not always easy to optimize the displaced volume. Cylinders are probably the most common shape of deep sea instrument housings. Though not as structurally efficient as spheres, they are relatively easy to make and, as a rule, less expensive. More complex geometries (eg. ring stiffened cylinders) either lack structural integrity or have more involved analytical solutions to their state of stress, precluding their wide spread use.

For the Flying Fish, a cylindrical housing has one distinct advantage: it can be exploited as a central structural backbone.

3.3.1.2 Material Selection. The three most common materials used to make

deep ocean pressure housings are titanium, glass, and aluminum. Because strength to weight was deemed a critical design parameter, two additional materials were investigated: fiber wound epoxy and alumina. In addition to strength to weight ratios, machinability, corrosion resistance, reliability, and practicality were of major importance. For the prototype, an aluminum alloy housing (7075-T6) was used because the material was inexpensive, readily available, and adaptable to design changes. Second generation profilers could switch to titanium to reduce the potential for corrosion problems with an acceptable cost increment.

3.3.2 The Flying Fish Housing.

The main pressure housing has a depth limitation of 6900 meters. The six inch inner diameter dimension for the housing is an industry standard which was considered desirable since this would increase the number of available sensor systems that could be readily integrated into the profiler. The length of the housing results directly from the payload requirements.

The forward endcap has 18 penetrators, 2 to power the release mechanism, 6 for the recovery flash tubes (see Section 3.7), 6 for the hydrophone-preamplifiers (2 for power, 4 for signal, and 4 spares). In addition, the forward endcap has a built in shuttle valve to allow dry air to circulate inside the housing during battery recharge to prevent the build up of explosive gasses (see Figure 3.3). The aft endcap can accomodate four 12 pin electrical penetrators of which two are reserved for the hydrographic sensors and the other two (for a total of 24 pins) are used to drive the control surfaces (see Sections 3.5 and 4.8). The

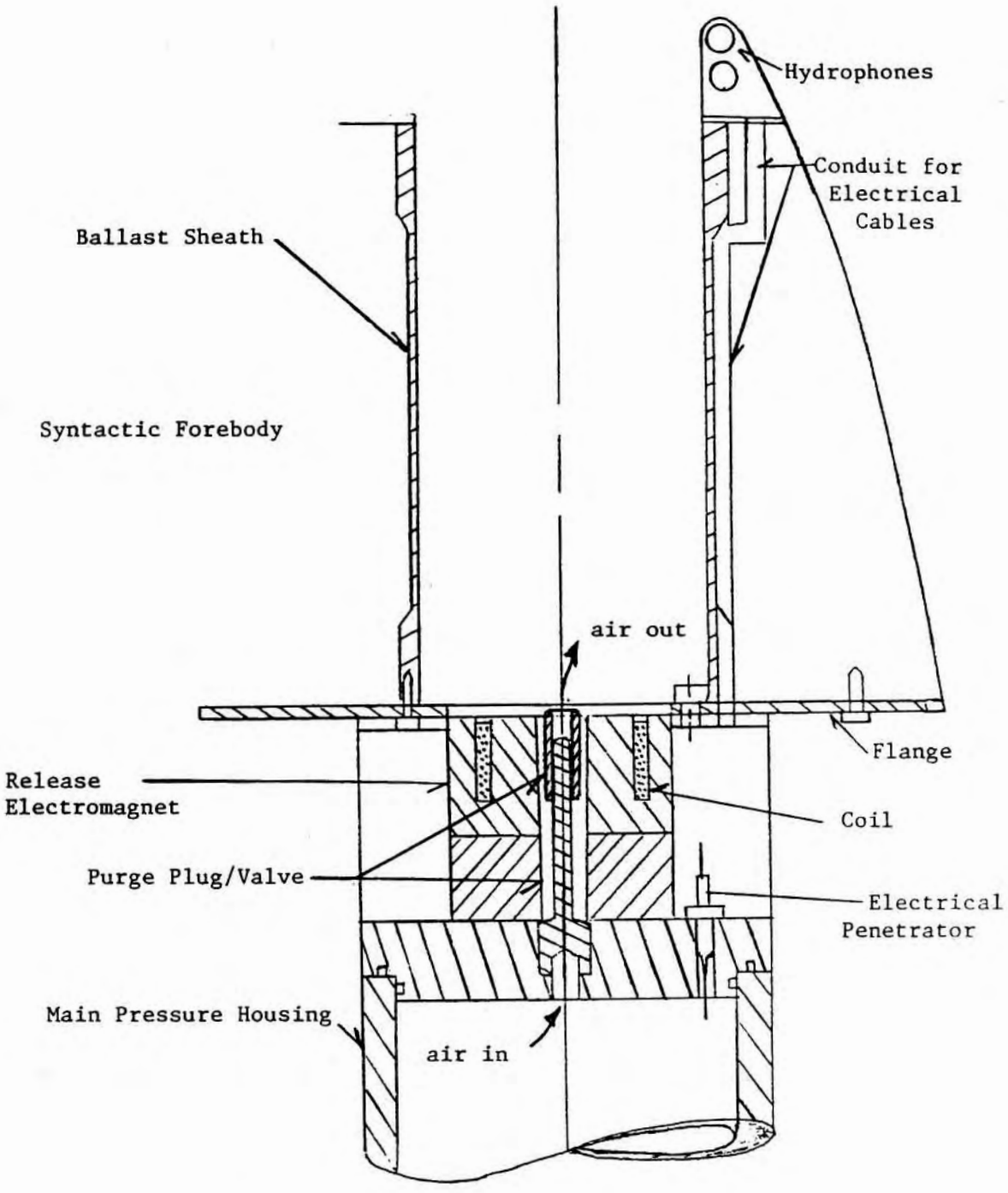

Figure 3.3 Drawing of the Flying Fish Forebody.

final geometry of the aft endcap will change as the mechanical details of the fish/sensor interface are established (beyond the scope of this thesis).

3.4 THE FLOTATION MATERIAL

3.4.1 Approaches to Buoyancy Generation.

Two general schemes for generating buoyancy at depth exist: passive and active. The first method requires no positive change in displacement and is usually accomplished by dropping a ballast weight. This ballast weight must be sufficiently large to overcome the buoyancy of the instrument and to carry it down.. The attractions are: this method is simple, effective, easily actuated, and the results are instantaneous. The second, active, method involves changing the displacement of the vehicle. This can be done either mechanically (eg. with a pump) or chemically (eg. generating gasses which do not dissolve in water). Either approach to actively changing the buoyancy has drawbacks including: (1) no inherent failsafe capability, (2) long actuation time, (3) not easily implemented, and (4) diminishing efficiency at pressure.

The passive approach to buoyancy generation requires materials which have a density less than water yet have the strength to withstand full ocean pressure. For deep ocean flotation, large hollow glass spheres (the largest commercially available glass spheres are 17 inches in diameter) provide the best buoyancy per pound but have several fundamental drawbacks: (1)they are bulky and hard to pack efficiently in a given space. Substantial volume is wasted. (2) If one flotation sphere catastrophically destructs due to a structural flaw, adjacent

spheres tend to implode in sympathy. In such a case, any reserve buoyancy (and the instrument itself) is lost. A composite material, syntactic foam, was developed to provide buoyancy at depth without these drawbacks.

3.4.2 Syntactic Foam.

Syntactic foam is a composite material of glass microballons (typically 200 microns in diameter) embedded in an epoxy resin matrix. The resin has a specific gravity 1.3, the composite material has a specific gravity between 0.4 and 0.6 depending on the hydrostatic pressures expected. The buoyancy results from the volume displaced by the glass spheres. Ideally, the hydrostatic stress is shared by the glass spheres and the resin. The mixture can be cast and machined without adversely affecting the structural integrity of the bulk material--a property which is ideal for prototyping where changes are made on a day to day basis and patches can easily be made in the field. If a structural failure of the composite occurs, it is not catastrophic. Instead there is a long term degradation of the material that is a function of the number of cycles and the ambient pressure during each cycle. For the Flying Fish, where several dives/ day are expected, this degradation can be monitored by recording the ascent rate (as measured by the pressure vs. time).

Syntactic foam is generally cast in one cubic foot blocks (1 X 2 X 1/2) which are subsequently glued together and machined to shape. For the Flying Fish, this approach would result in 70% wastage of the block material. For this reason, cast to shape syntactic was pursued. Patterns

and molds for the prototype were made in house; the casting was done by an outside contractor. The final result was a slightly heavier foam (a specific gravity of 0.59 VS. 0.56 for block material).

3.5 THE CONTROL SURFACE ACTUATOR.

3.5.1 Background.

A control surface is designed to induce an attitude change in the main fuselage by developing a relatively small lift force at some distance from the center of gravity (CG) of the body. Control surfaces may be located either forward or aft of the CG but any surfaces forward of the CG will contribute to static instability. Figure 3.4 schematically shows the major components in the control surface actuator. These include: (1) the control surfaces; (2) the motors; (3) the gear train; (4) the opto-interruptors; and (5) the pressure compensator. The role that each component plays in the system design is described below.

3.5.2 The Control Surfaces.

Control surface actuators belong to one of two broad categories: (1) those that generate lift with changes in camber and (2) those that generate lift with changes in angle of attack. Several interesting actuators, which are impractical in the present application, belong to this category: bladders (in which fluid is pumped from side to side); bimetallic strips (in which heat causes differential expansion). The second category includes actuators in which all or part of the control surface pivots around an axis orthogonal to the flow field. Full flap

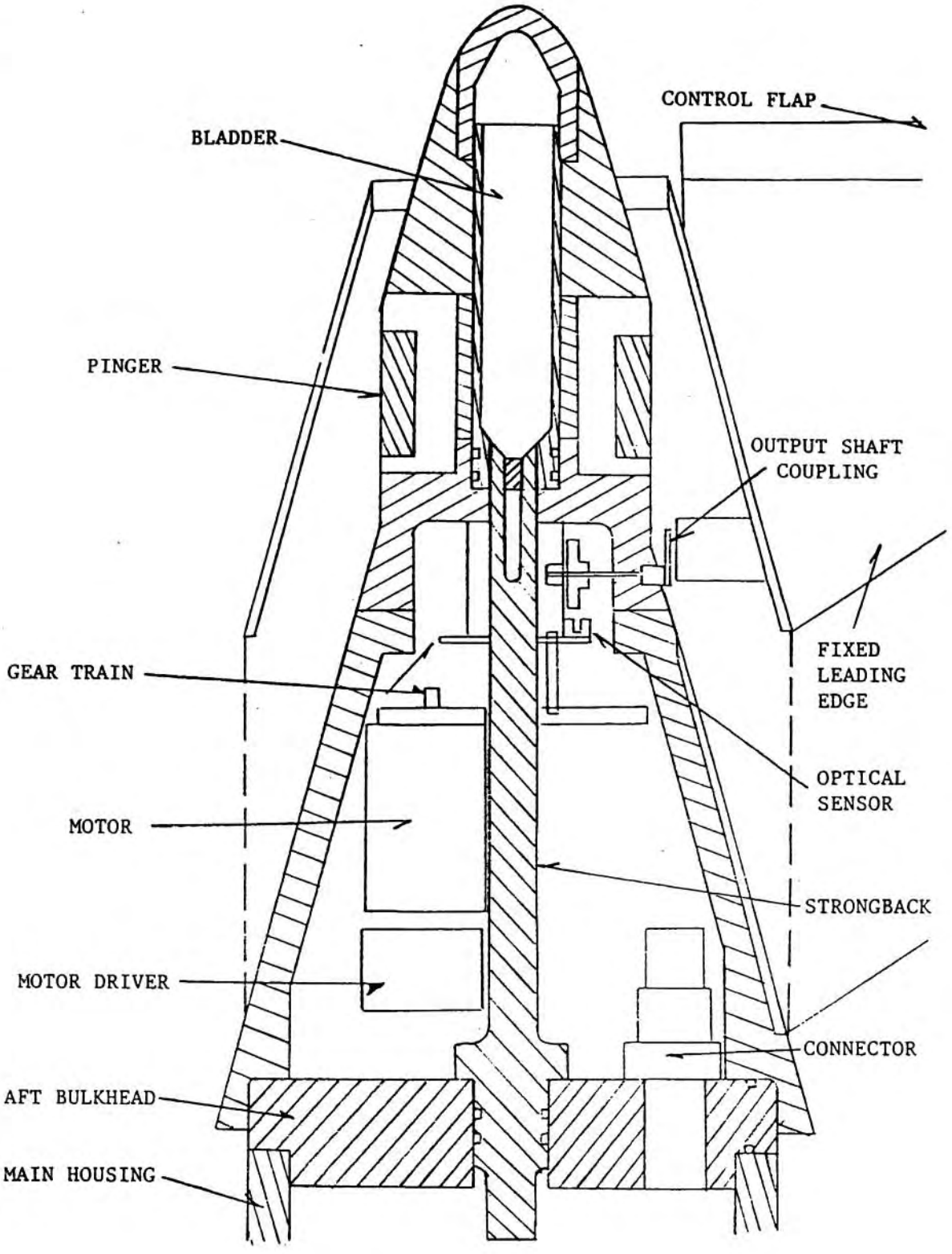

Figure 3.4 Drawing of the Flying Fish Stern Gearbox Sub-assembly with Exploded View of Control Surfaces.

controls are more efficient lifting surfaces (Fehlner, 1951) but are more susceptible to damage because the entire control flap is cantelevered. The partial flap control surface appended to a fixed leading edge can be modelled as a fully movable flap of reduced efficiency. This reduced efficiency, and the corresponding hydrodynamic model, were discussed in Section 2.6.

For applications where the direction of desired lift is known in advance (eg. an airplane wing), both camber and angle of attack may be exploited to generate lift. For applications in which the direction of desired lift is unknown (eg. a rudder), the control surface must be symmetrical.

For the Flying Fish, a partially movable hinged flap attatched to a fixed cruxiform/annular wing was chosen for structural integrity. The 2-Dimensional NACA 0012 foil shape was chosen for its lift and stall characteristics which are described in detail in Section 2.3.2.

With the flap and wing geometry fixed, the next step in the actuator design is to quantify the hinge moment, and specify the actuator torque requirements. The data describing the hinge moment was generated from wing tunnel tests conducted during the 1940's (see Bibliography).

3.5.2.1 Predicting the Hinge Moment

The hinge moment is generally calculated using wind tunnel tests because the strong influence of the boundary layer is neglected in 2 dimensional lifting line theory. The variables with a strong influence on the assessment of the hinge moment include: (1) the angular deflection of the flap; (2) the speed through the water; (3) the ratio of

the total chord to the flap chord; the shape of the leading edge of the flap; (4) the gap between the fixed and movable portions of the fin; (5) and the hinge point. The actuator is typically designed for the maximum static moment produced at steady flow since these values are not exceeded in normal manuevers (Fehlner, 1951).

3.5.2.2 The contribution of angular deflection, speed, and flap geometry to the hinge moment.

To keep hinge moments to a minimum (which was crucial in World War I when hydraulic actuators were unknown and the pilot provided the actuator force), the control surfaces are often balanced by putting the axis of rotation near the chord center of pressure. This center of pressure is a function of aspect ratio, angle of attack, and geometry (Fehlner, 1951; Abbott and von Doenhoff, 1959; deYoung, 1947). The center of pressure is near the 25% chord for high aspect ratio wings and as high as 45% chord for low aspect ratio wings (Weinig, 1947). Figure 3.5 gives the pertinent hinge moment data for the NACA 0012 profile with a 30% chord flap. The bibliography includes extensive data showing the additional degradation in performance resulting from a gap between the fixed leading edge and the flap.

For the Flying Fish, the speed and flap geometry have already been fixed. Thus the maximum hinge moment, as shown by Figure 3.5, is given for an angular deflection of 15 degrees. The maximum hinge moment is approximately 120 in-oz.

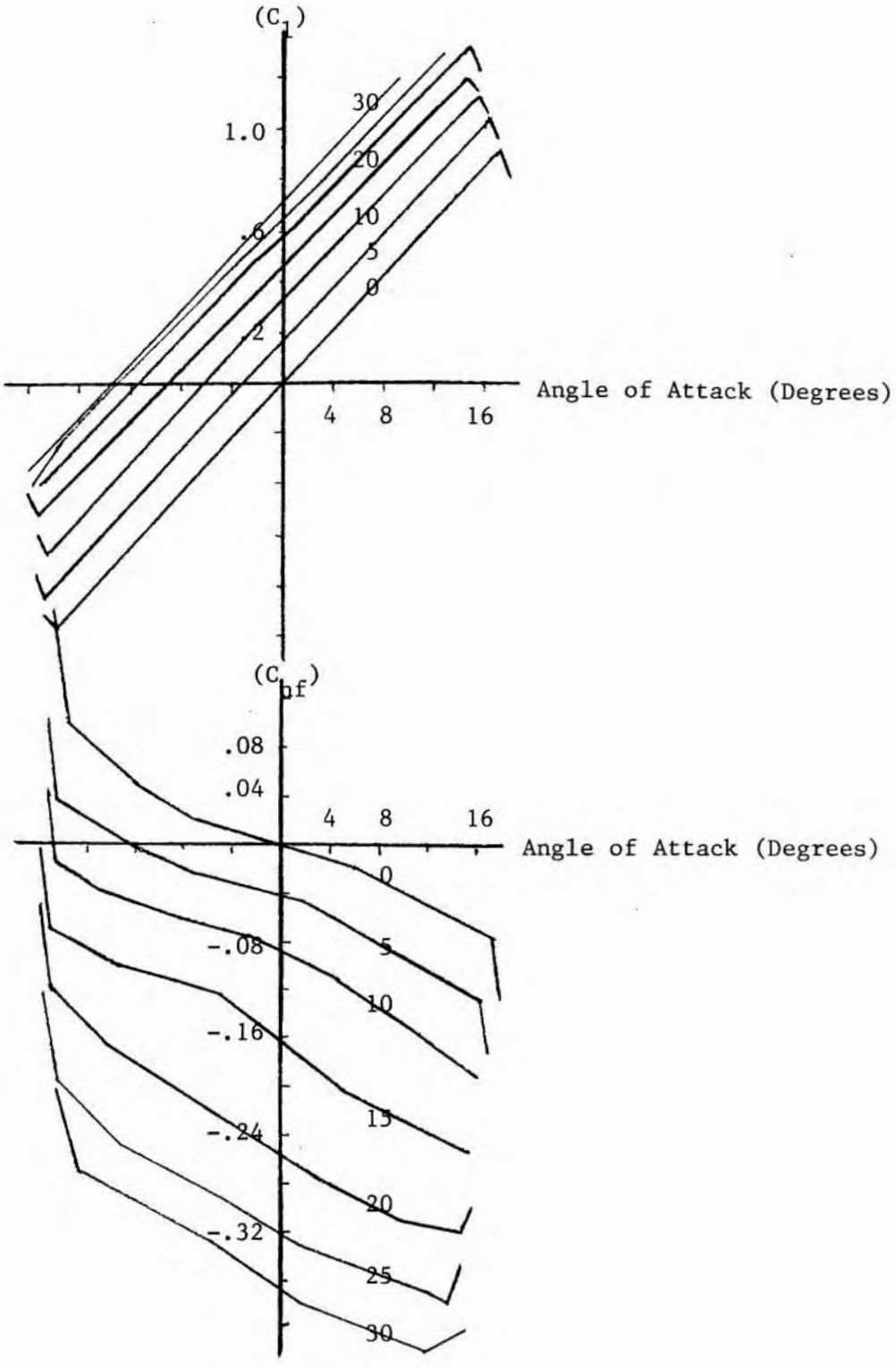

Figure 3.5 Non-dimensional Hinge Moment and Lift of a 30% Control Flap on a NACA 0012 Foil with No Gap (after Garner, 1944) Plotted for Various Flap Deflections as a Function of Angle of Attack.

3.5.3 Motor Selection.

Choosing motors for deep ocean applications involves more than the usual torque vs speed considerations: (1) the corrosive environment and (2) the high ambient pressures, are additional constraints. Standard shaft seals cannot withstand large pressure differentials, and must be used only in pressure compensated systems. Magnetically coupled motors have the advantage that the windings can be in air at atmospheric pressure but eddy losses in the pressure bulkhead are unacceptable when the motor is designed to withstand 10,000 psi. ambient pressure. Pressure compensated motors can be designed to run in high pressure gas (which requires a large reservoir) or liquid (which gives rise to parasitic drag). The fluid must lubricate and have relatively low viscosity. Brush commutated motors, when run in oil, produce carbon grit which destroys bearings and results in a short mean-time-to-failure. Stepper motors address the above considerations and are well suited to digital drive circuitry. They are, however, grossly inefficient for servo motor applications. Their torque vs speed characteristics (see Figure 3.6) force the designer to size the motor based on a worst case analysis which results in a large, heavy, power hungry actuator.

Brushless DC motors with rare earth magnets have the best mechanical attributes (power to weight ratio; power to size ratio; see Figure 3.7) but are electrically more complex to control and require a greater number of electrical penetrators. This added complexity is more than offset by two outstanding benefits: the Hall Effect sensors used to commutate the windings can be exploited as (1) position and (2) velocity feedback sensors to be used in the motor control algorithm. Specifically, the two

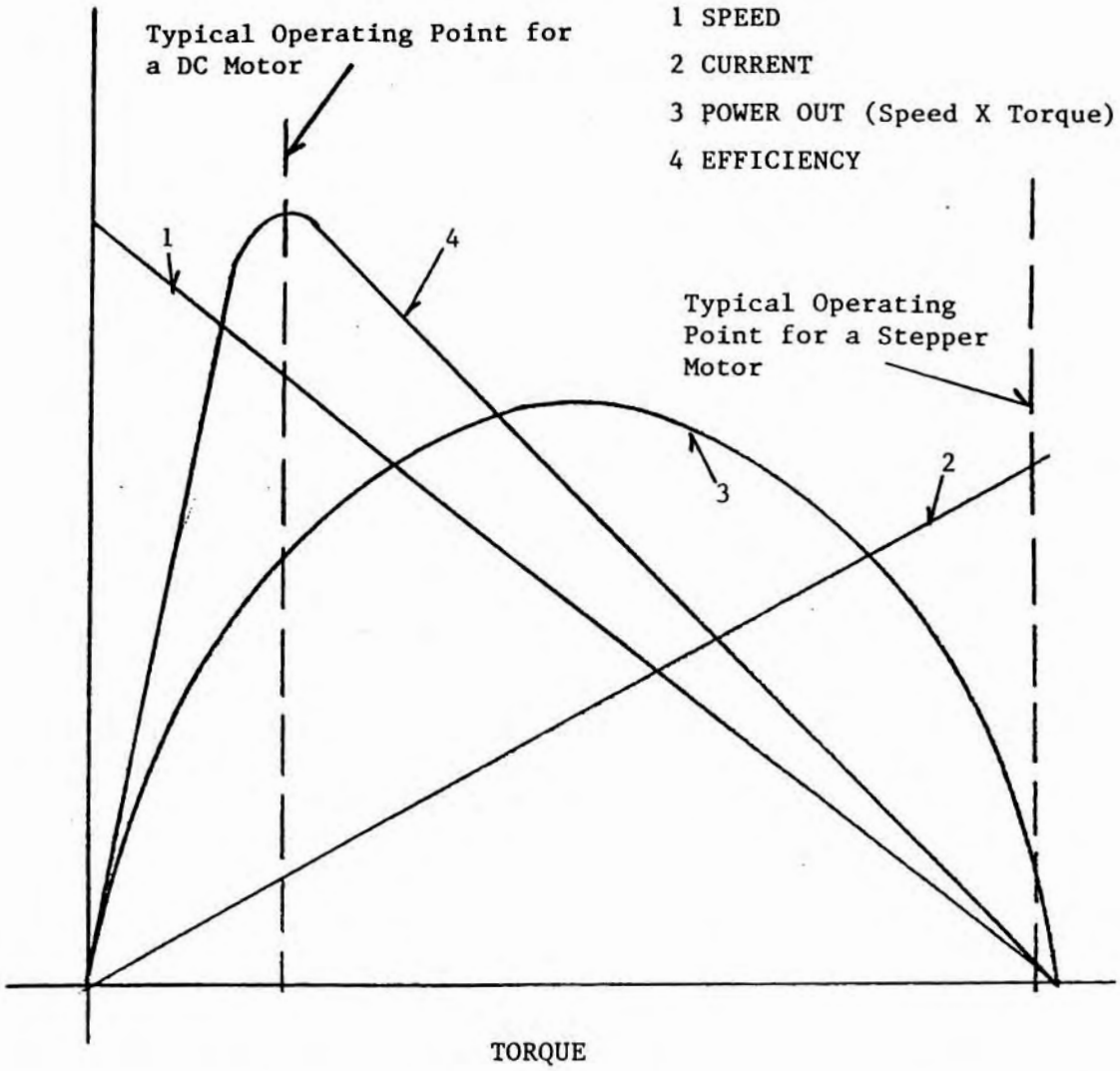

Figure 3.6 Idealized Motor Characteristics as a Fixed Drive Voltage. Note: Efficiency is defined as (Speed X Torque)/(Voltage X Current).

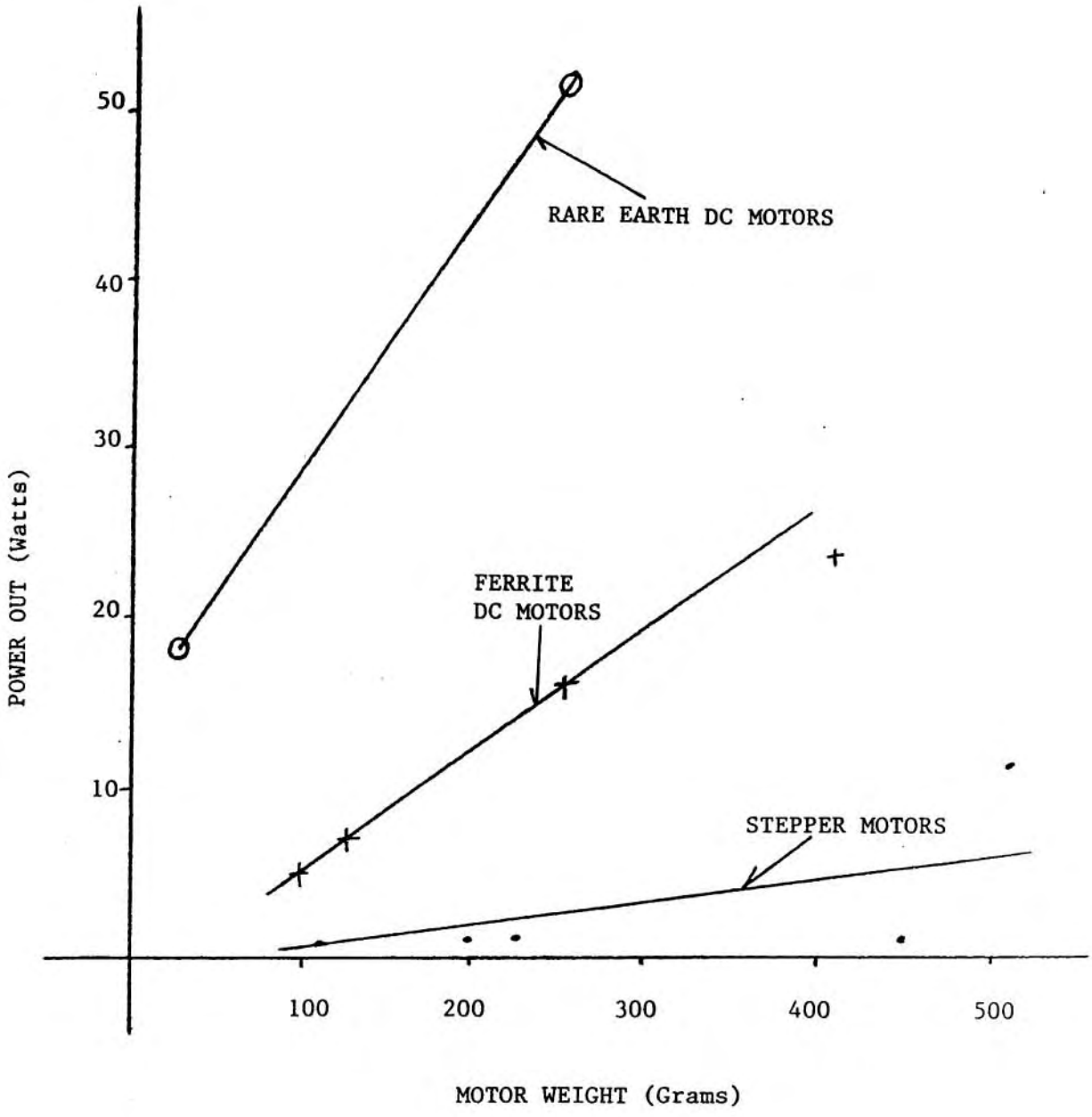

Figure 3.7 Maximum Power Out as a Function of Weight for Several Motor Types (taken from Manufacturers Data Sheets).

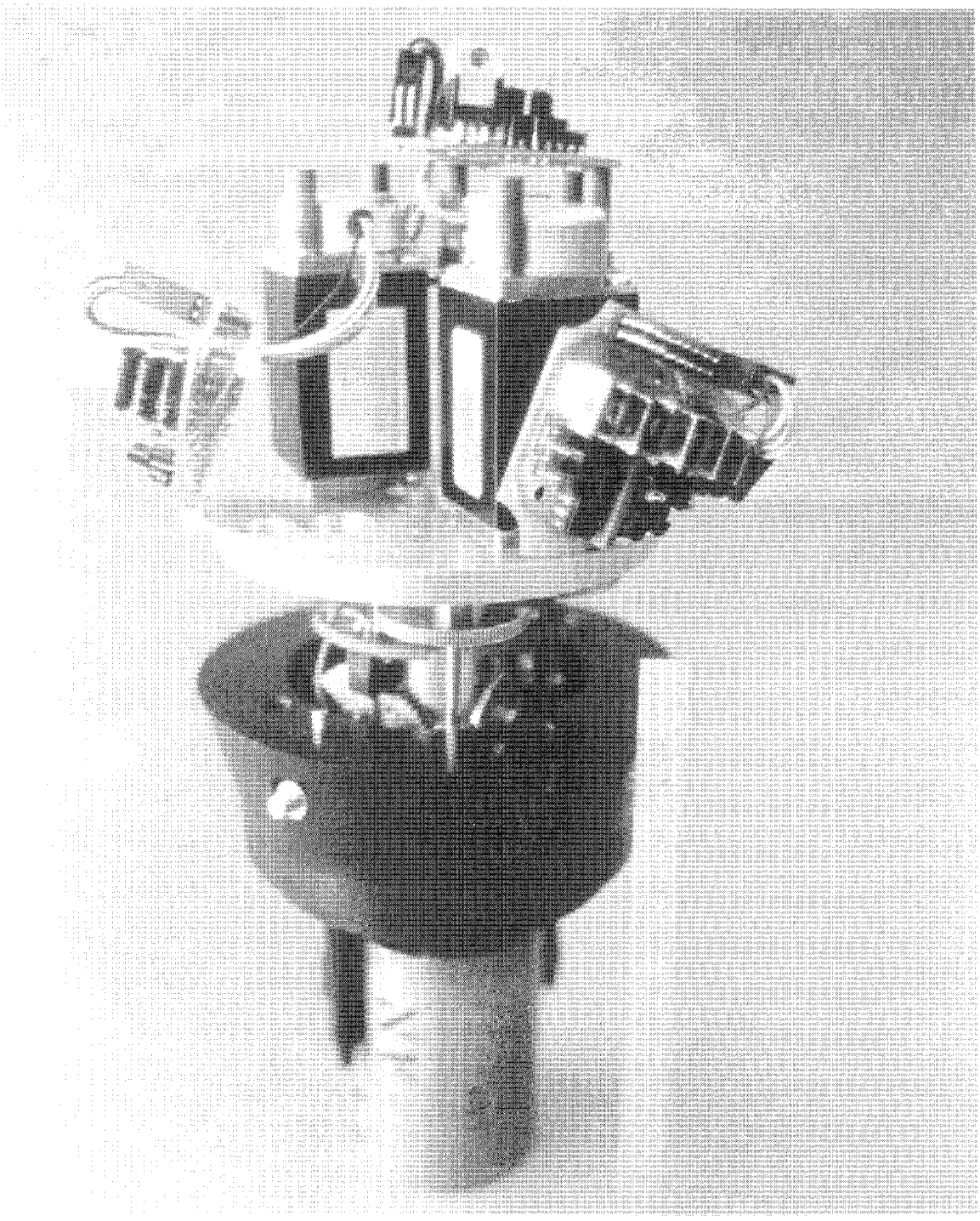

Figure 3.7 The stern mounted gear box: 1) Motor driver; 2) Brushless D.C. motor; 3) Gear train; 4) Optical interruptor; 5) Output shaft; 6) Electrical penetrators to the pinger.

Hall Effect signals are two 5 Volt logic signals in quadrature. Thus, by looking at the sign of one signal on the rising edge of the other, one can tell the direction of the shaft rotation. If an independent means of initializing a counter is used (see Section 3.5.5 below), then pulses from one Hall Effect signal can be used to increment or decrement the counter depending on the direction of the shaft rotation. This counter acts as a position encoder where the resolution depends on (1)the number of windings in the motor and (2) the gear reduction. Similarly, if the duration of the pulse is measured, the rate of rotation of the shaft can be calculated.

The number of bulkhead penetrations was minimized by placing the drive electronics in the oil filled gear box. No failures have resulted from subjecting the drive electronics to high pressure. The motor controller is a single chip microcomputer discussed in detail in Section 4.8.

The effects of parasitic drag resulting from running the motors in 20 cps silicone oil are shown in Figure 3.9. Roughly 20% of the motor efficiency is lost due to fluid drag between the stator and the rotor when run at no load (worst case).

3.5.4 The Gear Train.

The principal considerations involved in designing the gear train for the Flying Fish included: (1) the desired output torque, (2) the speed of response, (3)the least count of the control flap, (4) size, (5)efficiency, and (6)mechanical stops which prevent self-destruction during testing.

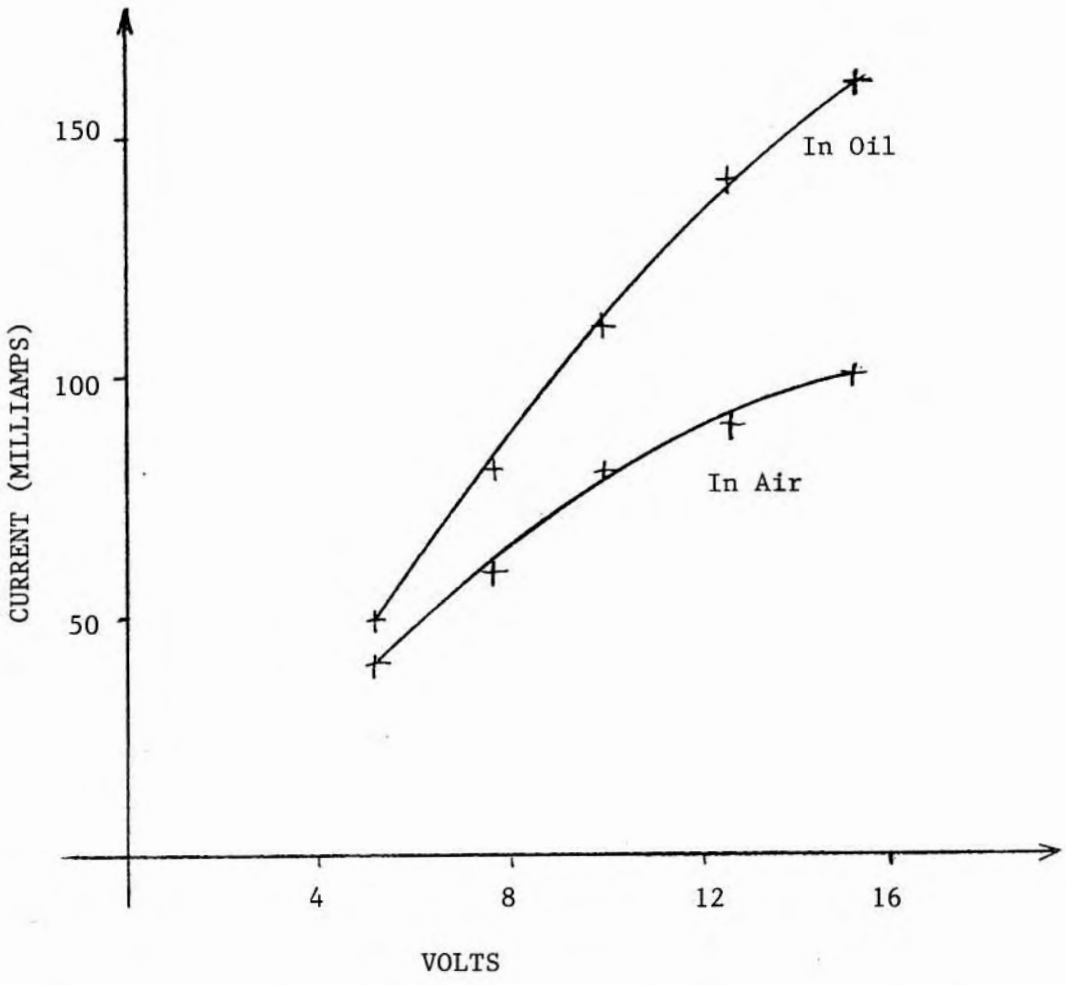

Figure 3.9 Quantifying the Viscous Losses Resulting from Running a 10 Watt Brushless Motor in Silicone Oil (200 Cps.) with No Load.

The control surface actuator torque is specified by the hinge moment coefficient described above. For the Flying Fish, the worst case torque is 120 in-oz. The motor output at stall is about 4 in.oz. with 28 Volt battery.

The least count sensitivity as determined by the hydrodynamic considerations outlined in Section 2.4 should not be less than 1 degree. Thus, for a motor which steps 180 degrees betweens windings, a minimum gear ratio of 180 is necessary.

The final design consists of a 500:1 gear reduction to provide a stall torque of 2000 in.oz. The least step count is 0.3 degrees. A worm drive was chosen as the final output gear because it is compact, provides a large reduction,and is a right angle translation. The inherent inefficiency of a worm drive is a desirable trait in as much as it is not backdrivable and the power to the motor can be turned off once a set points is reached.

3.5.5 Auto centering opto-interruptor.

An independent sensor for centering the fins was deemed desirable for startup and failsafe reasons. This one bit position sensor is an optical interrupt located on the output shaft. Figure 3.10 shows a schematic of the output shaft, complete with interruptor, worm gear, and mechanical stop. The interruptor is positioned so that a logical transition (from light to dark) occurs when the fins are centered.

In addition to helping during the initialization process, the interruptor output can be used as a diagnostic to monitor gear slippage. Every time a logical transition occurs on the optical

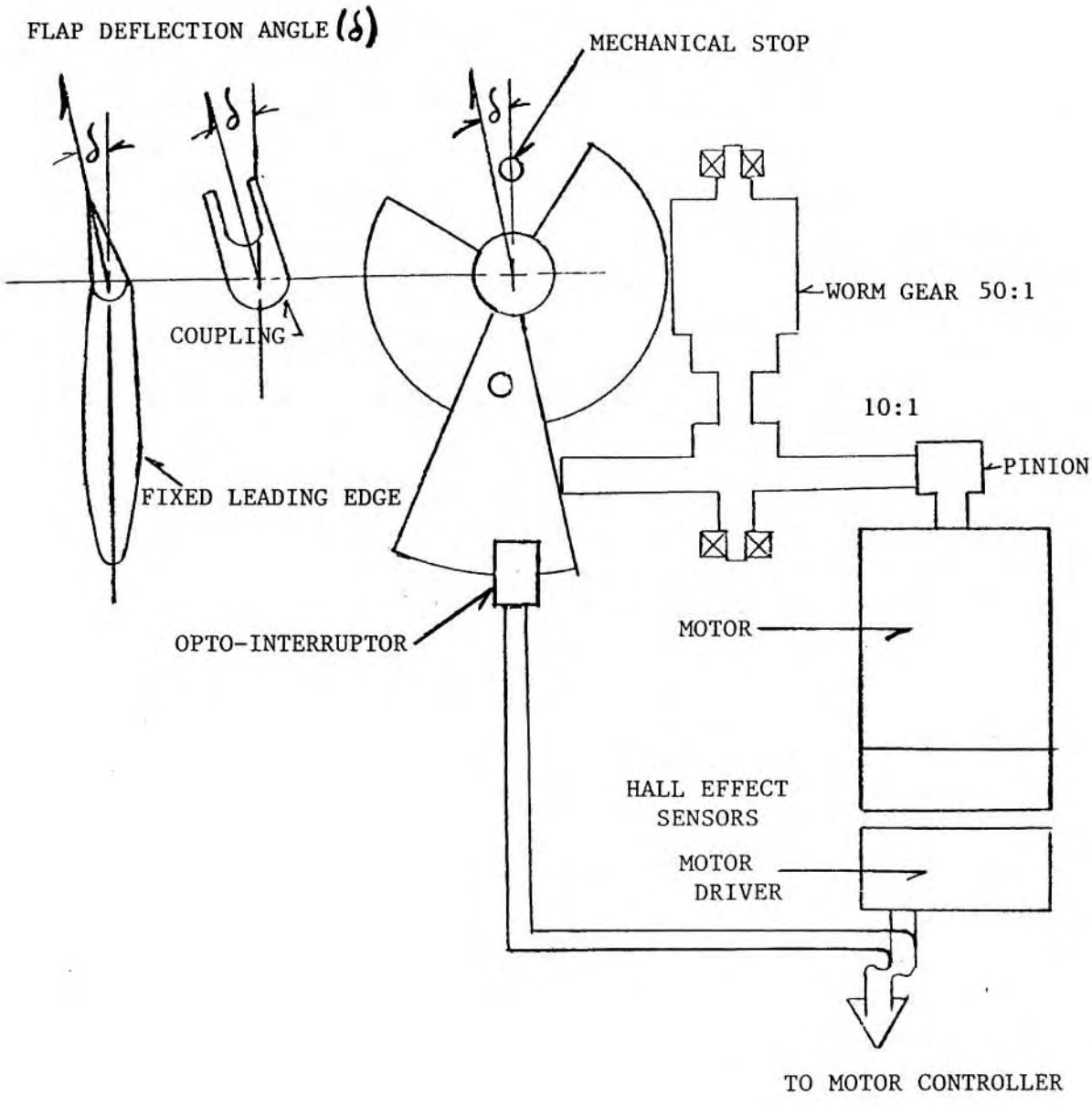

Figure 3.10 Drawing of Control Flap Actuator for the Flying Fish.

interruptor, the present position of the shaft is compared with the ideal center value. If the discrepancy is within an acceptable deadband, no gear slippage has occured.

3.5.6 Pressure Equalization.

The motor/gearbox assembly was designed to run in a silicone oil at ambient pressure. A diaphram was incorporated into the strongback running through the center of the gear box to accomodate differences in compressibility between the oil and sea water. The change in volume due to pressure and temperature effects can be as great as 10% of the gearbox housing volume.

3.5.7 Output Shaft Alignment.

The strongback running through the center of the gear box could, under load, deflect sufficiently to affect the alignment of the output shafts. For this reason, the entire gear box floats inside the housing. Alignment with the tail fin control surface could not be maintained due to tolerance limitations in the casting of the tail fin assembly. A flexible coupling between the actuator output shaft and the flap was designed to accomodate this potential for misalignment.

3.6 THE TAIL FIN ASSEMBLY.

For structural and handling reasons (see Section 2.3.2), an annular foil was chosen to provide the desired hydrodynamic stability. To support this structure and provide the desired control a rigid leading edge with movable flaps was chosen despite the better performance of

all-movable flaps. For reasons of simplicity in actuator design, an unbalanced aileron was chosen. The theoretical hinge moments as a function of deflection angle for this flap were used to determine the motor/gear train output torque requirements. The fin shape and size are discussed in Section

The tail fin assembly is by far the most vulnerable part of the fish. For this reason, it is a separate casting that can be replaced in the field without opening the gear box. The flaps are an integral part of the casting. Because of the large dimensional tolerances of such a casting, it is imperative that the actuator output shaft need not be colinear with the flap hinge in order for the control surface to be operable. Figure 3.10 shows how the output shaft and the hinge are decoupled. Any misalignment results in a small and acceptable amount of sliding between the shaft and the flap. Figure 3.11 shows the cruxiform being removed from the gear box.

3.7 DEPLOYMENT AND RECOVERY AIDS.

Though the vehicle is intended to maneuver to the ship, it will on occasion be unable to do so (no signal at the acoustic receivers, failed motor windings, software glitch, etc.). To monitor fish progress during deployment, a 10 KHz pinger located in the tail of the fish allows the ship to track the range and bearing to the fish. Special ping sequences have been established to signify key operations such as ballast release. Should a problem arise, the master controller can abort the dive by dropping the weight. The default condition for the vehicle is to center the control surfaces and head straight up (actually a small spin

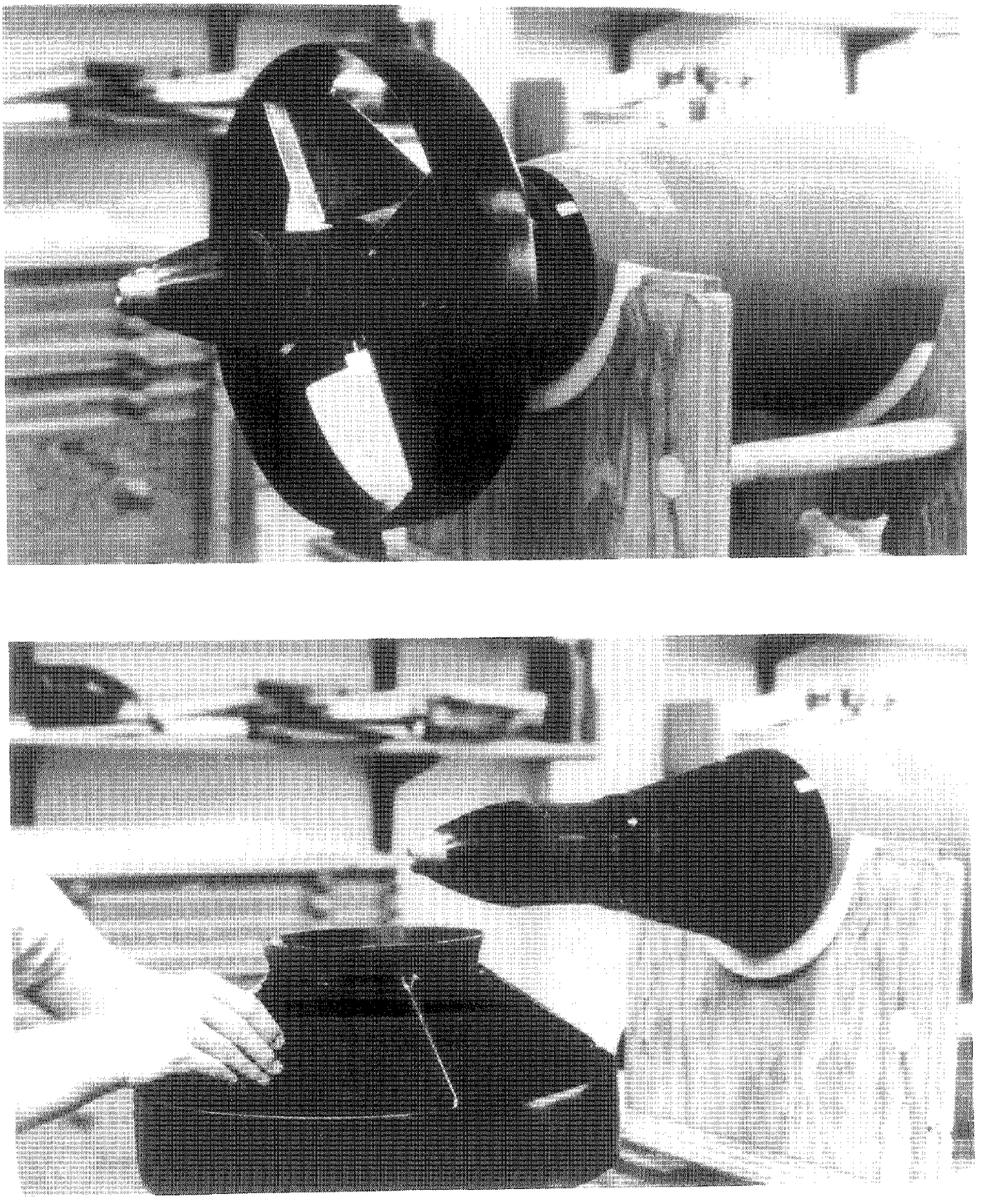

Figure 3.10 Stabilizing fins and control surfaces are removable without disassembling the motor housing and gear box.

is induced to take out any tendency to glide in a particular direction). Should this happen, recovery aids are essential. Several such aids have been built into the fish: (1)two strobe lights are faired into the forebody of the fish and (2)the fish is painted fluorescent orange. The strobes and reflective paint are intended to increase the visibility of the fish once it has reached the surface.

IV ELECTRONIC ARCHITECTURE

4.1 THE IMPACT OF THE SCIENTIFIC MISSION ON THE ELECTRONIC DESIGN.

Like the mechanical design of the fish, the design of the electronic circuitry which governs the data collection and controls the vehicle homing is constrained by the scientific mission. These requirements are summarized here:

4.1.1 The Data Volume.

During operation, two types of data will be collected by the fish, raw scientific data and engineering data. The scientific data will consist of (nominally) one to ten meter vertical averages of conductivity, temperature, and depth and totals about 200 KBytes per deployment. The engineering data will be used to monitor failures and long term degradation of the fish and consists of vehicle attitude (yaw and pitch), control effort (time history of control flap deflections), ascent rate (to measure changes in vehicle buoyancy), and key system voltages and currents (eg. battery condition). These data need not be collected as often and storage requirements can be as low as 50 KBytes. Thus 256 KBytes will be adequate for all data logging requirements.

4.1.2 The Time Between Deployments and the Data Transfer Rate.

The minimum time required between deployments should not exceed the time it takes for a ship to go from one hydrographic station to the next (of order one hour). Thus, the fish must be able to discharge a complete data set (256K Bytes) and be ready for another deployment within one hour

of recovery. This requirement was used to define the data transfer rate between the fish and the shipboard computer and establish the communications protocol. If one includes a communications overhead requirement of 100% (for handshaking purposes), and assumes serial data communication, a minimum of a 4800 Baud communications link is required to meet the one hour data transfer time. To ease interfacing problems with commercial sensors and not restrict the type of shipboard computer used, the choice of electrical interface was restricted to IEEE standards.

An additional set of engineering data can be generated between deployments when the fish is exercised by the deck computer (the details of this are beyond the scope of this thesis). This data will be able to monitor degradation of the hydrophones and will amount to an additional 100 kBytes. To allow for this added self-test capability, the serial communications link was increased to 9600 Baud.

4.1.3 The Time Between Deployments and the Choice of Battery Chemistry.

The short turn around time specified by the scientific mission affects not only the choice of communications interface, but the selection of battery chemistry. If primary (non-rechargeable) cells are used, a simple method is required to monitor their energy storage and to replace them when necessary. Secondary (rechargeable) cells have lower energy density ratios but need not be replaced on a regular basis. The detailed battery selection is discussed in Section 4.11.

4.1.4 Support Systems and Infrastructure Requirements.

The fish should be usable by two members of an operations team with a minimum of training or support infrastructure. To achieve this goal, the complexity of the electronic hardware must be transparent. This transparency must cover three areas: (1)use, (2)maintenance, and (3)repair. Traditionally, oceanographic measurements have been somewhat successful in addressing ease of use, but maintenance and repair have required substantial infrastructure in the form of highly trained people to support equipment both prior to and during large oceanographic experiments.

To attack this problem, a modular electronic architecture, in which each module is built around a micro-processor, was pursued. The benefits of this architecture are two fold: (1) each processor, in addition to performing a core function within the fish, can perform a number of self-test algorithms to help isolate a fault, and (2) once the fault is found, the module can be replaced as a single entity without affecting other components within the fish. These modules were tied together with a standard communications protocol so that additional modules and sensors can easily be interfaced. Each intelligent subsystem is capable of being interrogated and controlled by external hardware (eg. the main cpu or the deck computer)or by the operator.

4.2 THE DESIGN PHILOSOPHY: SYSTEM OVERVIEW

Figure 4.1 shows the Flying Fish surrounded by the required shipboard support equipment. This support gear, which was designed in parallel with the fish (and is formally beyond the scope of this thesis)

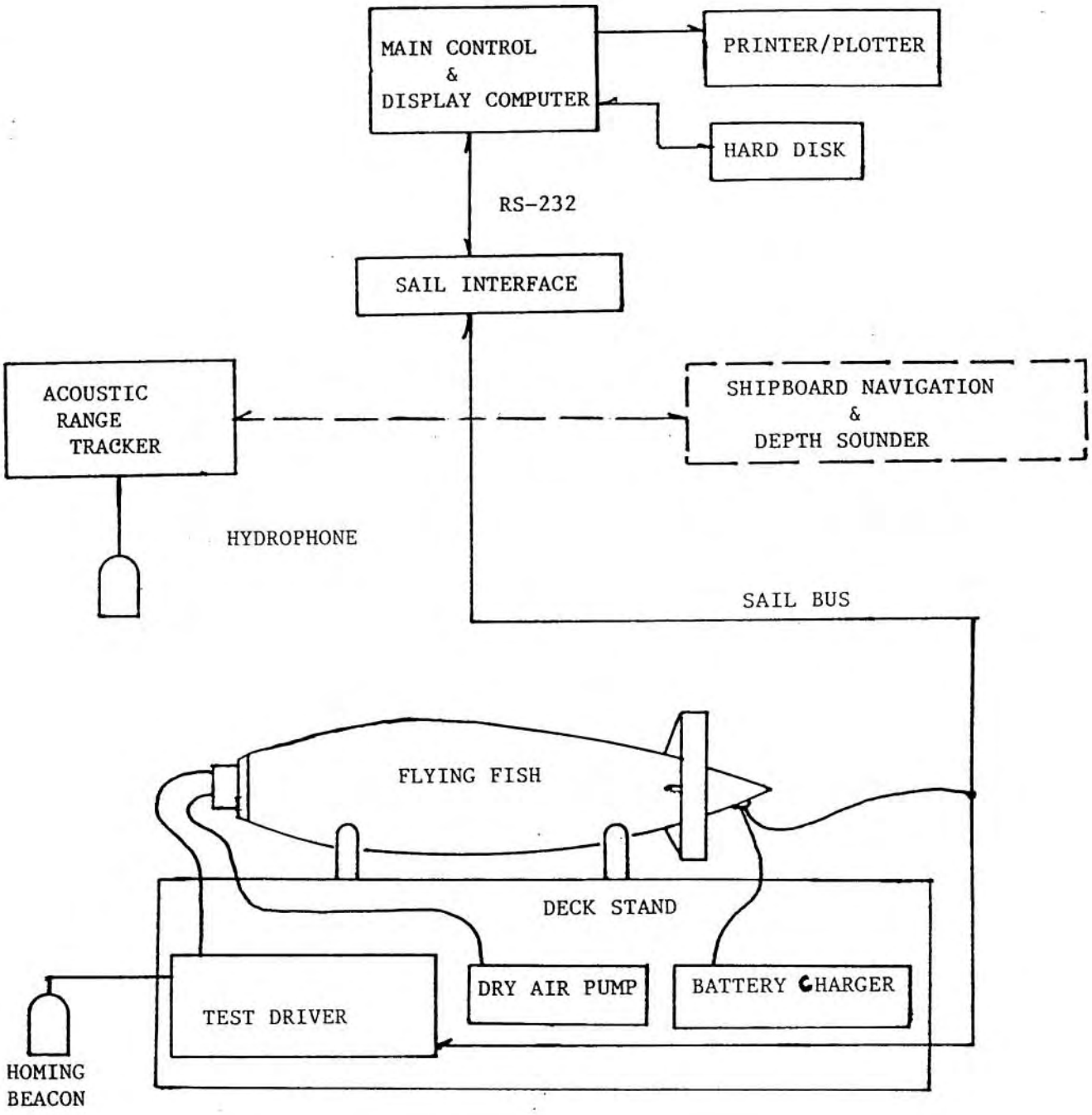

Figure 4.1 Schematic of major shipboard system components. Dotted lines show potential for automation.

is of a stand alone nature. The dotted lines show the potential of tying this equipment together with a serial communications network to enhance system automation.

Figure 4.2 shows the major electronic sub-assemblies of the Flying Fish. These include the main data logger, the receiver, the phase comparators, the motor drivers, the ballast release, the pinger, and the recovery flashers. The resulting architecture includes eight microprocessors aboard the fish. These processors are arranged in a hierarchical fashion.

Although all the processors are executing assembly code at roughly the same speed, each level in the hierarchy is performing a function that can be characterized by a time constant. For example: The main data logger interfaces to the shipboard computer and controls the overall system (turning on/off sub-systems, dropping the ballast, logging data, etc.) on time scales of minutes. The lowest level in the hierarchy is made up of the "end effectors" that actually measure the phase differences, run the motors, and drive the pinger. The characteristic time scale on this level ranges from 0.1 to 0.002 seconds.

Between each level in this hierarchy is a communications protocol which serves several purposes:

-To transfer data from one level to another. Data transfer between two processors running asynchronously and connected by a limited bandwidth communications link gives rise to several interesting problems which are discussed below.

-To signify a sub-system failure. Sub-system failure can occur either during testing or during a deployment. In either case, some

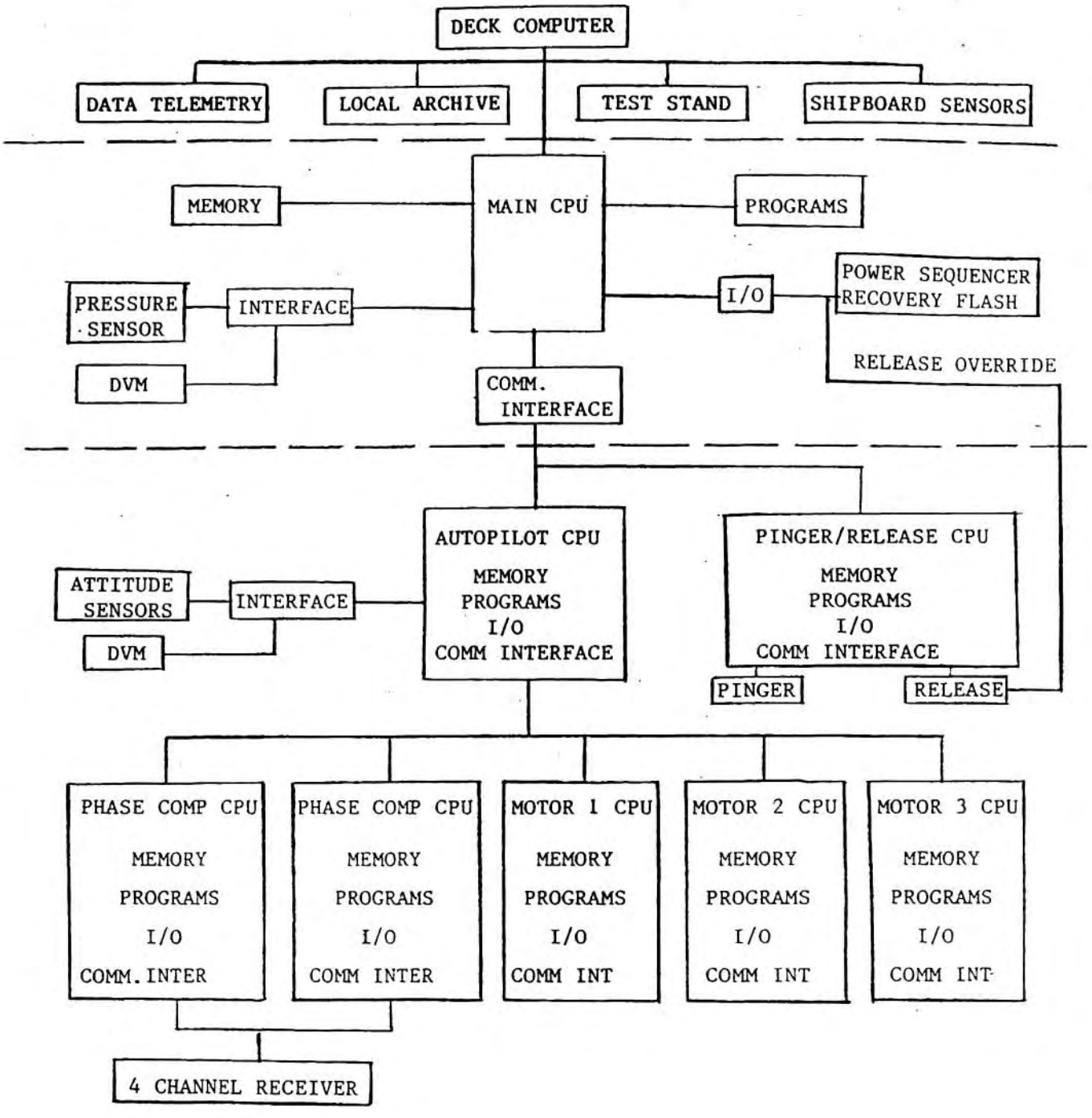

Figure 4.2 Outline of the Micro-processor Hierarchy in the Flying Fish.

mechanism must exist to notify the main cpu, and, ultimately, the person in charge of the fish. In the case of failure during deployment, the information should force the fish to abort the deployment (ie. drop the weight and change the ping rate to notify the surface vessel that a problem exists). For a failure during testing, the communications between the main controller and the slave processors can be exploited to isolate the problem (both the problem source and the problem type).

In addition to the operational advantages of a modular architecture based on intelligent sub-systems, there are several advantages immediately evident to the designer:

-Each sub-assembly can be designed, built, and tested independently of others.

-Software routines can be written to test each module and isolate faults.

-By implementing the design in software, the prototype can be easily tested and adapted to a variety of missions. For example, the autopilot feedback gains can be manipulated in the field via the serial interface without opening the main pressure housing.

-Software implementation allows for the inclusion of exceptions within the algorithm. These exceptions allow a module to employ default conditions in the event of a sub-system failure.

There are three key factors which determine the applicability of distributed intelligence within a single instrument:

-each sub-system must be well defined, the peripheral chips kept to a minimum. For the Flying Fish, where vehicle size is of importance,

circuit size takes on added importance.

-the interface (both mechanical and electrical)should be standard and simple (each processor up and down the hierarchy should be required to know a minimum about the other processors).

-the task should be I/O intensive. If much processing is required, a single microcomputer optimized for number crunching should be implemented.

In the Flying Fish, each phase comparator (one for each axis) and motor driver circuit is built around a single chip micro-computer. When the fish is actively homing on the surface beacon, the phase comparators are sampling the phase difference at about 100 Hz. This information is averaged over 32 cycles and processed by the autopilot sub-assembly which contains a simple model of the fish dynamics (see Chapter 5 for model derivation). The results of this processing are sent to the motor drivers as set points. The motor drivers are closed loop servos which move the control surface to the desired position. The inter-processor communications are via an open collector Serial ASCII Intrumentation Loop (SAIL) bus operating at 9600 Baud (Mesecar and Dillon, 1981; Bradley and Terry, 1983, IEEE 997-1985). The cycle is repeated at a 20 Hz rate.

There are several problems which arise as a result of distributed intelligence within a single instrument. These problems are: (1)control (how do you get each module to do its job?), (2)monitoring (how do you know its correctly executing a given task?),and (3)system synchronization (when passing data from one processor to another, how do you know the data is valid? in the case of passing 16 bit arguements on a 9600 Baud serial link, how do you insure that the first 8 bits are from the same

measurement as the second 8 bits?).

4.2.1 Control of Slave Processors.

Each processor in the hierarchy is controlled by and responsible to the processor above it. The phase comparators, for example, are controlled by the autopilot which is in turn controlled by the main cpu. The main cpu should be able to over-ride the autopilot. Similarly, the deck computer or the operator should be able to over-ride the main cpu. This capability allows for enhanced testing and fault-finding programs at all levels within the hierarchy.

4.2.2 Monitoring slave processors in a hierarchical architecture.

As a primary system design consideration, it is important that the communication protocol include some handshaking capability to insure that each slave module is running correctly. This is done with a status byte which is generated by each module and up-dated frequently. As each module begins a task in its program, a unique status flag describing that task is set. As each task is successfully completed, the flag is cleared. Should a problem arise and a task be left undone, the flag quickly indicates the point of exit from the program. This status flag can serve to indicate and isolate faults. During a deployment, a fault indicated by any of a number of status flags will begin the execution of a default program that will abort a dive and hopefully save the fish. The default architecture depends on whether a specific module is an information source (eg.sensors) or an information sink (eg. actuators). In the Flying Fish, information sources use the status flag to denote the

quality of the information that they are generating (a 1 bit quality control flag). These sources continually attempt to generate valid information with no fundamental change in their algorithm. Information sinks, on the other hand, use the status byte to initiate specific default sequences. Examples include: (1)dropping the ballast weight to abort a dive and (2) moving the control flaps to a benign position (zero deflection angle).

Two types of status flags are used in the fish: generic flags, which are common to all sub-systems, and module specific flags. The generic status flags are shown in Table 4.1; the module specific flags are described in the sections pertaining to each module. Should a slave processor program have initialized, but not begun any tasks, the status byte will be "*". "Z" signifies that the module is idling in a low power mode with all periferals shut off. As part of the handshake, each slave starts a timer each time it is addressed. Should the local manager not address any module within a given window (for the Flying Fish, a 1 second window is used), the slave will set the status byte to "T" and may begin execution of a default program. This ability to default is particularly important for actuators (motor drivers, pingers, and release mechanisms). A second timer is reset every time a complete loop through the slave program is executed correctly. This insures that the data generated by the slave is relatively fresh. If this timer (also set at 1 second in the fish) counts out, the status byte is set to "?". If all systems are running correctly, a "!" is generated by each slave module. This information is passed on to the local SAIL loop manager (in this case the autopilot) and constitutes the only essential exchange between

*	Program initialized
Z	Module is asleep (required for passthrough)
T	Communications Loop Breakdown
?	Program lost
!	Program functioning correctly
I	Ignore status (to prevent default programs from over-riding during a test sequence)

Table 4.1 Summary of generic status flags (ie. those common to all processors in the Flying Fish.

8	Continuous Measurement Flag
7	New Measurement Flag
6, 5	not used
4, 3, 2, 1	A/D Channel Control

Table 4.2 A/D Control Word Bit Assignment

8	Gyro Power Control
7	Accelerometer Power Control
6	Motor Power Control
5	Phase Processor Reset (control of slave processors)
4	Motor Processor Reset
3	Status Ignore/Active
2	Homing Enable
1	Sleep Enable

Table 4.3 Autopilot Control Word Bit Assignment

levels in the processor hierarchy. The autopilot, in addition to checking to see that its own status is valid, checks to see that the status of each slave processor is also valid. If all is OK, a single status byte (!) is passed on up the chain of command to the main cpu. System level decisions of whether to abort a dive or change ping rate are made at the highest level in this chain of command (ie. by the main cpu).

During testing, it is inevitable that one or both of the timeouts that form the basis for the two way interprocessor handshakes will occur. To prevent the default condition from overriding a test, a status ignore "I" command can be sent to the slave processors to invalidate any default program.

4.2.3 System Synchronization.

The Flying Fish is a mutil-processor instrument. As described earlier, these processors are arranged in a hierarchy. This hierarchy is characterized by extensive dialogue among processors at a single level and minimal exchange (only initialization is passed down and sub-system status passed up) between levels. Faced with the problem of recording the core of the dialogue that is transpiring on any given level, one can either (1) design separate data loggers for each level or (2) establish a protocol for communications between levels and use the main data logger to record all the variables of interest. The first approach requires additional hardware and merging the data sets from several recorders requires that time be logged redundantly at each level. A second approach is to pass the data up to the main cpu so that the engineering parameters can be merged with the scientific data string. This

necessitates one of the following two implementations:

-The different levels must be synchronized. Since each level is running a distinct program with a different execution time, this forces one of the programs to be artificially slowed to the pace of the other. As additional tasks are loaded onto either processor, care must be taken to re-synchronize the two programs.

-A buffer can be filled with the data that is being passed between levels. Appended to this buffer must be a second handshake to signal that new data is available or that the data is old and should be ignored. This second approach, while complicating the inter-processor communications protocol, is immune to any changes in program length. It also allows each program to be executed at top speed without artificially slowing the system down. Should the main program be faster than the autopilot program, a NEW DATA FLAG set by the autopilot will validate the data string which will then be stored in the main cpu mass storage (RAM). If the autopilot program is faster, then the NEW DATA FLAG will always appear valid. In the second case, some data will be lost but the logger will be working at full capacity.

This additional handshake was implemented using the bit assignment shown in Table 4.2. Bits 0, 1, 2, and 3 are the A/D channel select bits which are then appended to the data string as identifiers of the source of the data. Bit 7 causes the A/D to sample a specific channel continuously in a short loop to aid in fault isolation. Bit 6 is the NEW DATA FLAG.

4.3 THE BASIC BUILDING BLOCKS

Since the physical capabilities of the microprocessors and the attendant serial communications protocol are the building blocks of the modular electronic architecture of the fish, a small detour to describe the characteristics of each is in order. Further details are given in the manufacturer's data sheets and in the Bibliography.

4.3.1 The Hitachi 6301

The Hitachi 6301 is a single chip 8 bit microcomputer that is at the heart of each autopilot sub-system. Not intended for heavy processing tasks, its strengths lie in the following list of capabilities:

-built-in Universal Asynchronous Receiver Transmitter (UART) for serial communication (reduces the number of peripheral chips required).

-three 8 bit I/O ports (good for I/O intensive tasks).

-built in timer with input capture and output compare capability (for measuring and generating waveforms).

-9 vectored interrupts (simplifies programming overhead by jumping to a different interrupt routine for each type of interrupt).

The details of how these attributes are exploited vary for each module and are explained in each section below.

4.3.2 The SAIL Protocol

A hierarchical SAIL communications bus is used throughout the fish (Mesecar and Dillon, 1981; Bradley and Terry, 1983; IEEE 997-1985). The monitor was written by Dr. Albert Bradley of W.H.O.I. The principal

attraction of this approach is its simplicity. SAIL is a single degree of freedom system with no limitation on how the data is encoded or on the communications speed (eg. information may be encoded in changes in voltage, current, phase, or frequency, and a various baud rates). Each module on the SAIL bus is individually addressible and controllable. To access processors on other levels of the hierarchy, SAIL pass-through (Bradley and Terry, 1983) can be invoked to make the intermediate processor transparent to any transactions. Specifically, those processors which separate any two levels within the heirarchy are designed with two UARTs, one for transactions on the upper loop and one for transactions on the lower loop. This two-level communication is time multiplexed to allow transactions on both levels simultaneously. If the pass-through mode is invoked, characters that are input on one UART are quickly output on the other so that the processor is effectively transparent to any transactions between levels. Figure 4.2 shows a three layer SAIL hierarchy with the main data logger at the apex, the pinger/release and the autopilot on the second level and the phase detectors and motor drivers on the bottom. There is no fundamental limit to the number of layers allowed with this approach but a practical limit is enforced by the mental gymnastics required if more than three layers are involved.

Though the details of the SAIL structure and the monitor built into the Flying Fish is beyond the scope of this work, several key points about this approach highlight the advantages and disadvantages:

(1)Small parts count. The open collector SAIL bus which is used within the instrument, requires only one transistor and one resistor.

Between the fish and the deck computer, a single chip commercially avialable 20ma optically isolated SAIL interface module is used to increase noise immunity.

(2)All transactions are in ASCII. The main advantage is that all transactions on the SAIL bus can be monitored with a simple terminal. The disadvantage is that ASCII encoding requires a 30% to 40% overhead (compared to binary encoding) which directly affects the absolute rate of communication.

(3)Several instruments can be attached to a single SAIL bus. Since each processor on the bus has a specific address, it will ignore any transactions which are not specifically targeted for that processor. The advantage is a minimum of cabling. The disadvantage is that each address is several characters long. This additional overhead further cuts down the speed of communications.

An upper limit on the data rates is determined by the speed of the processor (its ability to keep up with the flow of data, a function of the crystal oscillator frequency) and the overhead requirements. This overhead can take the form of (1)inefficient coding and (2)individual addresses. The status handshake (see Section 4.2.2) also diminishes the effective communications rate. How critically the effective communications is impaired by these overhead requirements depends on the application. In the Flying Fish, the internal data rates are determined by the need to dump 256 KBytes in a one hour period and the need to process incoming phase information and generate motor set points within a time span that is short when compared with the characteristic time constant of the fish dynamics. As presently configured, the phase

comparators can make bearing measurements at about 100 Hz. The phase comparators are interrogated and the motor set points generated at about a 20 Hz rate (limited by processor speed). Thus, five bearing measurements can be averaged for each motor set point. This averaging is done in software.

As stated earlier, one of the advantages of a microprocessor based prototype instrument is the flexibility gained from having programmable parameters. If one agrees with the notion of distributed intelligence (ie several processors) within a single instrument, the hierarchical SAIL architecture allows direct access to all programmable constants on all levels within the hierarchy. For example, the motor controller gains can be easily changed just minutes prior to deployment without opening the pressure case.

4.4 THE MAIN DATA LOGGER.

The detailed design of the main cpu was done by Albert Bradley of Woods Hole and is not a part of this thesis. Its block diagram, shown as part of Figure 4.2, is fairly conventional. Its major attributes are (1) very low standby power and (2) it supports the SAIL protocol (including pass-through). This processor interfaces between the deck computer and the fish sub-systems (including the sensor payload). In addition to acting as go between, this processor board is the main data logger for both scientific data and engineering data. An A/D appended to the cpu is used as a digital volt meter (DVM) to measure critical voltages throughout the system and is a major component in the system fault isolation capability. This processor also controls the power

distribution throughout the fish. This power distribution is discussed in detail below.

For the purposes of this thesis, the main cpu can be considered the equivalent of a commercially available data logger with some I/O capability to control the power distribution in the fish.

4.5 POWER DISTRIBUTION

The design of the power distribution system is driven by two primary considerations: (1) the voltage and current requirements of the various system components; and (2) the need for a low power standby mode where all auxiliary components are shut down but can be brought up in an orderly fashion. Additional considerations include the efficiency of converting from the battery voltage to the various system voltages and the noise level on critical power lines (eg. to the receiver preamplifiers). Figure 4.3 shows schematically the power distribution architecture within the fish. The main cpu is always powered up and can power switch all other components. The 5 volt digital supply to the main cpu is generated from a +/- 5 volt switching regulator where the -5 volt supply is used in the local power switching network (a 10 volt difference between the source and the gate is required to turn on the Field Effect Transistors (FET) sufficiently hard). The release, flashers, pinger, and motor driver were all designed in house and all work off the raw battery voltage (their design is described elsewhere in this thesis). To improve the noise immunity of the receivers, their 5V supply is derived separately from the digital 5V supply. Individual spot regulators for each channel were used to reduce cross talk between channels. The

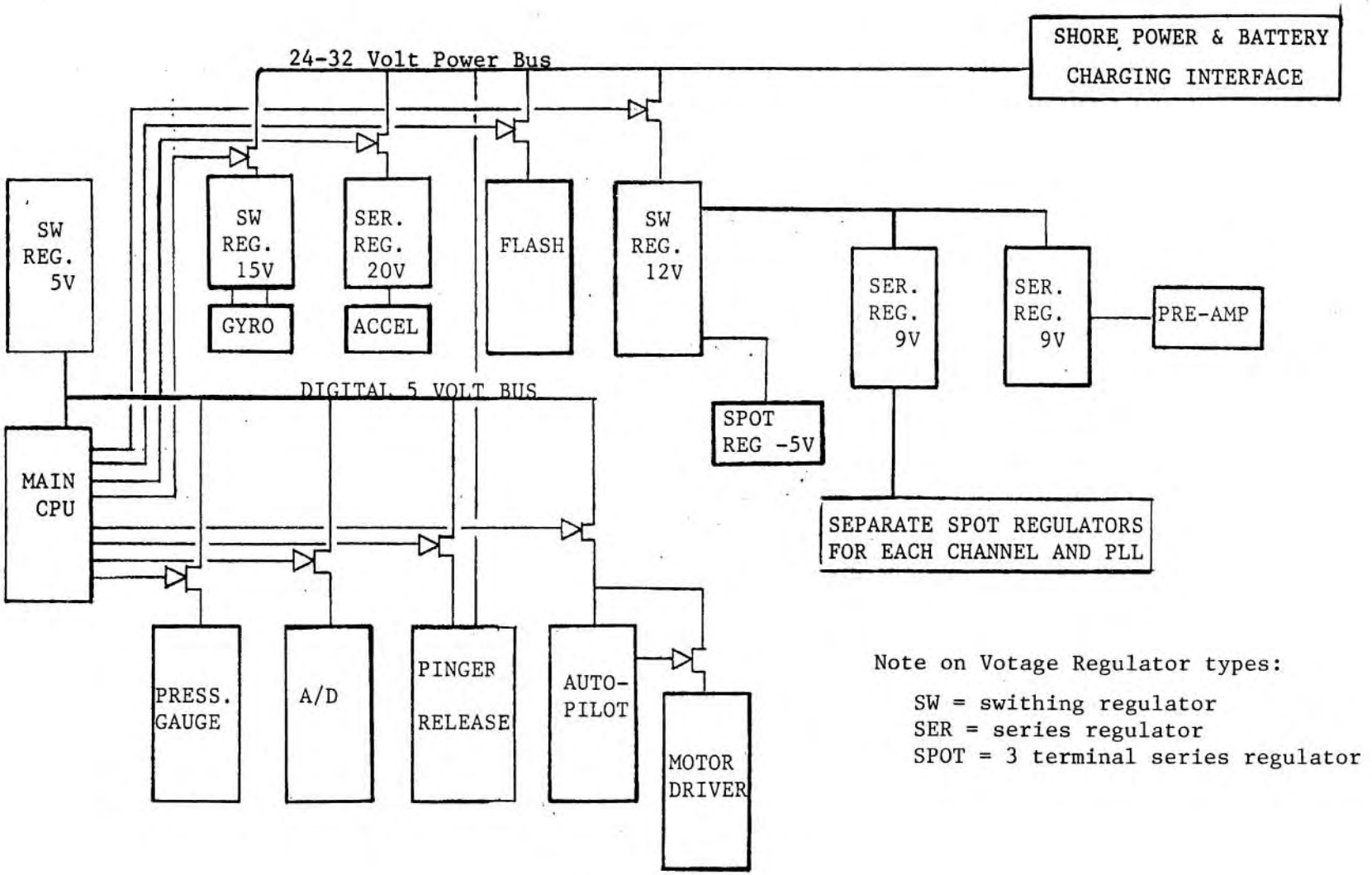

Figure 4.3 . Power Distribution Network within the Flying Fish.
Note the ability of the Main CPU to shut down all sub-systems within the Fish.

breadboard receiver suffered from power supply coupling between the Phase Locked Loop (PLL) output (a 5 volt square wave) and the receiver input (a low level analog signal). To address this, separate spot regulators were designed into each PLL circuit. The two commercial sensors, the rate gyro and the accelerometers, have unique voltage requirements as shown.

The battery charge circuitry is designed so that the instrument can be tested using shore power. Current surges (eg.for the pinger) are handled by large electrolytic capacitors. Battery selection is discussed in Section 4.11.

4.6 THE RECEIVERS.

4.6.1 An Overview.

To simplify the control algorithm, an effort was made to decouple pitch and yaw dynamics. This led to an axisymmetric vehicle with a four element phased array arranged in two orthogonal axes. Each axis consists of a hydrophone pair (two hydrophones), the separation forms the baseline from which interferometric measurements of an incoming cw acoustic signal are made.

As the signal passes through each stage of the receiver, phase shifts may occur. Further, the phase shift in each channel may differ due to hydrophone misalignment (see Section 3.1.2) or simply due to differences in component values (see Section 4.7.4 for a discussion of sources or error in the phase difference measurements). Thus, for a common input signal, a finite phase difference may appear at the receiver output. As long as this phase difference is constant over the operating range (both phase and temperature) of the fish, an additive offset in the

control algorithm will negate the effect of these phase shifts. If, between deployments, the measured phase difference can be tested against a known reference, any long term trends in the receiver/hydrophone performance can be monitored. A test generator has been built to monitor the phase input/output characteristics of the receivers and the hydrophones but is not part of this thesis.

A block diagram of the entire receiver/phase comparator module is shown in Figure 4.4. The major elements in the block diagram include the band pass filter, the limiter, the phase locked loop, and the multiplexer. These sub-system components are described below.

4.6.2 The Receivers as a Servo Loop.

A review of the hydrodynamic analysis conducted in Section 2.7 shows that, given: (1) an operating frequency, (2)the ambient noise, (3)signal attenuation and spreading losses, and (4)desired phase resolution, one can derive a relationship between source strength and receiver bandwidth. To reduce the acoustic power put into the water, a narrow band receiver is desirable.

The operating range of the receiver is 100 Hz wide to account for Doppler shifts in the homing beacon frequency due to forward motion of the fish. This operating range puts a lower limit on the bandwidth of the phase lock loop at 10 Hz. This limit arises from the capture characteristics of the PLL (Gardner,1966). As long as the fish and/or beacon do not get displaced such that the phase at the receiver changes 3600 degrees per second (1 meter per second), the receiver should track the homing beacon. Since the fish is designed for constant velocity

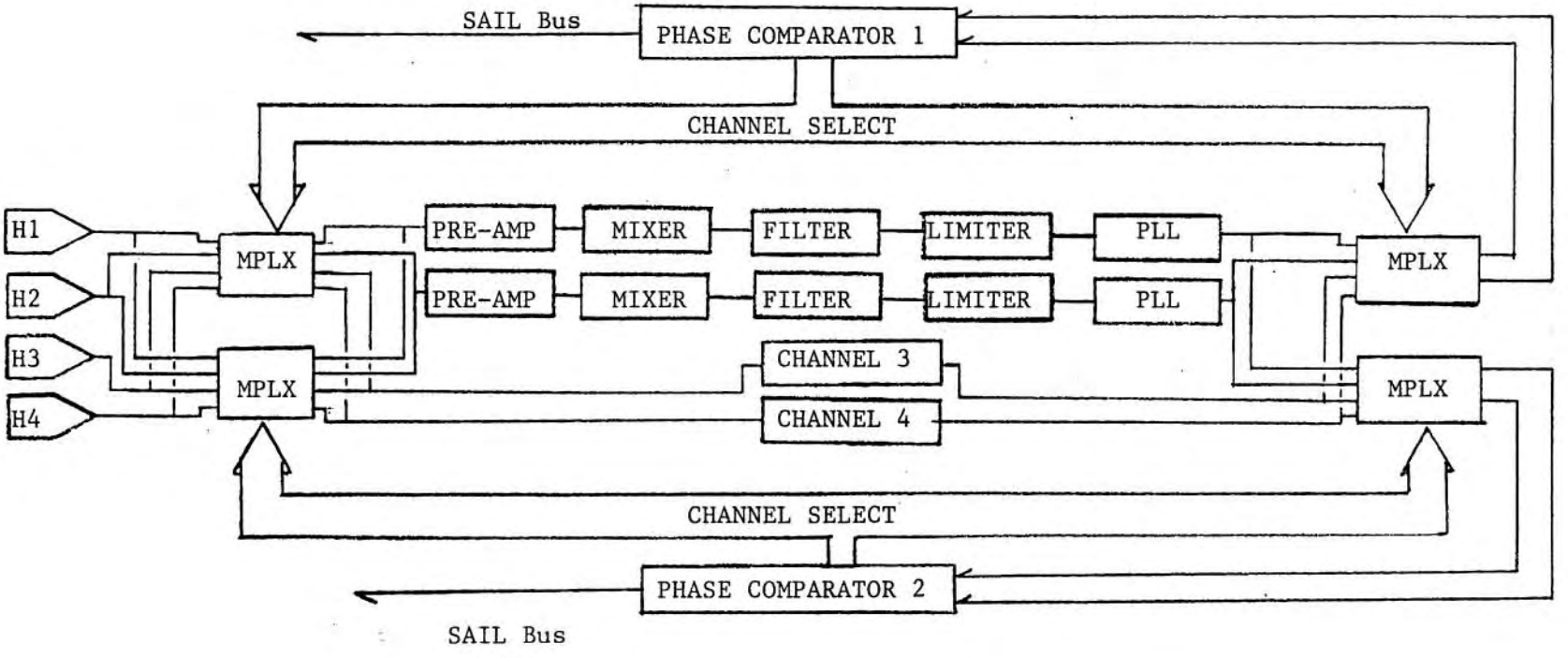

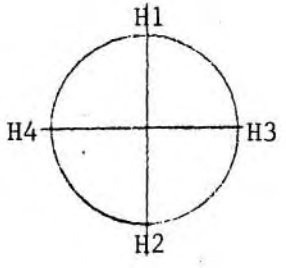

Figure 4.4. Block Diagram of the Hydrophone-Receiver-Phase Comparator Sub-System for the Flying Fish.

manuevers, tracking the beacon should not be a problem.

4.6.2.1 The Limiter. Since all the desired information is contained in the phase, the incoming signal is amplified and hard limited. The signal is then essentially a square wave where the zero crossings contain the phase/bearing information. Given a nominal signal strength calculated from (1)the assumed pressure field at the hydrophone and (2) the sensitivity specifications of the hydrophones, and if the limiter specifications are given by the manufacturer, the gain of the amplifier can be calculated. The schematics are shown in Appendix

4.6.2.2 The PLL/mixer. As described above, the PLL servos each receiver pass band to the apparent Doppler shifted frequency of the homing beacon. Unfortunately, like all servo systems, the PLL is driven by an error signal. This finite error appears on the output of the phase locked loop as a frequency independent phase jitter of order 3 to 5 degrees which is unacceptable (based on the hydrodynamic sensitivity analysis in Section 2.6). By mixing the incoming signal with a local oscillator, a difference frequency of 500 Hz., in which the original phase relationship is preserved, gives as acceptable phase jitter. This square wave signal goes directly into the phase comparator processor which uses an internal timer to measure (1)the period of the incoming signal on one channel and (2)the time between zero crossings on two channels. Thus, the phase difference resolution of the phase comparator is a function of only (1)the operating frequency (500 Hz) and (2)the resolution of the timer. This theoretical phase resolution is 0.3

degrees. In practice, the phase resolution is limited by the finite phase jitter of the PLL and is of order 1 degree; still within acceptable limits as specified by the homing error criterion derived in Section 2.6. This raw phase information can then be averaged if additional phase resolution is desired.

4.6.2.3 The Multiplexer. The multiplexer shown in the block diagram is used to switch any hydrophone to any receiver. If a fault exists on one channel, the hydrophone can be switched to a different receiver to help isolate faults during testing and to measure crosstalk between channels.

4.7 THE PHASE COMPARATOR

4.7.1 The Hardware.

The principal attraction of a processor based phase comparator is its simplicity (only three integrated circuits). The processor selected for computing the phase difference between two channels is the Hitachi 6301 described earlier. In addition to the built-in UART, the attractive feature of this processor in this application is the built in timer with its control registers. This allows the processor to measure the period of incoming square waves to within one clock cycle. For a clock frequency of 614 KHz and an incoming frequency of 500 Hz (after the mixer), the phase resolution is of order 0.3 degrees with no averaging.

During operation, the processor first selects a channel, measures the period of the incoming signal on that channel, then changes to a second channel to capture the phase difference between the two. The time delay between the two signals is divided by the period to make an

instantaneous measurement of the phase difference.

Additional advantages of a microprocessor based phase comparator include:

-a programmable averaging interval

-programmable phase offset due to hydrophone degradation.

-programmable receiver channel selection

-programmable hydrophone selection (independently programmable from receiver channel to isolate any problem).

-programmable local oscillator frequency (useful in the prototype only, this capability allows for some optimization of the mixer design)

-monitoring module status to warn the main cpu of a fault.

Because the phase comparators are an information source rather than a sink, no default condition is required. In the event of a malfunction, an error status flag is set but the phase comparators continue to try to make a phase measurement.

4.7.2 The Software.

Figure 4.5 is a block diagram of the software structure of the phase comparator that emphasizes the control and monitoring capability. The assembly language programs are archived at the Woods Hole Oceanographic Institution and may be accessed through Dr. Albert Bradley.

The phase comparator is controlled by a single word which is sent from the autopilot. This 8 bit word encodes the receiver channel selection. Default channel selections can be over-ridden by the main cpu

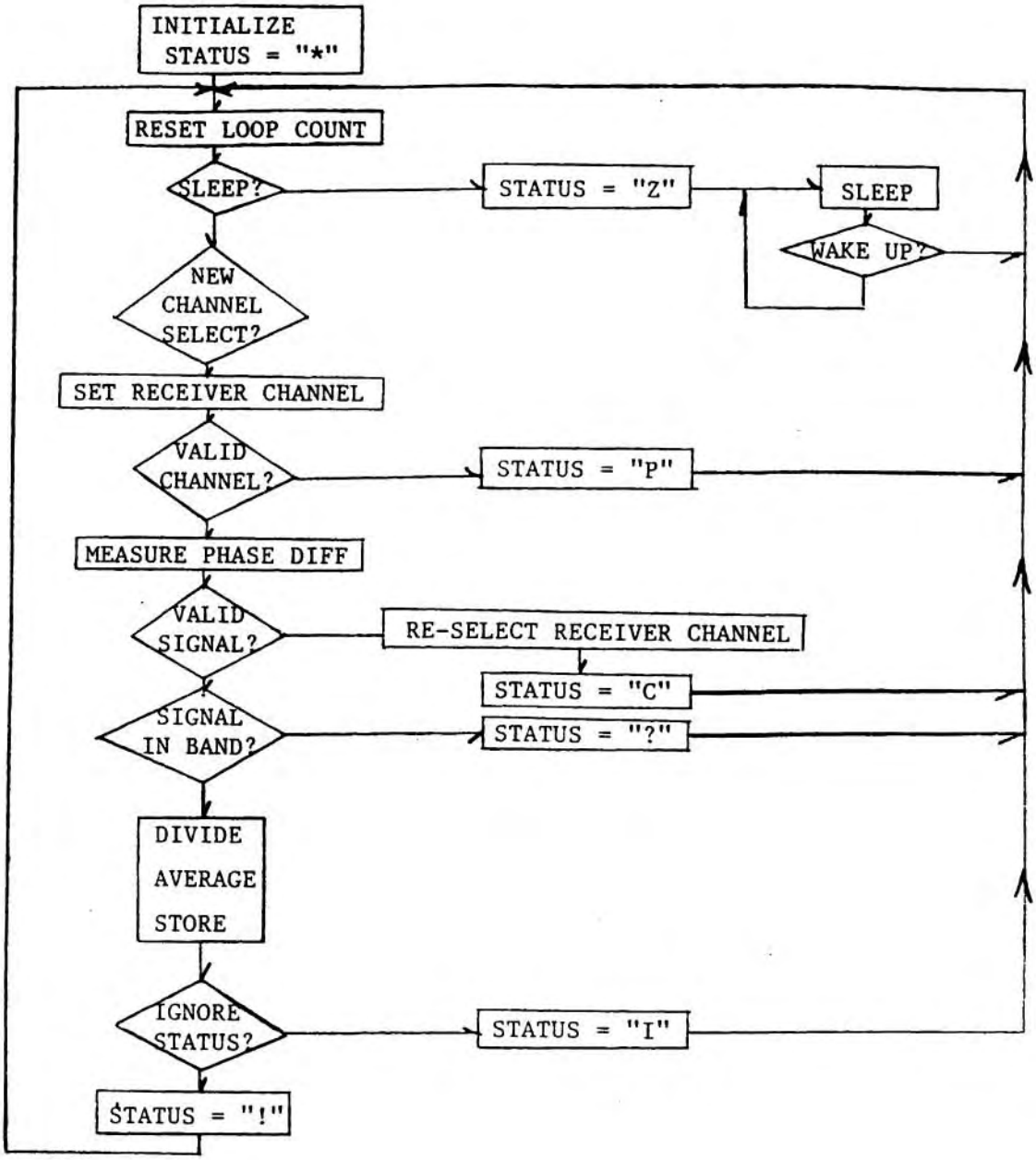

Figure 4.5 Block Diagram of the MAIN Program for the Phase Comparator Processors with Emphasis on the Structure of the Status Codes. Note that all system faults gives rise to successive attempts to make an accurate phase difference measurement; no explicit default routine is required by a data source (see Motor block diagram for an example of a default routine.

via SAIL passthrough for testing purposes. If no receiver channels are selected (ie, the control word is "00"), then the phase comparator has no imminent task and will enter a low power sleep mode. Similarly, if invalid receiver channels are selected, a status flag is set and the processor goes back to sleep. Any serial communications interrupt will temporarily wake up the processor but it will stay awake only if valid receiver channels are selected.

When testing other sub-systems, all receiver channels are turned off and the processor is put to sleep. For testing the motor drivers, for example, phase difference inputs are generated synthetically by simply down loading numbers into that RAM location reserved for measured phase differences.

Monitoring the validity of the phase measurements is done with the status word. The block diagram of the phase comparator algorithm shows the conditions under which status words are generated. In addition to the generic status flags discussed above, several status words are specific to the phase comparators. The first is if the receiver channel is invalid. The second is if no signal is present. The third is if the incoming frequency is out of band (ie. incoherent noise). For testing purposes, the status flag can either be ignored or overwritten when the module is queried by an operator.

If, for any reason, a bad status flag is generated, the measurement is ignored and the local manager (in this case the autopilot) is alerted that a malfunction exists (the autopilot can choose to ignore this bad status flag, a helpful option when testing).

For valid measurements, the raw phase measurement can then be

averaged (the number of measurements averaged is programmable but the default is 32 to roughly match the time constant of the phase locked loop). Though the capability to automatically average to a given noise level could easily be implemented, this has not been done to date.

4.7.3 Phase I/O relationship.

Inherent in the hydrophone, preamplifier, and receiver circuitry are phase shifts which may be functions of amplitude, frequency, filter gain, and temperature. The critical relationship is not the phase in to phase out shift but the change in this shift over the operating range of the fish.

Should a change in the phase shift exist, as long as it is consistent in all channels, useful information can be derived from the phase comparator. Figure 4.6 shows this input output relationship. This relationship could change from channel to channel and will almost certainly be unique to each fish. Consequently, a test signal generator was designed to check and measure this relationship. This test generator, while useful in the check out of the prototype, may also prove useful operationally as a way to monitor long term degradation of the hydrophone/receiver network.

To better understand how the measured phase difference may change over the operating range of the hydrophone/receiver network, assume that the major contributor to this phase shift is the two-pole RLC filter in the receiver pre-amplifier. Figure 4.7 shows the idealized amplitude and phase characteristics of several two pole filters. The temperature coefficents of the components in these filters can contribute to the

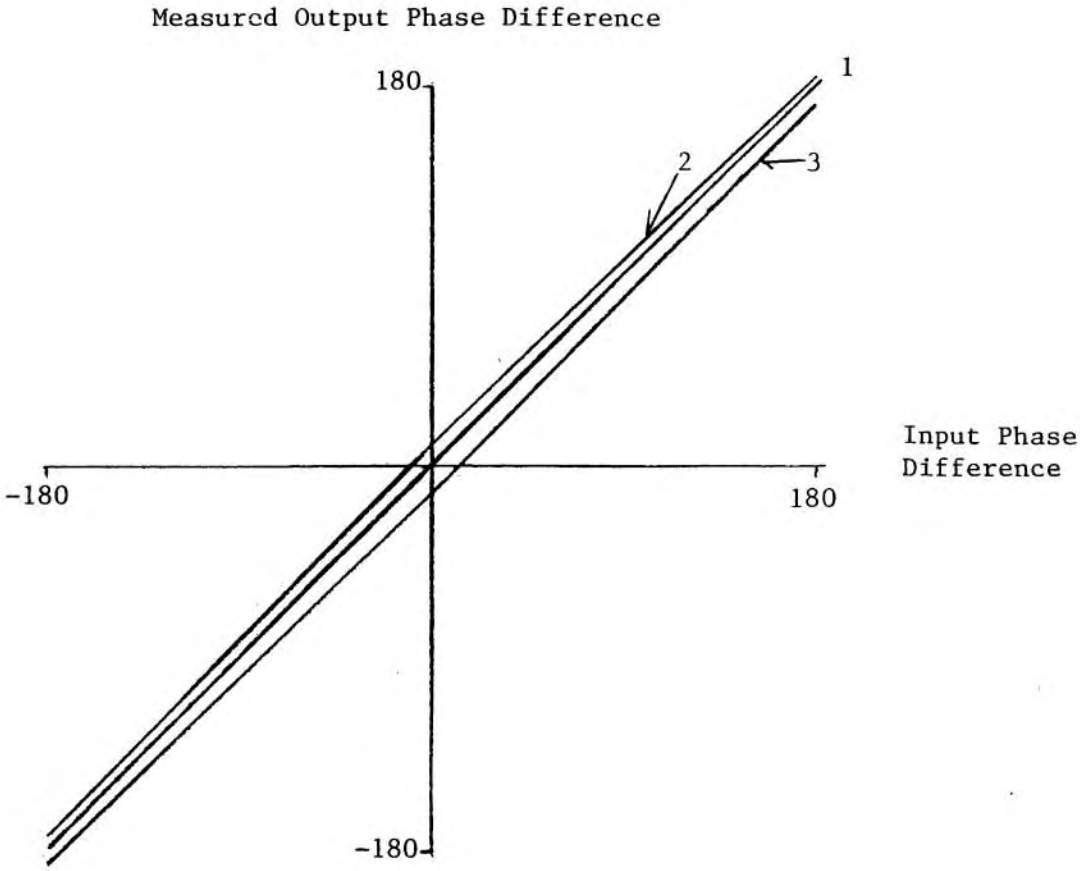

Figure 4.6 The Input/Output Phase Difference Relationship for the Flying Fish Hydrophone-Preamplifier-PLL Network: (1) Idealized; (2) As measured between Channels 1 & 2; (3) As measured between Channels 3 & 4. Data collected at room temperature with a 15,050 Hz Carrier.

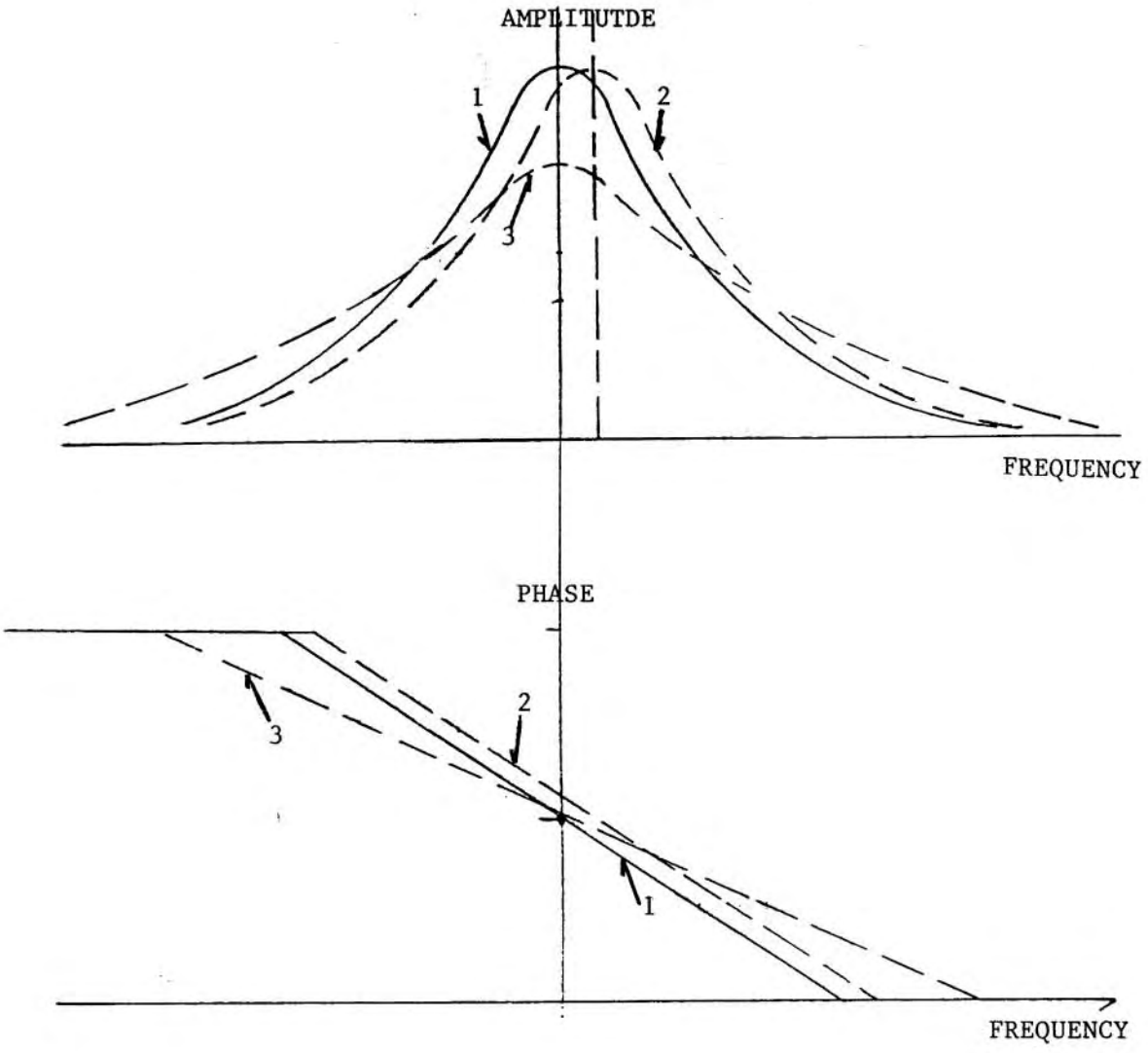

Figure 4.7 Amplitude and Phase as a Function of Frequency for Three RLC Filters. 1 & 2 have the same Q but their center frequencies are offset. 1 & 3 have the same center frequency but have different Q.

phase shift if (1)the two receivers are not tuned to the same center frequency and (2)the two receivers do not have the same Q. For the first case, the slopes of the phase VS frequency plots for the two filters are, to first order, parallel. Consequently, if both receivers are at the same temperature, no net change in the phase difference will be measurable. The presense of temperature differences between two receiver channels will give rise to a change in measured phase difference but is considered a second order effect. If two RLC filters have different Q, then the slopes of the phase VS frequency plots are not parallel and the phase difference in to measured phase difference out can vary dramatically as a function of temperature and input frequency. Thus, it is important to match the Q of all four receiver filters.

4.8 THE MOTOR CONTROLLER

4.8.1 Background.

The one aspect of the fish attitude controller that was expected to exploit existing commercial products with a minimum of modification was the motor controller. Several companies manufacture motor drivers that are compatible with the 4 pole brushless DC motor selected in Section 3.5.3 (including the manufacturer of the motor) but all these designs proved inadquate for a number of reasons:

-many motor drivers are designed as retro-fits for brush type motors with analog resolvers and tachometers. To convert these to digital signals is unattractive and consumes circuit board space.

-most motor drivers are designed to handle a range of voltages and currents that go well beyond those required in this application. The

resulting commercial circuits are over-designed, heavy, and bulky.

The approach taken in the design of the motor drivers used in the Flying Fish was to design to the power requirements of the 10 watt motors. The result is a compact circuit built around a microprocessor with a minimum of additional circuitry. Furthermore, no additional sensors are required to generate both position and tachometer feedback. A unique program in the motor controller synthesizes integral feedback to eliminate steady state errors. A detailed description of this design follows.

4.8.2 An Overview of the Motor Driver Design in the Flying Fish.

A block diagram of the motor driver/controller module is shown in Figure 4.8. To keep through hull penetrators to a minimum, the drive electronics were put in the oil filled gear box. The Pulse-Width Modulated (PWM) output eliminated the need for a digital to analog converter. An attempt was made to generate the individual pulses in software but the carrier frequency (lower limit determined by mechanical characteristics of the motor, upper limit determined by eddy losses in the core) specified by the motor manufacturers was too high (20 KHz) and some additional circuitry was built so that the processor only had to control the pulse width. The Hall Effect rotor position sensors, in addition to commutating the windings, are fed back to the processor. The opto-interruptor is an independent measure of the center position of the control surfaces.

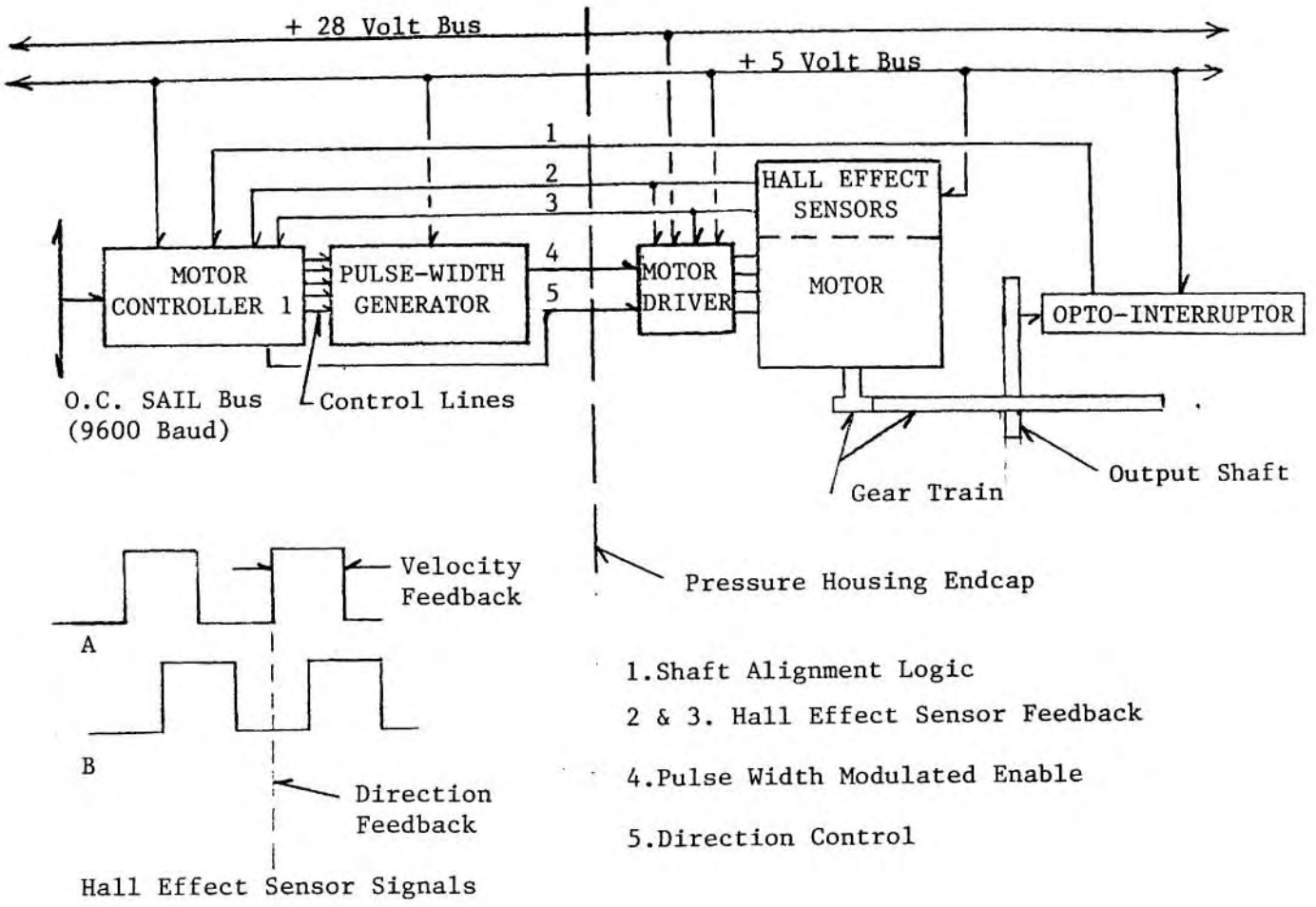

Figure 4.8 Diagram of Motor/Controller Sub-system (One of Three) in the Flying Fish.

4.8.3 The Motor Controller as a Servo Loop.

4.8.3.1 Position Feedback. On initialization, the optical interruptor is used to center the fins independently of the rest of the motor controller logic. Once the fins are centered, this position is the reference point from which all other control surface deflections are measured. The two Hall Effect sensor outputs used to commutate the windings are fed back to the motor controller. The two sensor signals are in quadrature. One sensor output is used to generate a timer interrupt which either increments or decrements the position counter depending on whether the other sensor input is high or low (see Figure 4.8). The position error is measured by the difference between the set point and the position counter. The control loop gains are programmable and can be changed without opening the housing by using SAIL passthrough (Bradley and Terry, 1983).

4.8.3.2 Tachometer Feedback. In addition to simply counting the pulses generated by the Hall Effect sensors, the timer input on the cpu can be used to measure the pulse width, which is a measure of the output shaft rotation speed. This information can be used to artificially dampen the dynamic response of the motor. For the Flying Fish, the parasitic drag generated by having the motor run in oil is a sufficient damper and tachometer feedback was never implemented.

4.8.3.3 Integral Feedback could be implemented by having a register which sums the position error but the actual implementation of this was very cumbersome. Instead, rather than penalize the accumulation of error, a

timer was the basis for increasing the drive to the motors. This timer is running whenever any error between set point and actual position exists and is reset when the error is zero. As a consequence, all errors are weighted equally in time. The result of this approach is that large excursions tend to cause some overshoot. This tendency was deemed acceptible.

4.8.3.4 A Linear Model of Motor Dynamics.

The primary purpose of using closed loop position control of the control surface is the ability to handle perturbations and errors in modelling the motor dynamics. The model used to predict the dynamic response of the motor/actuator/servo loop is shown in Figure 4.9 (after Ogata). If one ignores the winding inducance (in this case the electrical time constant is 1Δ of the mechanical time constant so this simplification in the model is valid), the transfer function between input voltage and output position is given by Equation 4.1.

$$\frac{\theta_{OUT}}{V_{IN}} = \frac{K_M}{S(T_M S + 1)} \qquad 4.1$$

where $K_M \sim \frac{1}{K_b}$

$$T_M \sim \frac{R_a J}{K_T K_b}$$

R_a is the winding resistance
K_b is the back emf constant
K_T is the motor torque constant

For Pittman motor P/N 3112-76T33, K_M = 29.4 rad/sec/volt
T_M = .112 seconds

Because of the large gear train, the load inertia and friction can be neglected. For the motor chosen (Pittman p/n 3112-76T33; see Section 3.5.3 on motor selection), the closed loop position servo transfer function, characteristic equation, the root locus for several proportional feedback gain constants are shown in Figure 4.10. Figure 4.9 shows the idealized linear model.

In addition to the unknown and unmodelled effects of non-linear motor characteristics and friction, are the known but unmodelled parabolic loading characteristics of the control surface as a function of deflection. This known quantity could be included in the model of the motor dynamics or could be left as an unmodelled perturbation in the control loop. Because of the 10:1 safety factor between expected hinge moments and maximum actuator output torque, the wing loading was left unmodelled as a perturbation to the control loop. This varying load, when modelled as flap deflection dependent friction, necessitates the inclusion of some form of integral feedback.

4.8.4 The Motor Controller as a Smart Module.

4.8.4.1 the Hardware.

Here again, the unique characteristics of the Hitachi 6301 have been exploited to make a minimum parts motor driver servo loop sub-assembly with a simple serial interface to connect it to the rest of the autopilot sub-system. Because of the unique internal communications protocol, the gain constants of the proportional, tachometer, and integral feedback loops can be manipulated without opening the pressure housing. The motor driver modules can be individually turned on or off and exercised by test routines in the deck computer.

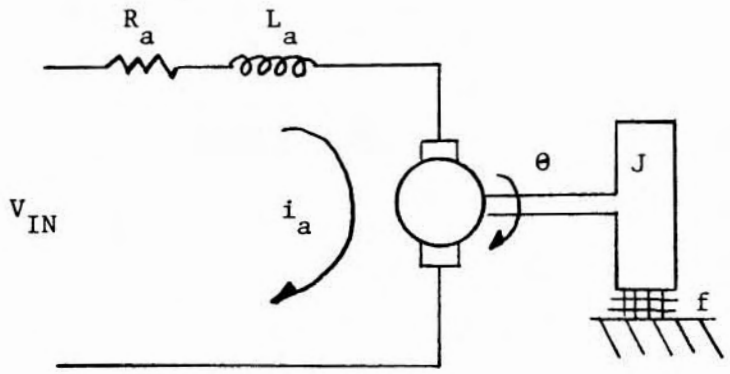

Figure 4.9 Motor Model (after Ogata, 1970)

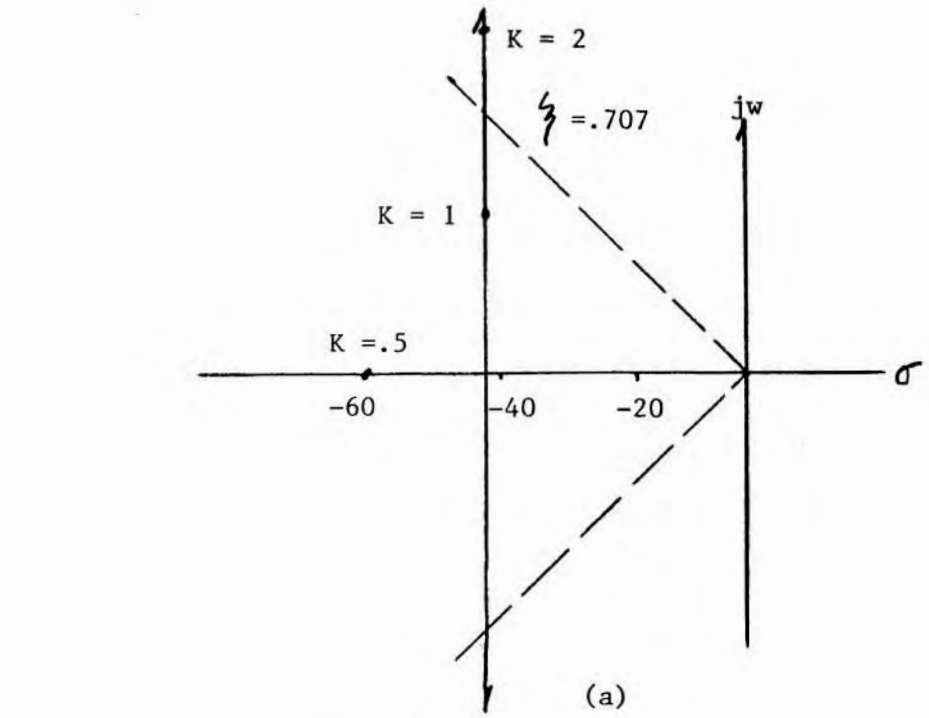

(a)

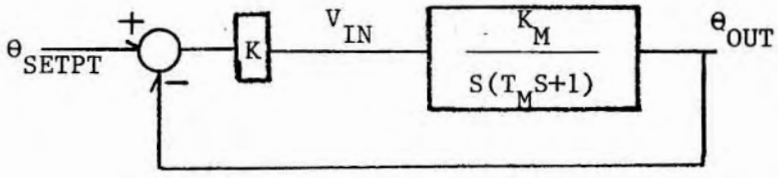

CHARACTERISTIC EQUATION: $S^2 + 83S + 2500K = 0$

(b)

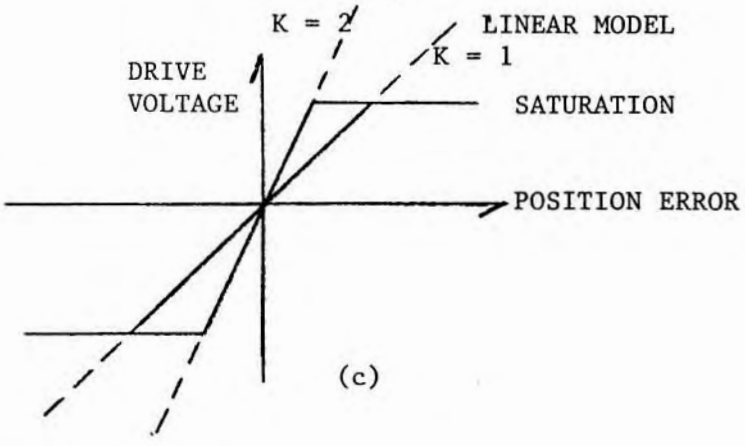

(c)

Figure 4.10 (a)Root Locus of Motors Used in the Flying Fish
(b)Closed Loop Model of the Motors.
(c)The Limitations of a Linear Model in a Slew Rate Limited Actuator.

In addition to the Hall Effect sensor feedback, the only other connections between motor controller and motor driver are the direction control and the PWM drive control. If all three motors share common power and ground, the number of through hull penetrators is 15 (if one also includes the pinger and opto-interruptors, the number of wires increases to 24).

4.8.4.2 The Software.

The main attraction of a processor based motor controller is that the various gain constants are programmable. Figure 4.11 is the block diagram of the motor controller algorithm (with timer interrupt routine). The detailed block diagrams and assembly programs are archived at Woods Hole.

On power up the processor goes into a low power standby mode. When the correct initialization command is given by the autopilot cpu, the motor controllers use the optical interruptors to center their fins. This center position is used as a reference point. The motor controller attempts to minimize the position error as measured by the difference between present fin position and set points generated by the autopilot. The safety counter and timeout counter are used to insure that (1)no breakdown in interprocessor communication has occured and (2) that the motor is operating correctly. If a bad status flag is generated, the motor controller defaults to the straight up condition. The status check can be ignored when test routines are employed.

4.9 THE AUTOPILOT

4.9.1 Sub-system overview.

The main purpose of the autopilot is to coordinate the activities of the phase comparators and the motor controllers. A simple model of fish dynamics

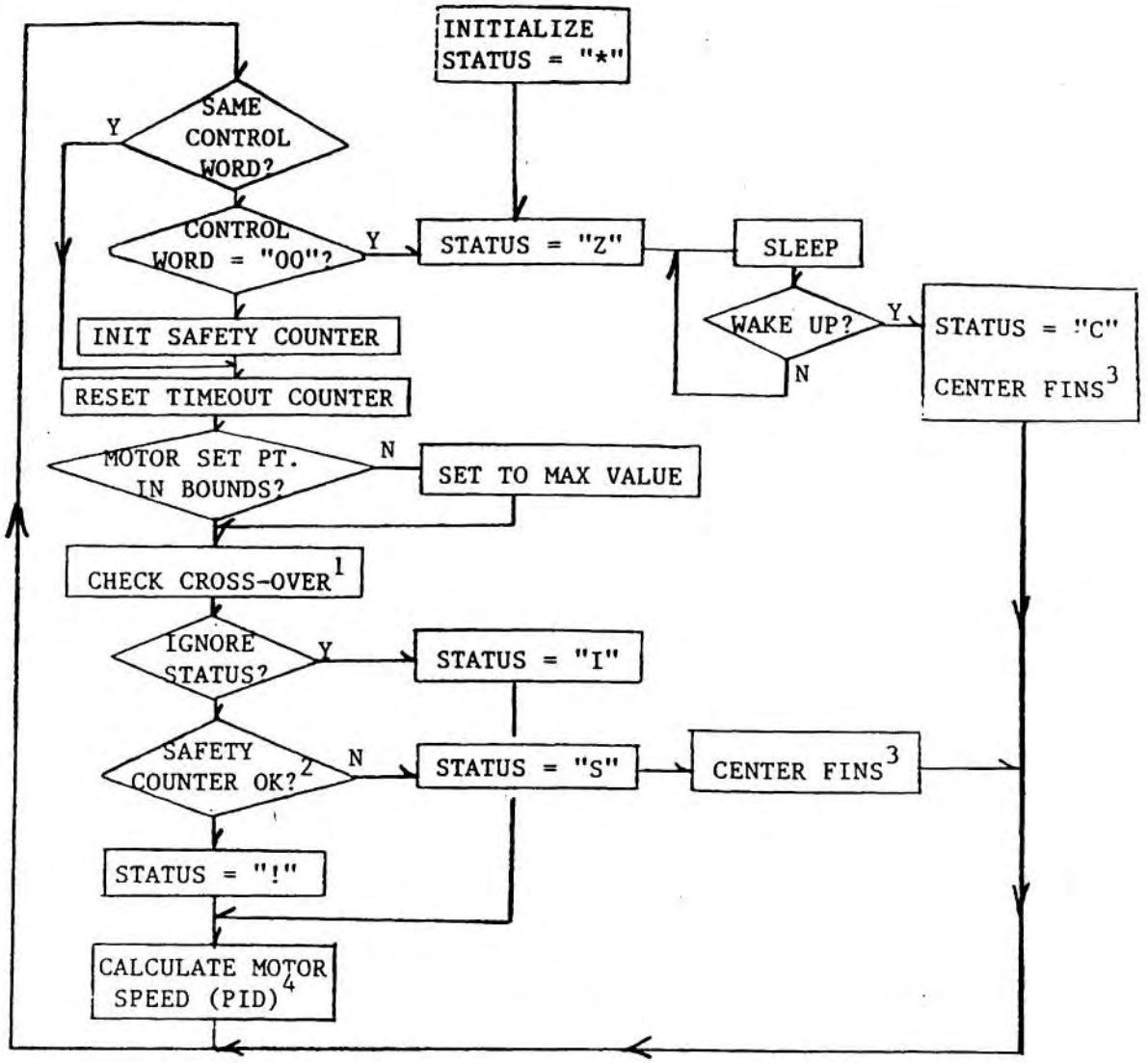

Figure 4.11a Main Motor Controller Program.

Notes:
1 Compare Optical Interruptor Transition with Expected Position (not used at present)
2 Safety Counter is Reset when Motor Controller is addressed by the Autopilot, an Indication that no Communication Breakdown has Transpired.
3 When fins are centered after SLEEP, the Optical Interruptors are used, otherwise the fins are centered using the position counter
4 The inputs to the PID algorithm are generated by the TIMER INPUT CAPTURE and the TIMER OVERFLOW Interrupts

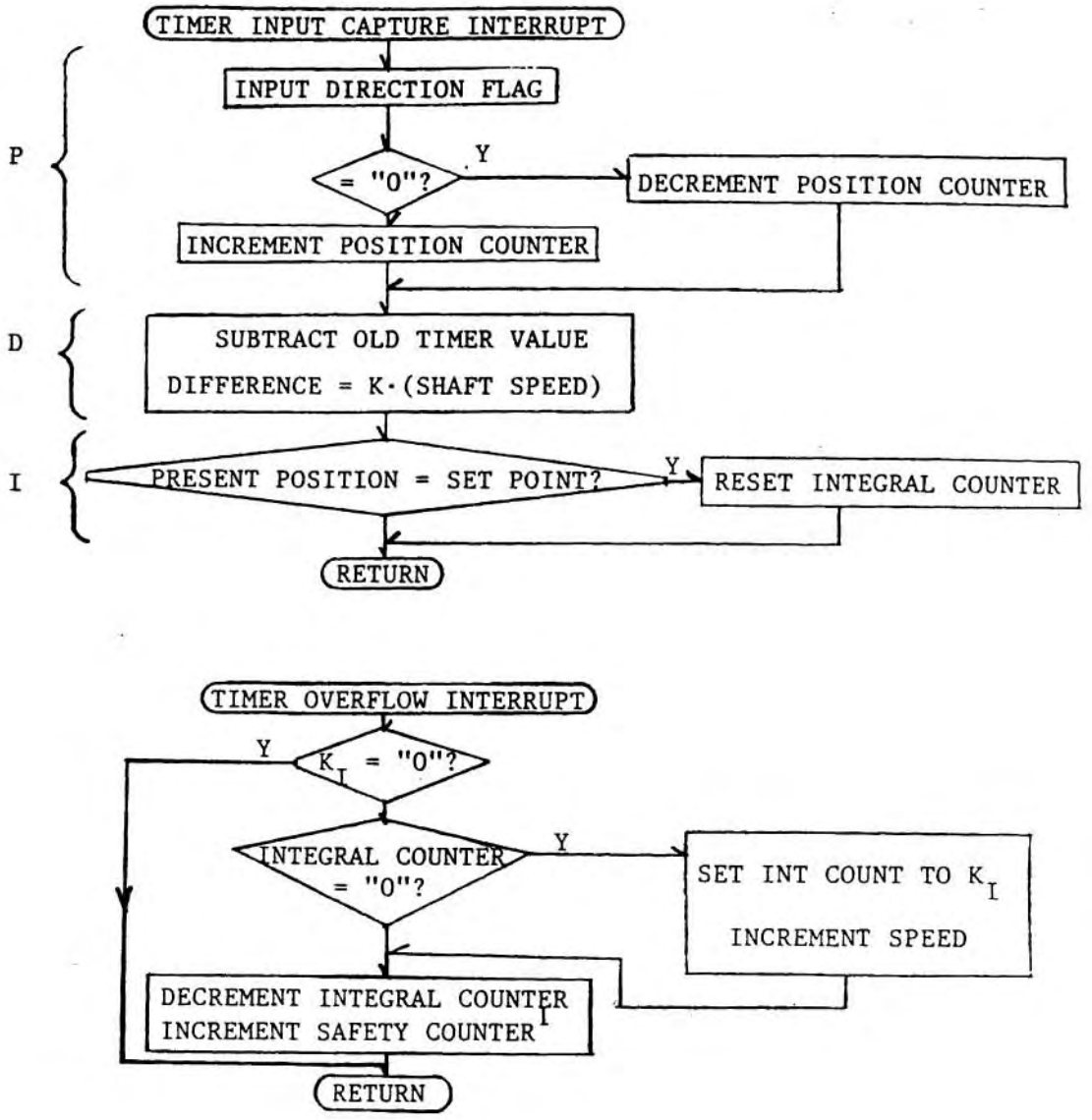

Figure 4.11b Block Diagram of TIMER INPUT CAPTURE and TIMER OVERFLOW Interrupts for the Closed Loop Motor Controller
Note: 1 safety counter reset when motor controller is correctly addressed by the Autopilot.

is included and the gains in this model are programmable. The model of the fish (discussed in detail in section 5.4) is severely damped but the gains can be changed to optimise the fish response.

A block diagram of the autopilot is shown in Figure 4.12. The two UARTs allow the SAIL pass through mode to enable higher level controllers to monitor and test the individual sub systems. Note that the autopilot is not concerned with the details of the phase measurements or the motor control (ie. it is unaware of the actual time varying position of the control surface). The autopilot program contains a simple model of the fish dynamics.

The autopilot cpu is only concerned with (1) the averaged phase differences; (2) the motor set points; and (3) the status of each slave module. If all five slave status values are valid, normal operation ensues. If any single status value defaults, a default mode is engaged until the slave status value becomes valid again.

The accelerometer and rate gyro inputs, in addition to being part of the control algorithm, are of engineering value in the evaluation of fish performance. Several methods of storing this data exist and were discussed in Section 4.2.3.

4.9.2 The Hardware.

In addition to the two UARTs used to implement the hierarchical SAIL structure, a 10 bit A/D is used to digitize the accelerometer and rate gyro inputs. Additional A/D inputs are used to measure system voltages and sub-system current drain as an aid to fault isolation. The autopilot cpu also has control over the power up of the accelerometers, the rate gyro, the phase detectors, and the motor drivers. The slave processors can also be reset by

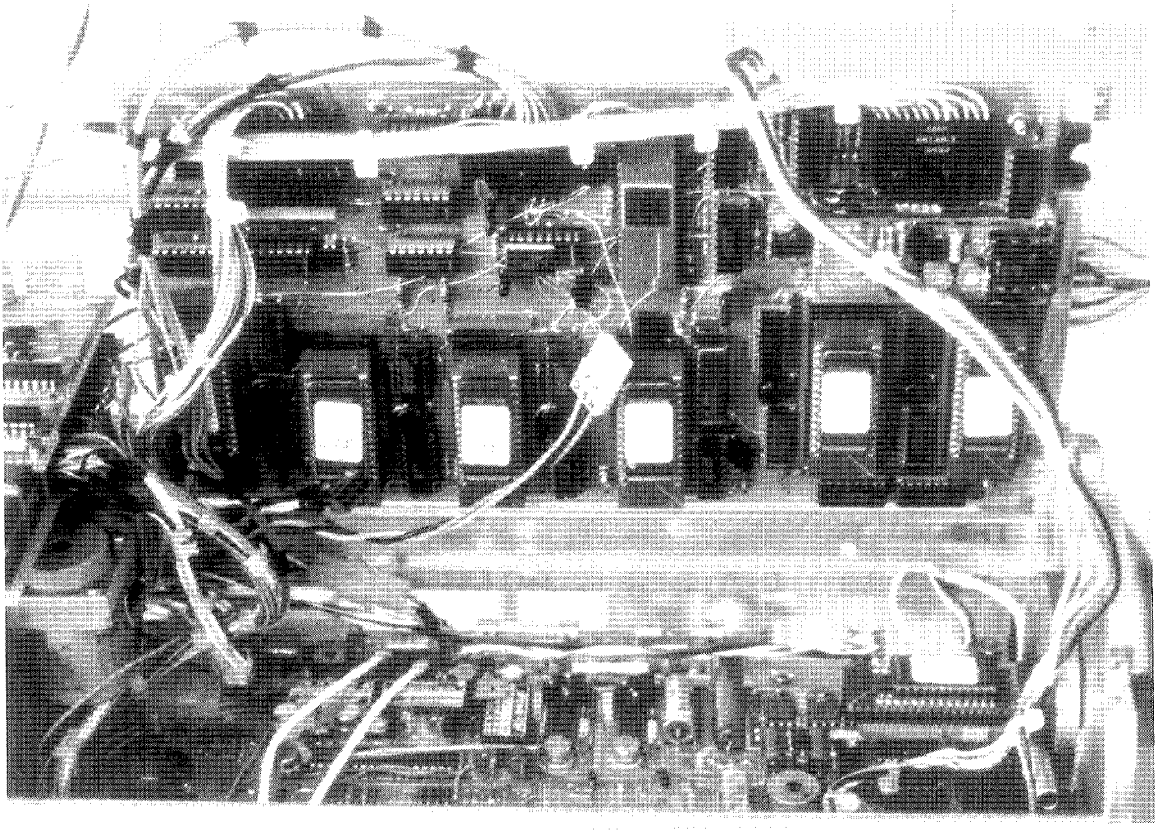

Figure 4.12 The Autopilot Sub-system is comprised of two phase comparators (one for each axis), three motor controllers (one for each axis and one for differential motion to eliminate spin), and one processor to coordinate data flow both within the sub-system and between this sub-system and the main CPU. All six processors are synchronized using a single crystal. An on-board A/D digitizes the signals generated by the accelerometers and the rate gyro and measures sub-system voltages and currents.

the autopilot.

4.9.3 The Software.

The Autopilot control word is an 8 bit word defined in Table 4.3. Bits 5, 6, and 7 of the control word determine which of the auxiliary components are powered up. Bits 0, 1, and 2 determine the operating mode of the autopilot. If bit 0 is set, the autopilot shuts down the slave processors and then goes into a low power standby mode. If bit 1 is set, the normal homing control loop is executed. If bit 2 is set, only the A/D is exercised. Since the A/D can be configured as a DVM, this last operating mode can be used to monitor system voltages and current drains during the fault isolation process. Figure 4.13 is a block diagram of the resident Autopilot program.

4.10 RECOVERY AIDS

4.10.1 The Pinger

The pinger module is another microprocessor based sub-system which can

-trigger a change in the ping rate to alert the surface of a major change in status (eg. dive abort or ballast drop)

-drop the ballast weight independently of the main weight release circuitry (an electrically ORed system).

The ping rate is programmable and constitutes the only communication between the fish and the surface ship during deployment. The pinger allows the ship to keep track of the range and bearing to the fish during deployment. Special ping sequences signify ballast release and loss of lock on the homing beacon. If communication between the pinger processor and the main cpu breaks down, the default condition is to abort the dive. In

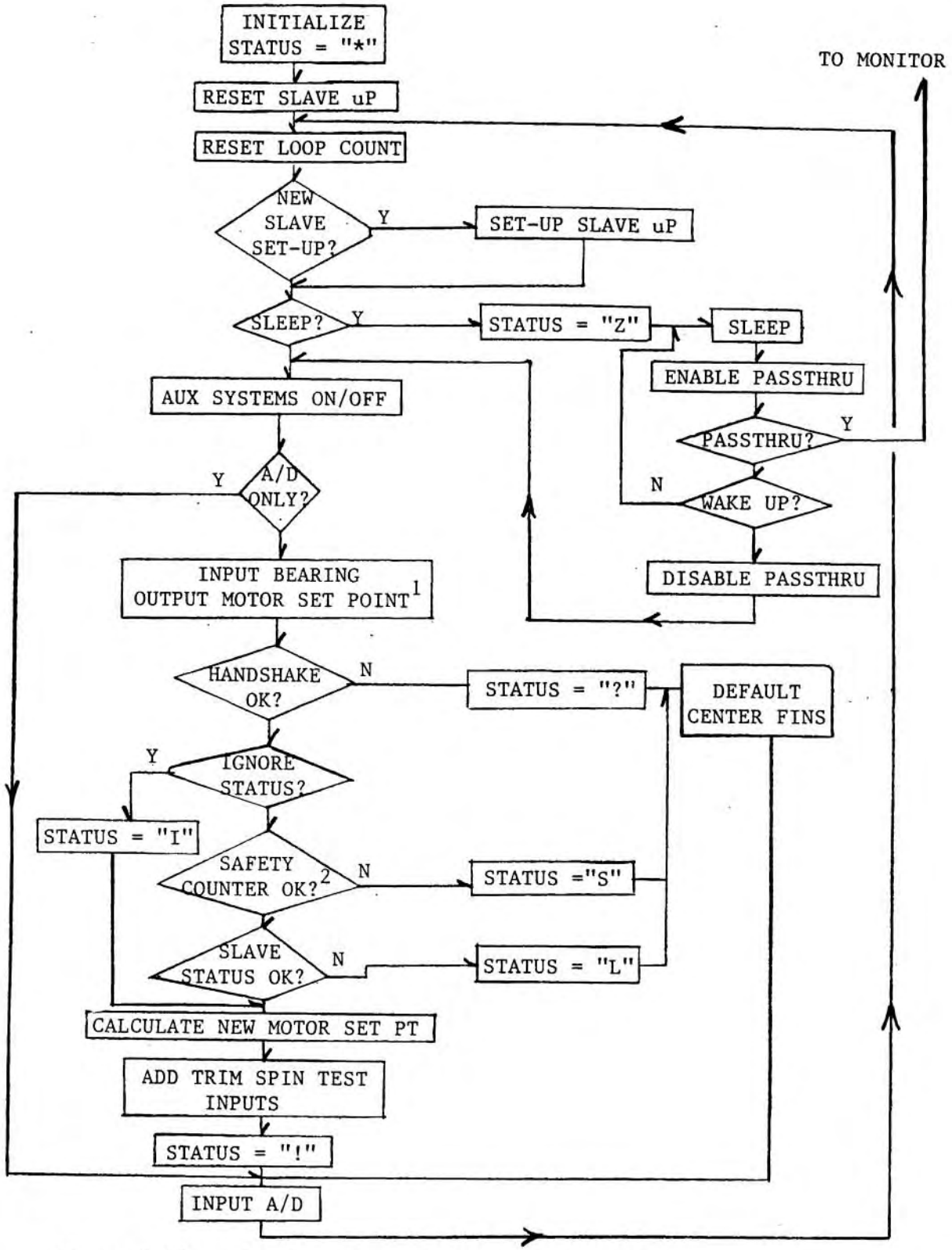

Figure 4.13. Block Diagram of Autopilot Program.
Notes: 1 Motor Set Point Generated from Previous Bearing Input
2 Safety Counter is Reset when Autopilot is Addressed by the Main CPU.

addition, if any of the subordinate processors should give a bad status byte, the dive may be aborted (ie. the main cpu drops the ballast weight, instructs a change in the ping rate, and attempts to home).

4.10.2 The Strobe Lights.

Two strobe lights are faired into the forebody of the fish to increase visibility at night once the fish is on the surface. They are held off by two logical signals from the main cpu which is programmed to turn them on and off as a function of depth.

4.11 BATTERY SELECTION

Under normal operating conditions the fish is not opened. A four conductor cable dumps data and recharges the batteries. By definition, this precludes the use of primary cells. Mission duration is roughly 30 minutes. Of this, the electromagnet only operates during decent and the three motors operate only during ascent. The total power consumption is closely tied to the control effort exerted by the motors. At worst case, the total power consumption is 10 Watt-hours per dive.

A 100-Watt-hour battery pack made up of rechargeable lead acid D cells was used in the prototype. Though a conservative choice from the energy per pound or energy per volume criterion, they are simple, inexpensive, reliable batteries with a long shelf life, low internal impedance, and good low temperature characteristics. The potential for hydrogen outgassing during battery re-charge was addressed with a purge plug used to circulate dry air around the electronics when the fish is on deck. During transportation, with all peripheral devices shut off to minimize quiescent power drain, the

instrument can continue to keep a real time clock and monitor its status for months.

5. VEHICLE DYNAMICS AND CONTROL

5.1 THE COMPLEXITY OF THE MATHEMATICAL MODEL.

Modern instrument design incorporates servo loop technology on many levels. In the Flying Fish, for example, one can describe the local feedback around each operational amplifier in a circuit in terms of servo loop vocabulary. On a larger scale, sub-systems such as the tracking receiver or the motor controller can be described in a similar manner. And of course the entire Fish attitude is servoed so that a zero phase difference is measured between the hydrophones within the array. The degree to which these servo loops interact determines the complexity of the model used to predict vehicle performance. The degree of interaction can be estimated by determining the characteristic time constants of each level within the servo loop heirarchy. Factors of 10 provide a practical boundary.

5.2 THE CHARACTERISTIC TIME CONSTANT OF THE TRACKING RECEIVER.

The response characteristics of the tracking receiver are set by the bandwidth of the Phase Locked Loop (PLL). As discussed in Section 2.7, a small bandwidth gives higher signal to noise ratios. The lower limit on the bandwidth is set by the capture characteristics of the PLL. This limit resulted in a tracking receiver bandwidth of 10 Hz.(ie. a characteristic time constant of 0.1 second.

5.3 THE CHARACTERISTIC TIME CONSTANT OF THE SERVO MOTOR.

The control surface actuator is slew rate limited and does not lend itself to linear modeling. An upper bound on the performance of the actuator is given by the linear model of the motor/gear train as described in Section 4.8.3. By including the gear train and limiting the actuator deflection to +/-15 degrees, a response time of order 1 second was estimated. For large excursions of the control flap, the motor drive is saturated and this linear estimate is no longer valid. In this case, a degraded response time of order 2 seconds may represent the motor dynamics more accurately.

5.4 THE CHARACTERISTIC TIME CONSTANT OF THE FISH IN RESPONSE TO RUDDER DEFLECTIONS.

5.4.1 Deriving The Equations of Motion.

The Flying Fish can be modelled as a rigid body moving through an infinite fluid. The vehicle dynamics include six degrees of freedom (corresponding to three linear and three angular velocities); body geometry, mass distribution within the body, and fluid properties are assumed to be the only variables of importance. The effects of cavitation, surface tension, gravity waves, separation, and Coriolis and centrifugal forces are neglected. For a streamlined free-fall body at terminal velocity with minimal maneuvering requirements, linearization of the equations of motion about steady straight ahead motion is a reasonable assumption (Abkowitz, 1969). This results in 6 (one for each degree of freedom) first order linear cross-coupled differential equations. For the case of an axisymmetric body, many of the

cross-coupling terms are zero and some of the differential equations can be decoupled. If the center of gravity of the fish is assumed to be on the axis of symmetry, the equations describing pitch and yaw motion are identical. Further, roll can be treated as a separate single degree of freedom system which is not critical to directional stability.

For motion in the X-Y plane (and by symmetry in the X-Z plane) and no roll, the equations of motion reduce to those including drag, lift, and pitch. For streamlined bodies, small changes in angle of attack have a negligible effect on the drag (Abkowitz,1969; Abbott and von Doenhoff, 1959), reducing the equations of motion to a system of two first order linear differential equations relating lift and pitch (see Equation 5.1).

5.4.2 Evaluating the Coefficients in the Equations of Motion.

Numerical values of the coefficients are needed to quantify vehicle response characteristics. Because adequate facilities were not available for model tests, existing theoretical and empirical methods, developed for airships, torpedoes, and missiles, were exploited and compared with the performance of a full scale prototype whose design was based on calculated values.

The dimensionless coefficients for ellipsoids moving through an invicid fluid were first derived by Lamb (Lamb, 1932). Because of the invicid assumption, the derivation does not predict drag characteristics. Nevertheless, a good first approximation of the pitching moment can be calculated. For the special case of an ellipsoid, the three planes of symmetry eliminate all cross-coupling terms in the equations of motion and only three unique quantities are needed to

estimate the vehicle motion. Figure 5.1 shows these quantities as a function of varying length to diameter ratio. The errors introduced into the diagonal terms in the matrix describing the equations of motion by modelling any axisymmetric streamlined shape by an ellipsoid with the same L/D is easily outweighed by the resulting simplification in the mathematical model of the vehicle (Abkowitz, 1969). However, additional off diagonal terms, which arise from fore-aft asymmetry, and which are not adequately described by Lamb, must be included in the equations of motion. The need to introduce fore-aft asymmetry is a practical result of the following two considerations:

1.Drag. Separation arising from the inability of the boundary layer to overcome an adverse pressure gradient over the aft section of the body can dramatically increase the form drag. This form drag is relatively insensitive to the shape of the fore body but is a strong function of the afterbody taper ratio (L/D of the body aft of the maximum diameter). For a given body length and maximum diameter, the drag characteristics can be optimized by moving the maximum diameter forward of the mid-chord.

2.Stability. A bare streamlined hull is inherently unstable. The addition of lifting surfaces aft of the center of gravity is essential if stable flight is to be guaranteed. Sizing the stabilizing fins is discussed in detail in Section 2.3.2.

The result of moving the maximum diameter forward and adding stabilizing fins in the stern introduces several off-diagonal elements into the matrix of coefficients that describe the equations of motion. Note that in the general case, these coefficients are time varying. For the purposes of this work, the manuevering is minimal and constant

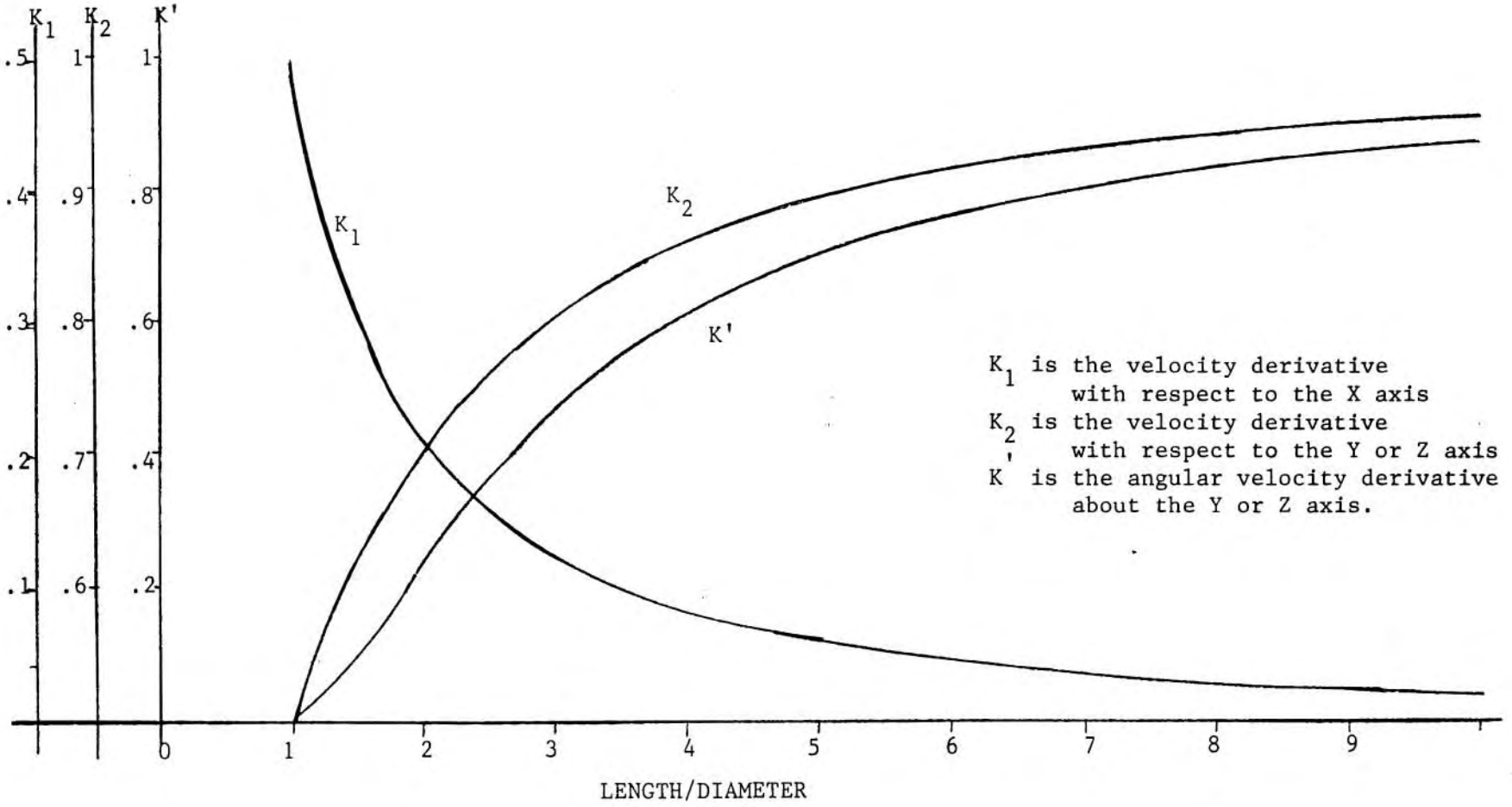

Figure 5.1 Lamb's Coefficients for Prolate Sheroids of Varying Length to Diameter Ratio (after Lamb).

coefficients are assumed.

Landweber's empirically derived velocity derivatives (see Table 5.1) and Abkowitz' derivation of the acceleration derivatives formed the basis of estimating the off-diagonal elements in the equations of motion.

Equation 5.1 shows the coupled pitch/lift relationship. For the Flying Fish, the two roots of this linear system of equations are -18 and -2.2. Both roots are real and separated by approximately an order of magnitude. Thus, the fish dynamics simplifies further to two first order systems where the faster time constant corresponds to pitch and the slower time constant corresponds to lift. The position of the pole corresponding to pitch dynamics is governed by the ratio of the bare hull upsetting moment to the stabilizing moment generated by the fins. If the stabilizing fins are made smaller, the pole moves toward the right half plane and the vehicle responds quickly to changes in rudder angle. If the fins are made larger, the response becomes more sluggish.

5.4.3 The Effect of Motor Dynamics on the Closed Loop Control of Pitch.

The Flying Fish is servoed to a specific heading relative to an incoming acoustic plane wave. Consequently, pitch is the dynamic response of interest. The characteristic time constant of the pitch dynamics is of order 0.5 seconds. Unfortunately, this time constant is of the same order as that which describes the motor-actuator dynamics. Thus, the motor dynamics must be included in any analysis of the vehicle response to perturbations in desired heading. The model used in this study is shown in Figure 5.2.

The set point can either be zero (in which case the trajectory is a

$$\begin{bmatrix} (Y_{\dot{v}} - m)S + Y_v & (Y_r - mU_o) \\ N_v & (N_{\dot{r}} - I_z)S + (N_r - mX_G U_o) \end{bmatrix} \begin{bmatrix} v \\ r \end{bmatrix} = 0$$

Equation 5.1 Coupled Pitch and Lift Equations for an axisymmetric shape, linearized about steady straight ahead motion (after Abkowitz).

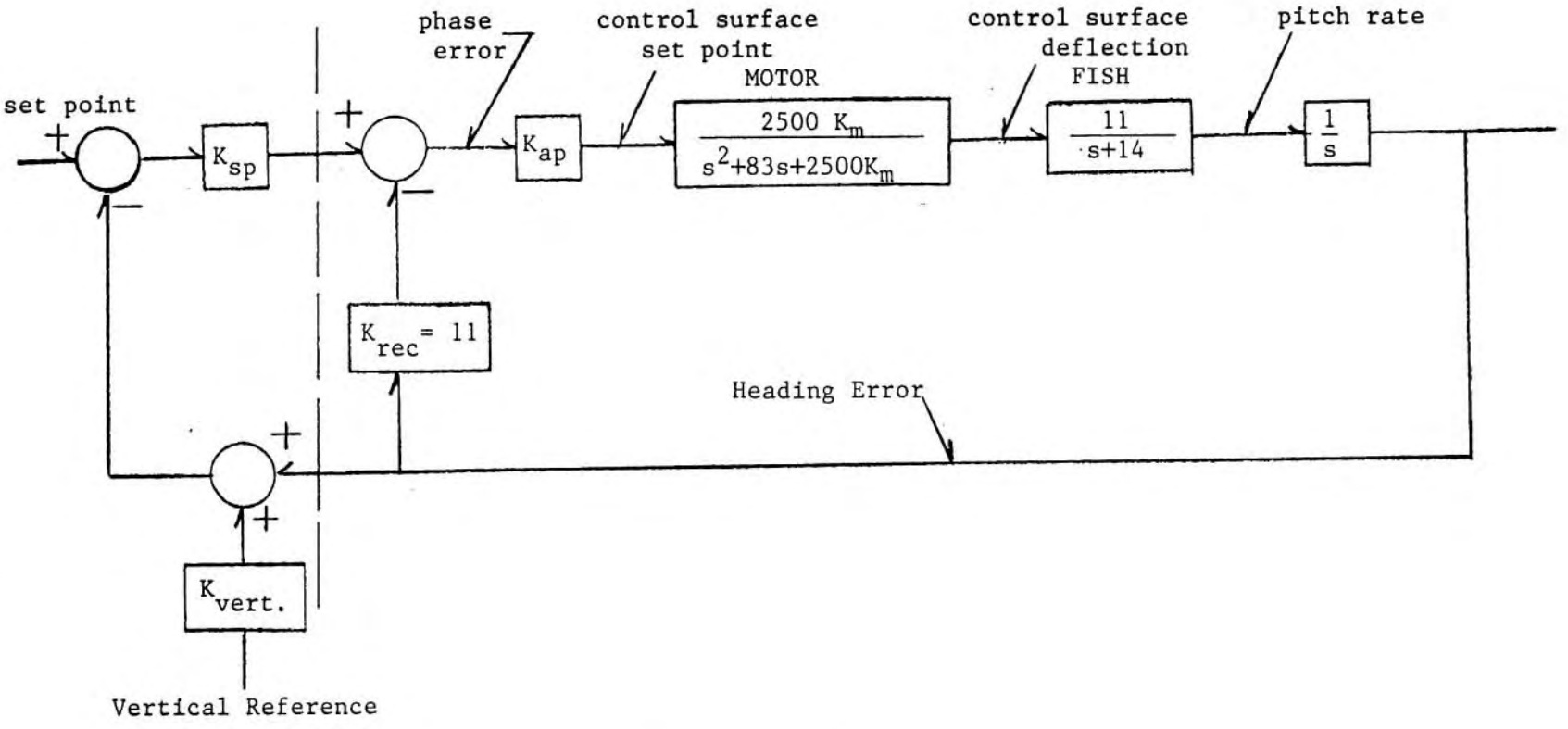

Figure 5.2. Block Diagram of the Control Loop (1) without a vertical reference input and (2) with a vertical reference input.

non-optimum logarithmic spiral as described in Section 2.5) or some value determined by an additional control loop that is measuring the local vertical (in which case the trajectory is a straight line toward the homing beacon. The gain of the hydrophone array relating the heading error to the phase error is determined by the hydrophone baseline and the homing beacon frequency. As stated in Section 2.7, this gain is fixed at 11 degrees phase per degree of heading. The motor transfer function relates the control flap set point to the actual position of the flap. The model of the fish dynamics relates the flap deflection to a pitch rate which must be integrated to give the fish heading. The autopilot gain can be varied to achieve the desired fish performance. In addition, there is some lattitude in independently programming the motor gain. The root locus plots for several autopilot and motor gains are shown in Figure 5.3. Despite some serious questions about the crudity of the model used in this analysis, several important conclusions can be drawn from these plots:

-The generic shape of the Root Locus is the same for all motor gains.

-A large autopilot gain can result in instability.

-A sluggish motor (low motor gain) will promote instability.

-Though the actual coefficients in the model may have large errors, this analysis is helpful qualitatively in analyzing the data generated by the sea trials and making adjustments in the field.

-The offset introduced to eliminate the tendency toward spiraling depends on the glide angle to rudder deflection ratio discussed in Section 2.6. For the limited operating range of the Flying Fish, this ratio is a constant.

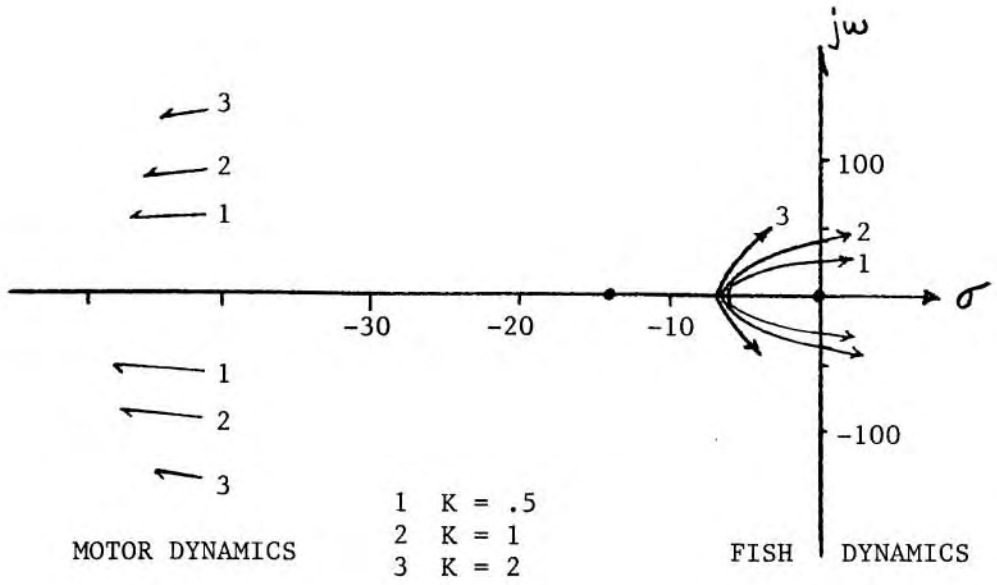

Figure 5.3 Root Locus of the Flying Fish as a Function of both Autopilot Gain and Motor Gain. The Motor Gain K was allowed to vary over a range which brackets the desirable damping coefficient of .707 as shown in Figure 4.10. As expected, a faster motor response improves stability but too high a feedback gain in the autopilot (between heading error and rudder angle) can lead to instability. Note that even though the motor poles are well to the left of the fish poles, they are responsible for shaping the trajectory of the fish poles and contribute to potential instability.

5.4.4 The Roll Dynamics.

From symmetry arguments, the roll dynamics can be decoupled from the pitch and yaw dynamics. Though the roll dynamics do not directly affect the stability of the vehicle, roll may affect the homing capability of the fish if the plane of actuation is allowed to rotate away from the sensing plane (ie. if, between sensing a phase error and changing heading, the vehicle is allowed to rotate. An additional reason to study the roll dynamics has to do with a future desire to spin the vehicle about its longitudinal axis for profiling currents electromagnetically.

Because of the vehicle symmetry, no restoring force exists. Thus the asymmetry results in a constant rate of spin. A first assumption is that any spin (caused by vehicle asymmetry resulting from imperfect weight distribution, faults in the syntactic foam or imperfections in the stabilizing fins) is independent of the angle of attack of the vehicle. The resulting constant rate of spin, which may vary from vehicle to vehicle or from dive to dive, could be offset with a constant deflection of lone of the fins. This, however, would require careful calibration of each unit. Further, mishandling at sea could require recalibration of the spin rate. A closed loop servo which senses angular rate and drives a differential to give zero spin would solve these problems and also handle spin arising from hydrodynamic sources. To simplify the mechanical design of such a differential servo, the differential motion was generated electronically rather that mechanically.

The roll dynamics are described by a first order equation whose time constant depends on the feedback gain. As long as the characteristic time constant is short relative to the length of the homing process, any

errors incurred by an initial tendency to spin will be negated. The model shows the characteristic time constant to be of order 20 seconds, short compared to the 15 minute ascent time. Figure 5.4 shows the interaction of this control loop with the control of vehicle yaw.

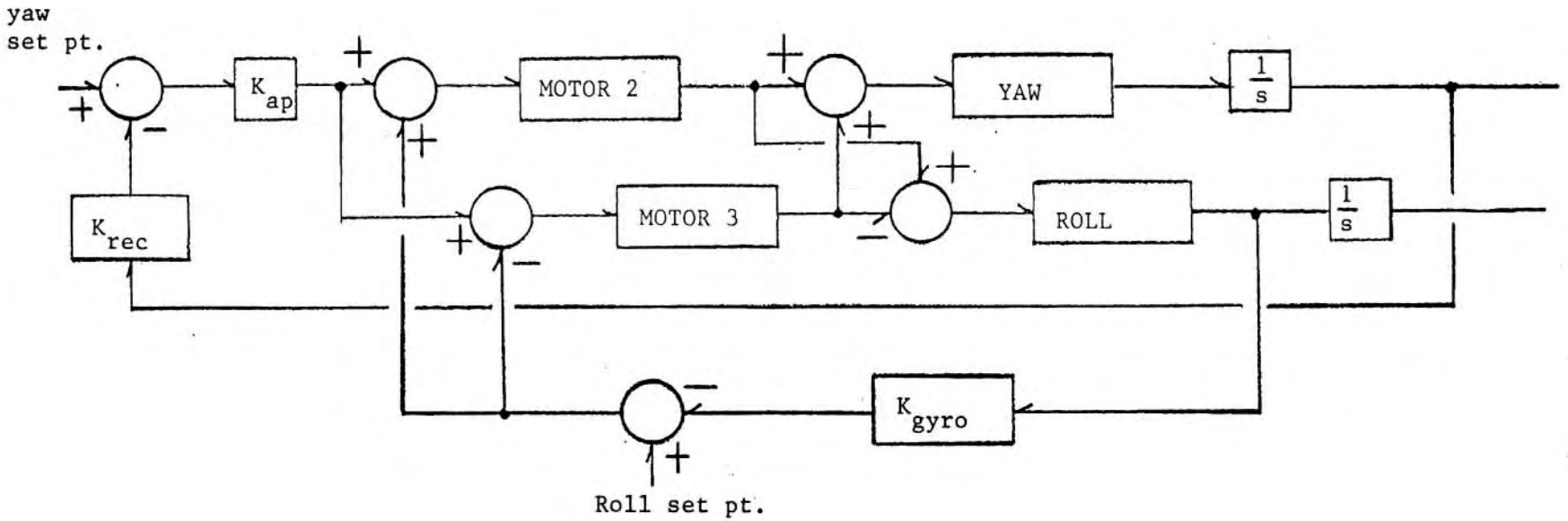

Figure 5.4. Roll Control as a source of differential motion.

6 FIELD TEST RESULTS

6.1 SHALLOW WATER TESTS (25 METERS DEEP).

Shallow water testing of the Flying Fish included: (1) measuring the reserve buoyancy of the vehicle, (2) measuring the vehicle center of buoyancy and center of mass, (3) testing the weight release mechanism, and (4) checking the structural integrity of the fish. These tests are succinctly summarized in Figure 6.1. In the near shore shallow water environment the acoustic multipath confused the receivers and prevented the Phase Lock Loops from acquiring the homing beacon signal. Moreover, the vehicle could not reach realistic speeds to test control surface actuation or vehicle manueverability. Consequently, tests of vehicle manueverability, stability, and homing capability were conducted in relatively deep water (greater than 200 meters).

6.2 HOMING AND MANEUVERABILITY TESTS (220 METERS DEEP).

A site on George's Bank, accessible using the R/V Asterias, in 220 meters of water was chosen for the steering trials. This water depth would allow the vehicle to reach its terminal velocity (30 meters minimum), lock onto the acoustic beacon, and maneuver. Because of the large number of expected problems during the early testing stages, going to sea aboard a large oceanographic vessel for weeks at a time seemed impractical. These logistical constraints were the only reasons for not deploying the fish in mid-ocean. The results of these steering trials, which show accurate homing capability, are discussed below.

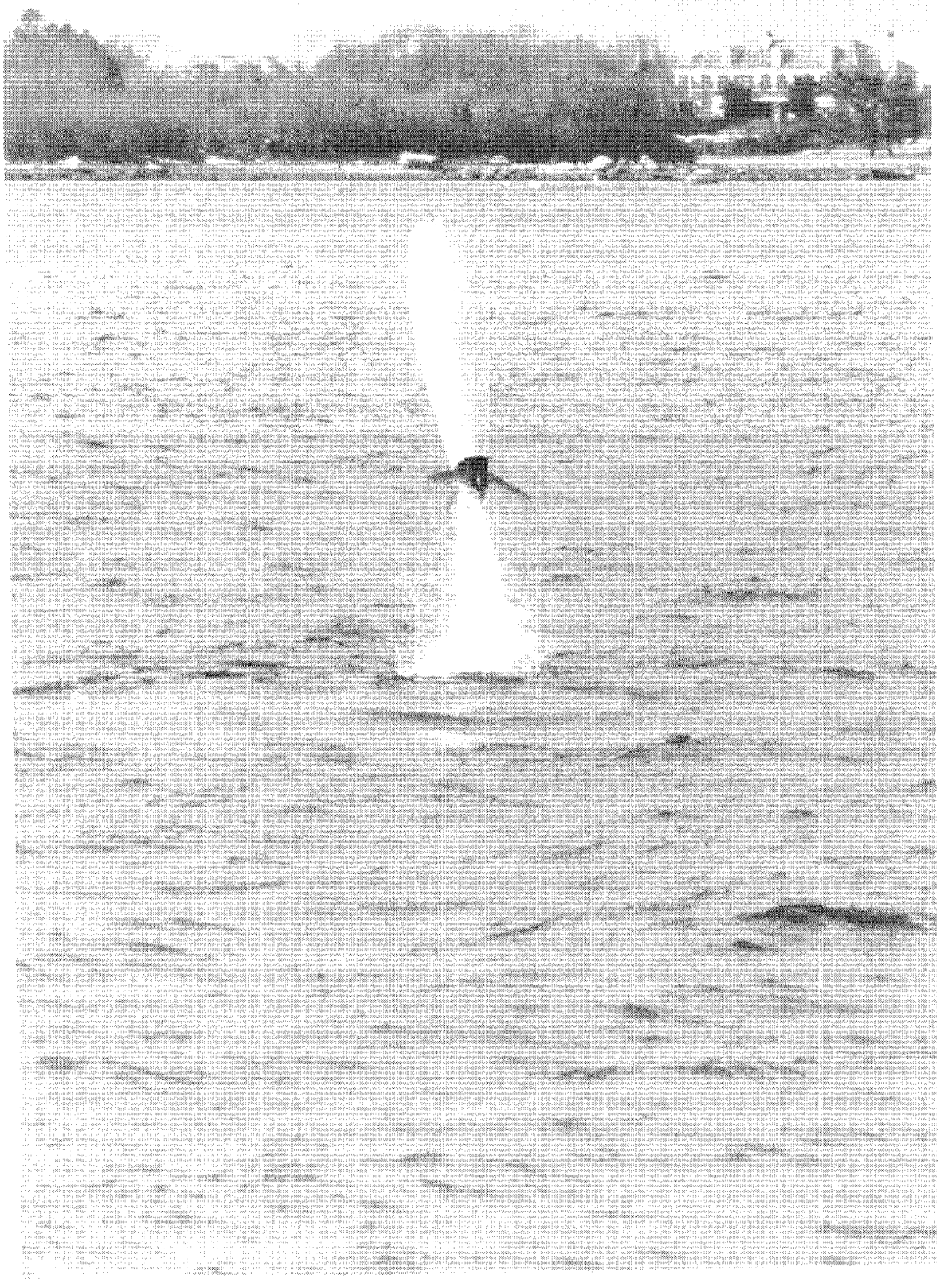

Figure 6.1 Shallow Water Testing of the Flying Fish.

6.2.1 The Deployment Program Used for the Homing Tests.

Figure 6.2 shows a block diagram of the field test deployment program resident in the fish. This program is divided into four parts: (1)Pre-deployment, (2)descent, (3)active homing on ascent, and (4)Recovery. Shown in Figure 6.2 are three conditions that result in the abort of a dive: (1)Sub-system failure, (2)Safety timer, and (3) at the pre-set depth for termination of descent. The last of these is the normal trigger for dropping the weight. Should all of these triggers fail, eventually the battery will drain and the electromagnet will drop the weight. During the trials, a dive was never aborted. During Dive 5, however, the safety timer was required because the pressure sensor malfunctioned.

On ascent, any subsystem failure will cause the instrument to send a new ping code which will alert the support vessel that a problem exists. During Dive 2, when the acoustic signal was fouled by the protective foam around the beacon, the default ping code was received at the surface vessel. Dives 3, 4, and 6 signaled the surface vessel that the fish was attempting to home. Reasons for inaccurate homing during Dives 3 and 4 were attributed to several problems which are outlined in Table 6.1.

6.2.2 The Deployment Procedure.

A total of 6 dives were made during these field trials on three separate excursions. An outline of the procedure used during these deployments is given in Table 6.2. Note that many of the steps in the outline can be automated in future work with the system. For example, the shipboard computer could access the phase difference synthesizer and

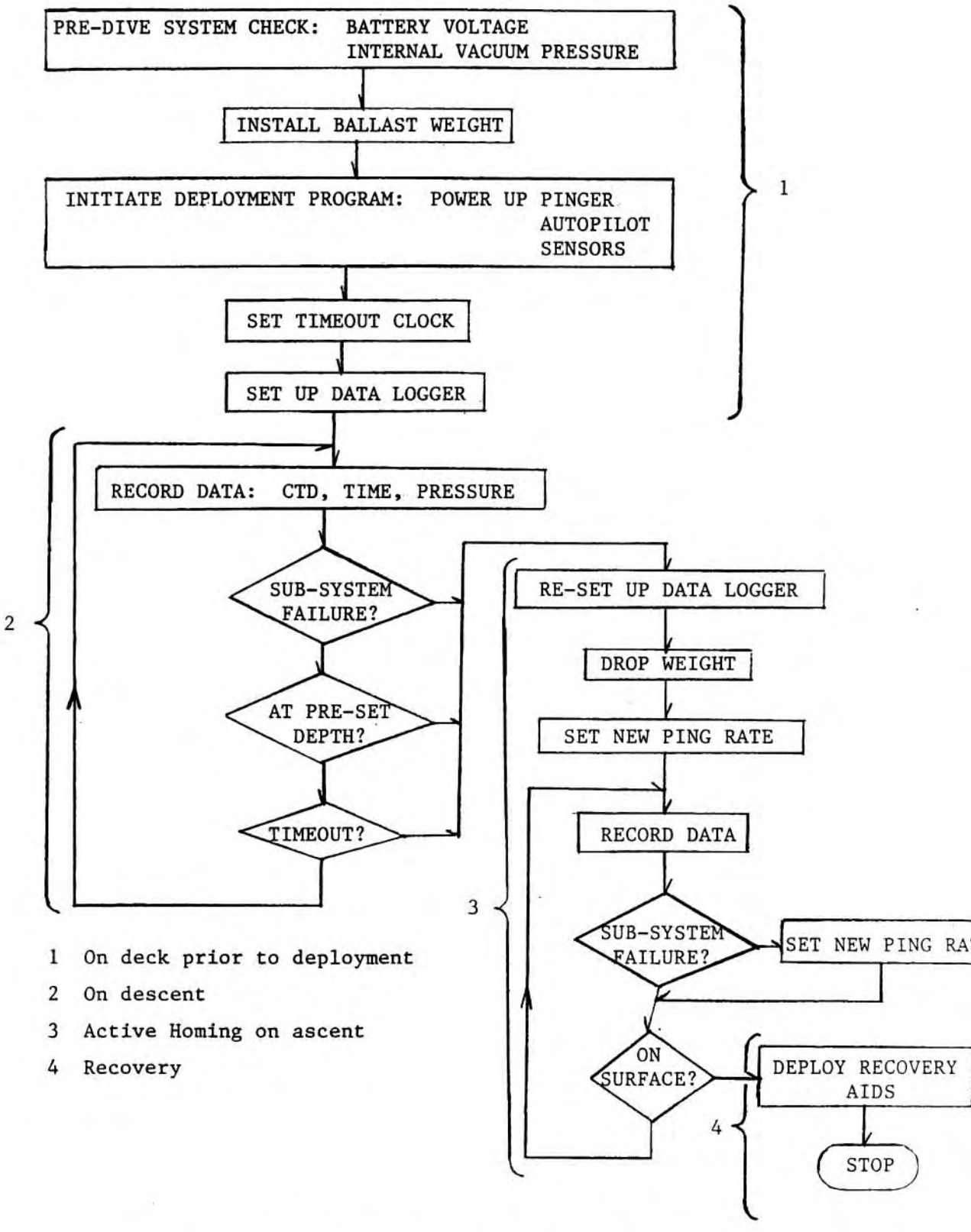

Figure 6.2 Block Diagram of Resident Program Used During Deployment of Fish.

Dive No.	Problems Encountered	Successes Achieved	Action Taken
1	Leak in compensation bladder; salt water shorts out batt. and power transistors; no data.	System together for the first time; all support gear works.	New bladder design; electronics isolated from potential shorts; motor drivers coated with epoxy.
2	Bad acoustic signal.	Full data set from all sensors.	Foam removed from surface beacon (small bubbles seem to absorb acoustic energy).
3,4	Not enough water depth for homing; one bad receiver channel.	Good acoustic phase tracking; full data set.	Designed a new release mechanism and deployment program to allow backwards deployment to eliminate turn around transient.
5	A/D failure; no pressure sensor; instrument hits bottom; no data.	Backup release timer works!	A/D design review.
6	Minor damage to tail during recovery.	Vehicle homed correctly to within 1 meter of surface beacon.	Celebration.

Table 6.1 Summary of Homing Test Dives

1 INITIALIZE SYSTEM (this short program powers up all the sub-systems in the fish and establishes two-way communication with all slave processors)

2 MEASURE PHASE OFFSET (input a known phase difference between the elements in the hydrophone array, then access each phase comparator and measure the offset)

3 ADJUST PHASE TRIM

4 INSERT BALLAST WEIGHT AND ENERGIZE RELEASE MAGNET (once energized, the program idles)

5 SET RELEASE TIMEOUT AND RELEASE DEPTH

6 BEGIN DEPLOYMENT PROGRAM

7 REMOVE SHORE POWER AND SAIL COMMUNICATIONS LINK

8 DEPLOY FISH, HOMING BEACON, AND TRACKING HYDROPHONE

9 MONITOR FISH PINGER FOR TURN-AROUND AND SLANT RANGE AND STATUS (determine whether the fish is actively homing or in default mode)

10 RECOVER SURFACE BEACON, HYDROPHONE, AND FISH

11 CONNECT SAIL CABLE (determine fish status, shut down recovery aids recharge battery and disgorge data onto disk)

12 BACKUP DISK, ARCHIVE RESULTS AND PLOT

Table 6.2 Outline of the Deployment Procedure Used during Homing Tests. Note that all steps could be either automated or prompt the user.

the fish phase comparators, plot the phase input to measured phase of the hydrophone-receiver network, and trim the phase comparators with the appropriate offset. Similarly, the shipboard computer could access the ship's depth sounder and automatically set the ballast release depth.

6.3 INTERPRETING THE FIELD DATA.

Sensors mounted in the fish which generated data during these tests include two accelorometers (pitch and yaw), a depth sensor, a rate gyro, two phase comparators, and three servo motors. In addition, the time and system status generated by the CPU were recorded. Key points in the record are highlighted to allow cross comparisons between the different data sets. "A" denotes the maximum depth measured on a given dive; "C" marks when the fish reached the surface.

6.3.1 The Pressure Record.

The pressure was continually monitored and recorded on board the fish. In addition the pressure sensor is used to trigger the weight release mechanism by comparing the pressure sensor output with a preset number. For near vertical trajectories, the pressure record, when plotted against time, produces a measure of the terminal velocity reached by the fish. Large deviations from a steady velocity are indicative of gross instability in the vehicle control loop. The pressure record near the inflection point at the bottom of the trajectory shows the temporal and spatial scale occupied by the bottom transient. This has several ramifications: (1)it is an indication of how close an approach to the ocean floor can be made without damage to the fish and (2)how long a

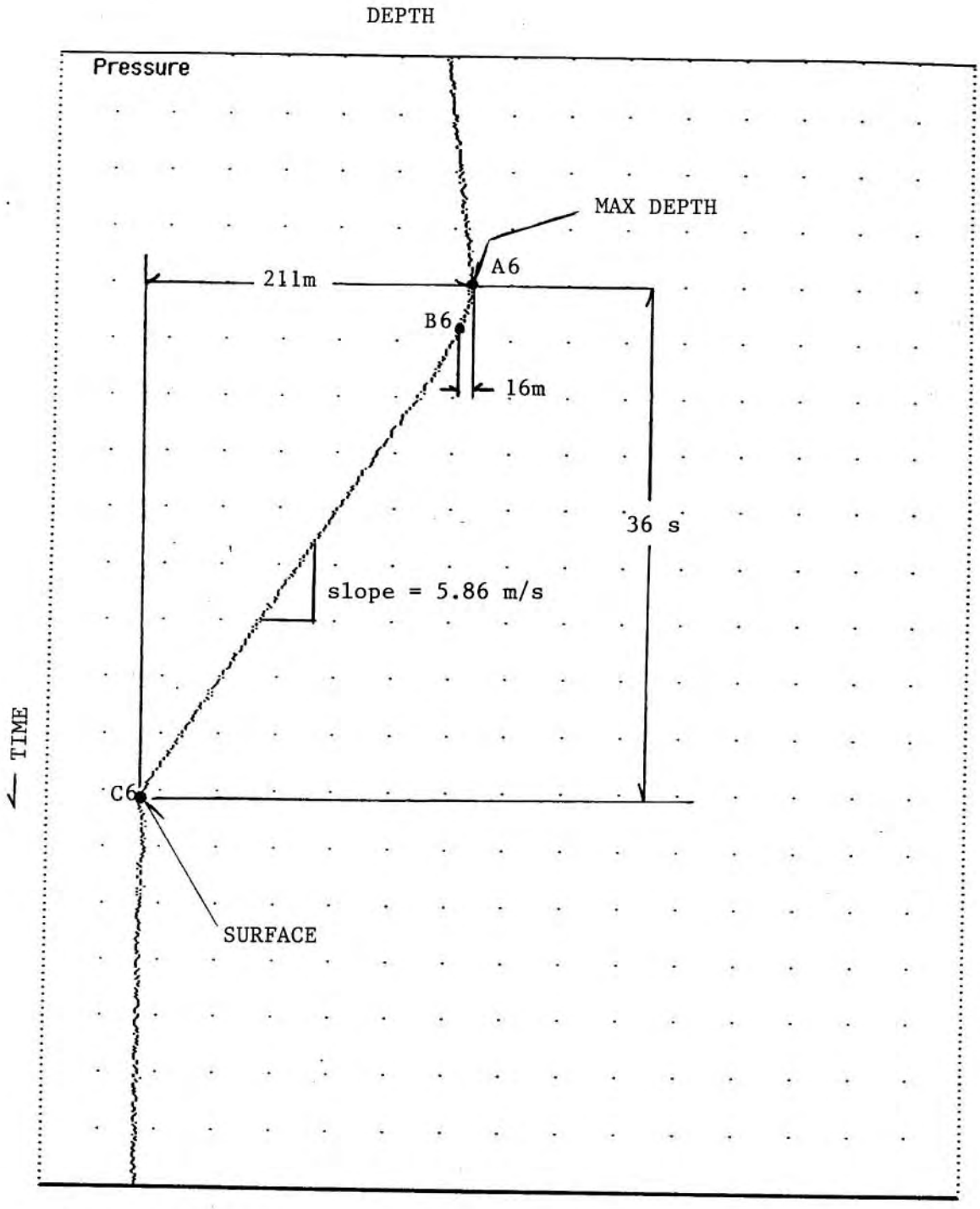

Figure 6.3 The Pressure Record From Dive 6.

delay between ballast drop and acoustic signal aquisition to insure operation within the correct acoustic image.

Of the six dives, four gave complete pressure records. Figure 6.4 shows a typical pressure record. For these early trials, the terminal velocity on descent was purposefully set to a low value (via a small ballast weight) so that the vehicle could crash into the bottom and allow a backup timer to drop the weight should the pressure sensor cease to work (Note: this backup was extremely valuable on Dive 5).

The terminal velocity during ascent ranged over 4 dives from 5.9 m/s to 6.7 m/s with the smaller value attributable to the addition of a release/recovery appendage on Dive 6 that is not an integral part of the fish.

6.3.2 The Accelerometer Record.

The accelerometer record serves three purposes: (1)To show the degree of stability of the overall attitude servo loop. The perturbations in the accelerometer record give a measure of the overall stability of the vehicle. (2)To reconstruct the vehicle trajectory during ascent. If one assumes that the major contributor to the accelerometer output is the instantaneous vehicle attitude relative to the gravitational vector (ie. any lateral accelerations are negligible), then the accelerometer record can be used as a basis for reconstructing the vehicle trajectory. This information is helpful in tuning the control loop gain constants. (3)To show the characteristic vehicle time constant. By correlating the motor set point record to the acceleromenter record, an estimate of the vehicle response

characteristics can be made.

6.3.2.1 The Transient at the Inflection Point (Just After the Ballast is Dropped).

When the ballast weight is dropped, the fish flips from a nose down to a nose up attitude. This dramatic maneuver far exceeds the operating range of the closed loop servo as shown in Figure 6.4. This turn around transient, as measured by the accelerometers, exceeds the temporal and spacial scales of the transient as measured by the depth sensor, showing the insensitivity of the vehicle drag to angles of attack as great as 25 degrees. The size of this transient is small when compared with the total depth of a mid-ocean deployment and has no detrimental effect on the homing capability of the fish. This transient does, however, have a marked effect on the success of shallow water testing. Specifically, by the time the vehicle has reached a stable vertical attitude, the maneuvering room is virtually non-existent. For this reason, subsequent testing in water less than 1000 meters deep is of value only if the vehicle is deployed backwards as done in Dive 6. The small size of the perturbations measured by the accelerometers (see Figure 6.5a) are indicative of a stable trajectory.

6.3.2.2 The Reconstructed Trajectory.

The only dive for which a trajectory can be reconstructed with any confidence is Dive 6. The fundamental assumption inherent in this reconstruction is that the vehicle is in steady motion and that the measured acceleration is related only to the instantaneous vehicle

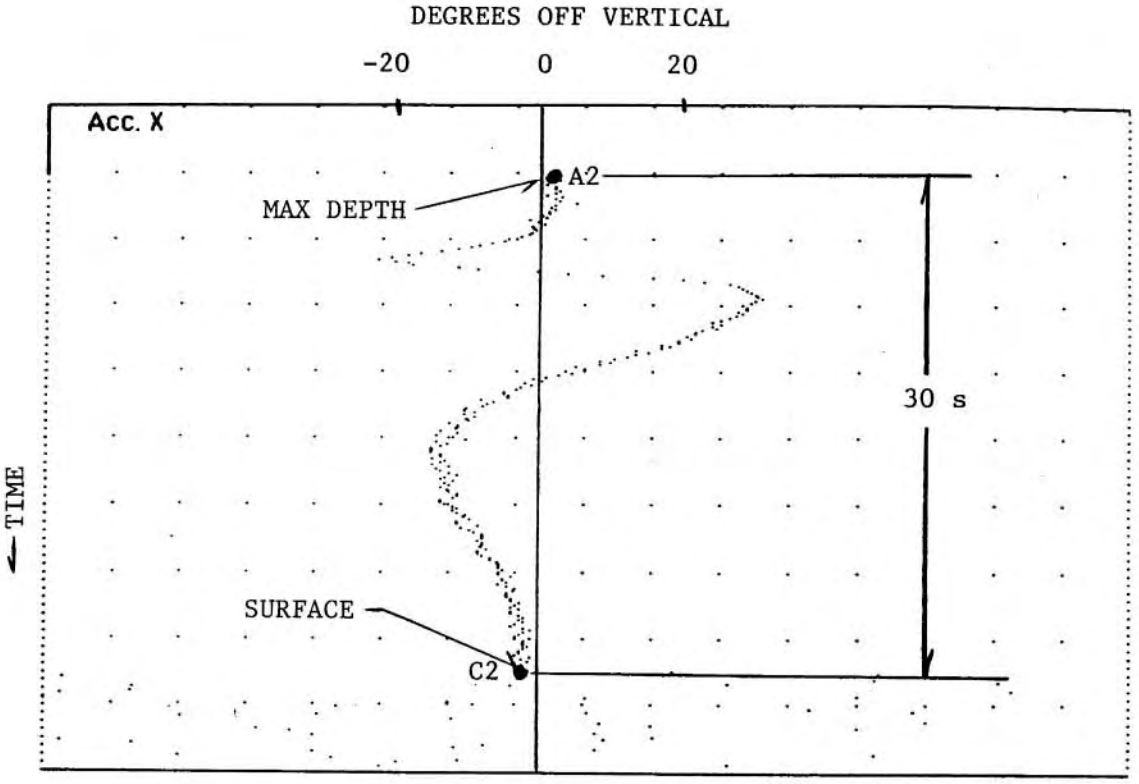

Figure 6.4 The Turn-around Transient as Measured by the X-Axis Accelerometer on Dive 2.

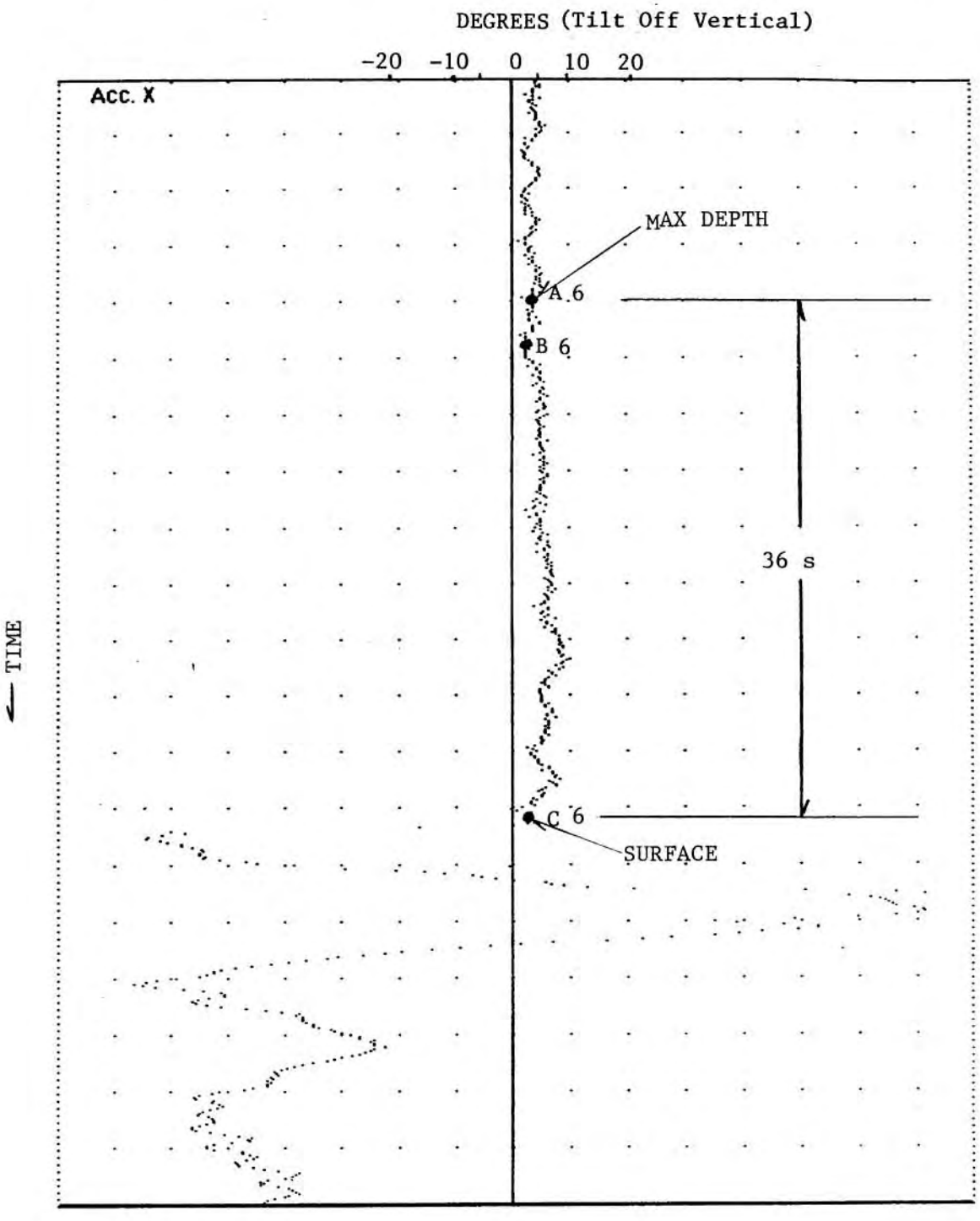

Figure 6.5a The X-Axis Accelorometer Record For Dive 6. Oscillation on Descent (Points above A) is Due to Backwards Deployment.

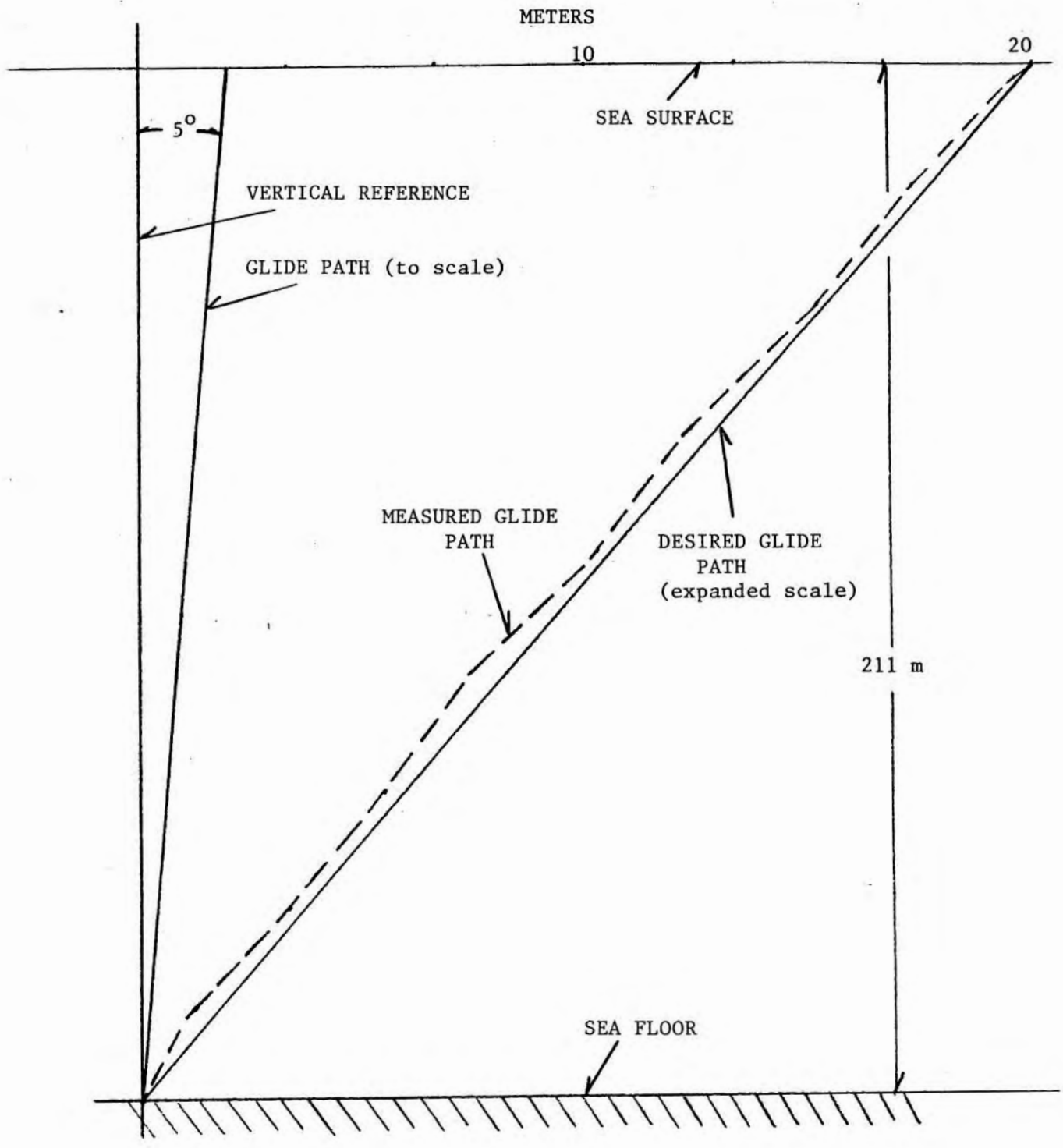

Figure 6.5b Reconstructed Glide Path for Dive 6. in line with the X-Axis Accelerometer.

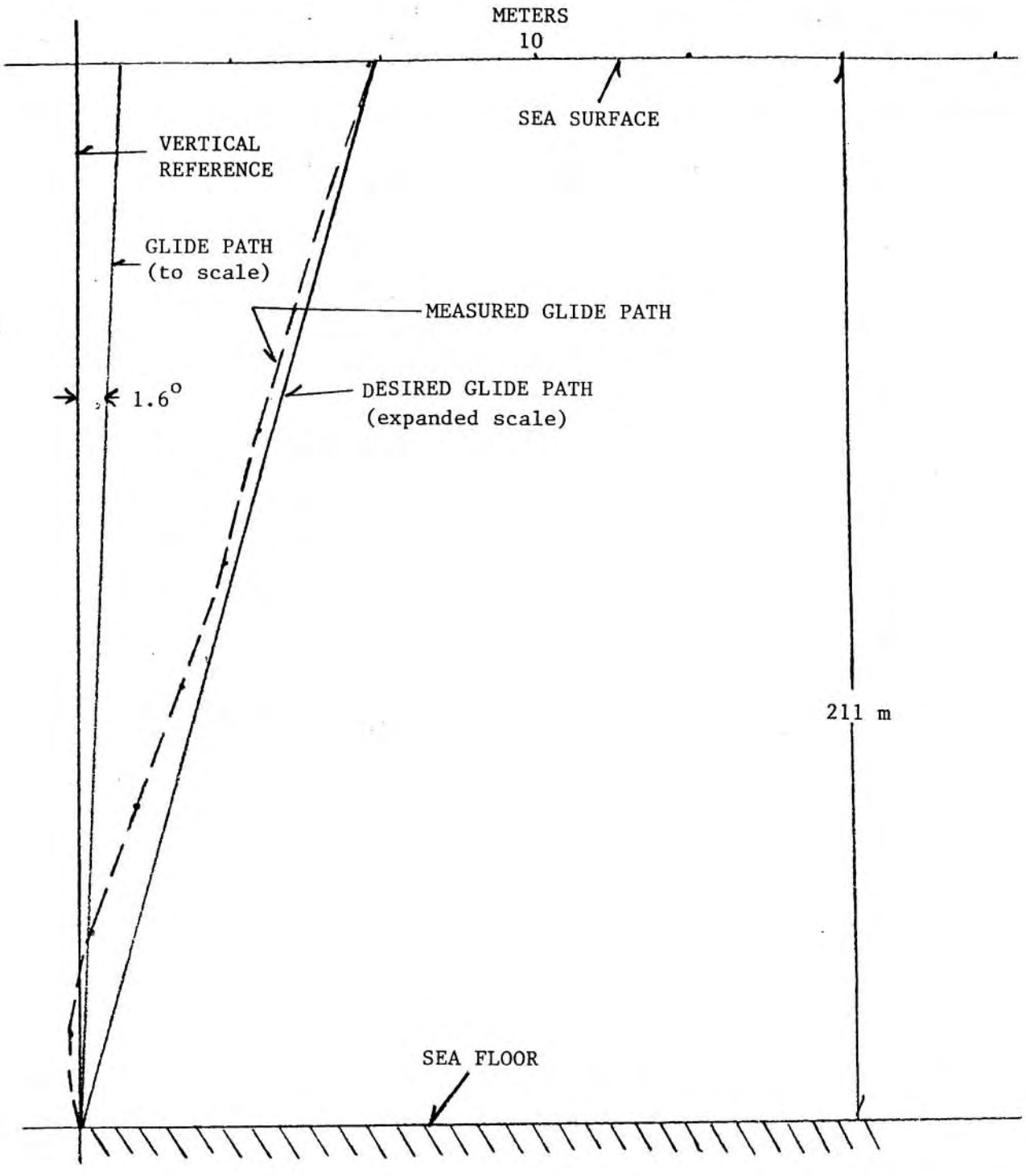

Figure 6.5c Reconstructed Glide Path for Dive 6 in Line with the Y-Axis Accelerometer.

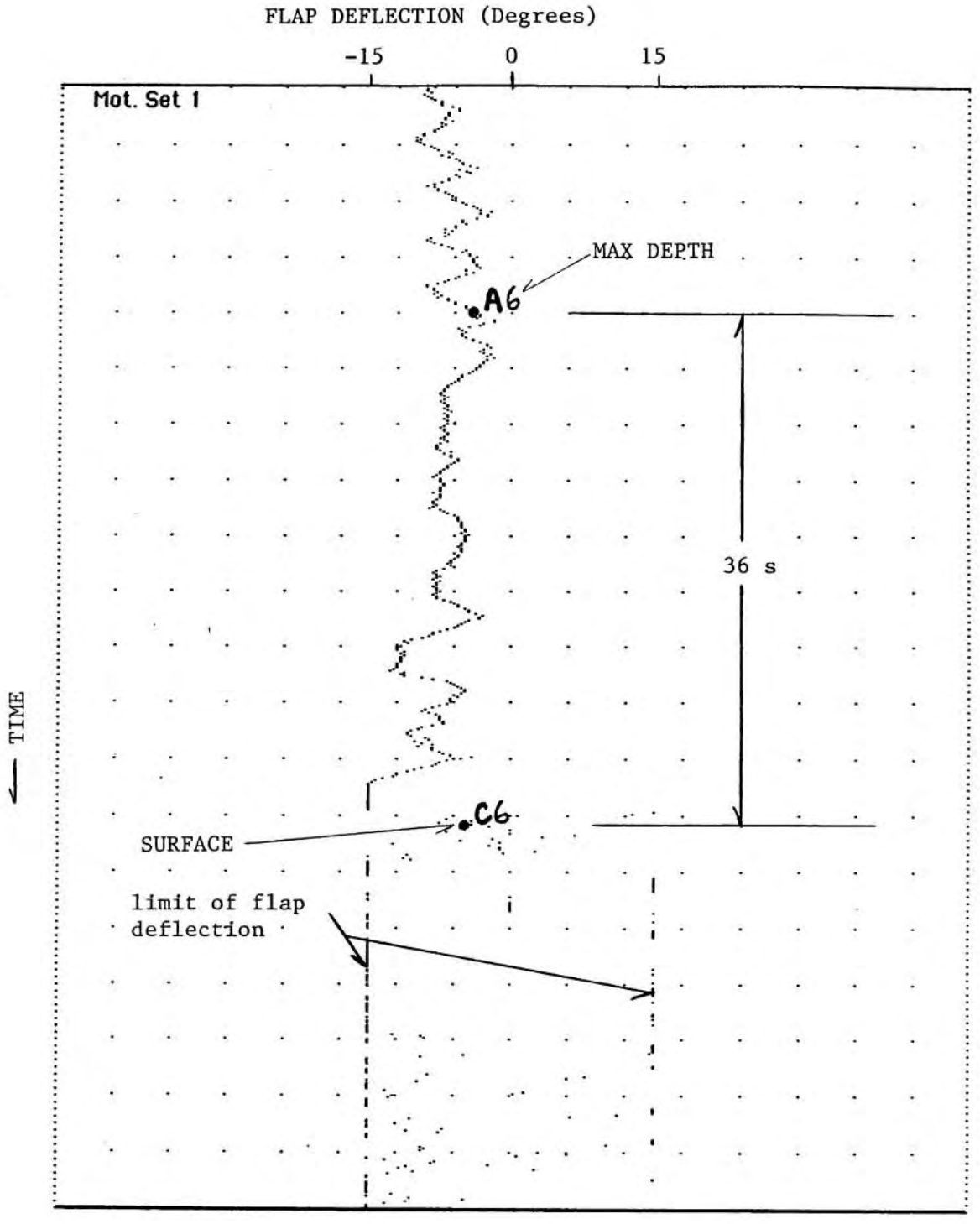

Figure 6.6 Motor Set Point Record for Motor 1 on Dive 6.

attitude. The desired and measured glide path for Dive 6 is shown in Figure 6.5b. The average glide angle for this deployment was about 5 degrees off the vertical. The fish came within half a meter of the beacon, well within the predicted circle of error.

6.3.2.3 The Measured Vehicle Response Characteristics.

By correlating motor set point (ie rudder deflection) to vehicle attitude, a measure of the vehicle response to rudder commands can be deduced. Figure 6.6 shows an attempt to correlate the accelerometer and motor set point data for Dive 6. An estimate of the characteristic time constant of the vehicle in pitch is about 5 seconds, in close agreement with the response predicted by the model derived in Chapter 5.

6.3.3 The Rate Gyro Record.

The rate gyro serves two purposes: (1) as an engineering diagnostic to determine the extent of vehicle asymmetry which was left unmodelled and (2) to measure vehicle rotation as the source of differential motion in the closed loop servo as discussed in Section 5.4.4. If the vehicle were to rotate on ascent, an apparent change in bearing to the surface beacon would result: a 180 degree rotation of the fish would result in a sign change in the measured bearing to the beacon. If this rotation rate were fast relative to the characteristic time constant of the fish in pitch, a potential source of instability would be introduced into the control algorithm. Because this asymmetry was left unmodelled and will change as refinements are made in the weight distribution of the fish, a closed loop servo to zero rotation via differential motion of the control

surfaces was implemented. Long term zero drift of the rate gyro output is assumed to be slow compared with the vehicle pitch response to changes in rudder angle.

Figure 6.7 shows the raw rate gyro record from Dive 4 and Dive 6. Dive 4 measured vehicle rotation but did not act on this information. Dive 6 included rotation in the control loop. During Dive 4, the vehicle appears to have rotated approximately two complete revolutions in 450 feet of water due to unmodelled asymmetry in the fish. Dive 6 had no measurable net rotation.

6.3.4 The Phase Comparator Record.

The phase comparator is an instantaneous measure of the error signal as measured by the short baseline acoustic interferometer (ie. it is a measure of the bearing to the surface beacon). This error signal is the input to the autopilot algorithm which determines the motor set points. The phase comparator signal is affected by (1)source strength, (2) multipath and cross coupling between hydrophones, (3) source frequency, (4) flow noise, and (5) vehicle rotation. Figure 6.8 shows the phase comparator record for Dives 2, 3, and 6. During Dive 2 the phase comparators had trouble aquiring the signal. This was attributed to small bubbles in the foam block that protected the homing beacon (in subsequent dives, the foam block was removed, resulting in good signal aquisition). As designed, when the system status reflected a problem with signal aquisition, the control surfaces defaulted to zero deflection.

The extreme variability in the phase signal in Dive 3 can be attributed to a number of problems including: (1) the turn around

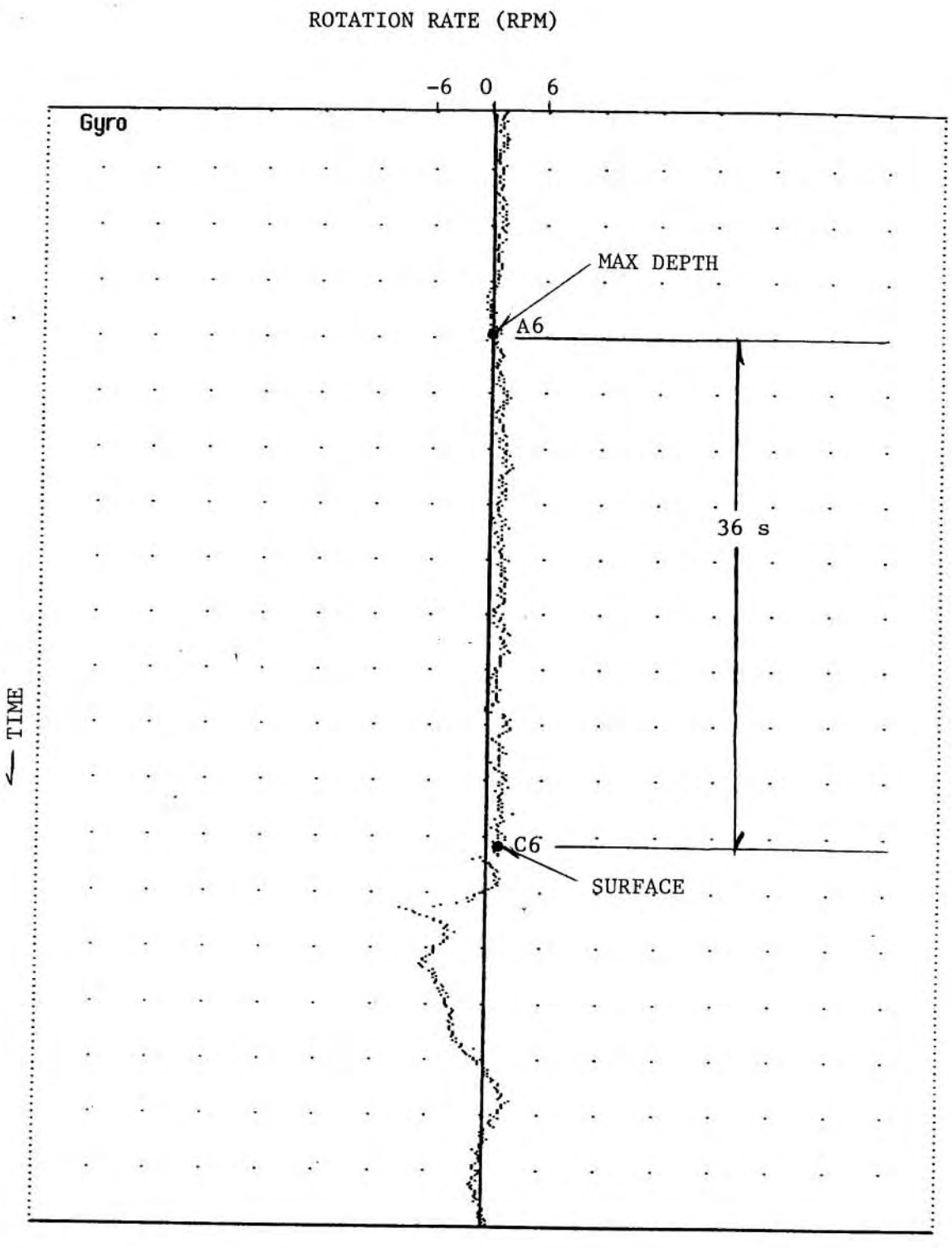

Figure 6.7a The Rate Gyro Record From Dive 6. Note that the rotation rate is much less that in Figure 6.7b where no differential control action was exerted.

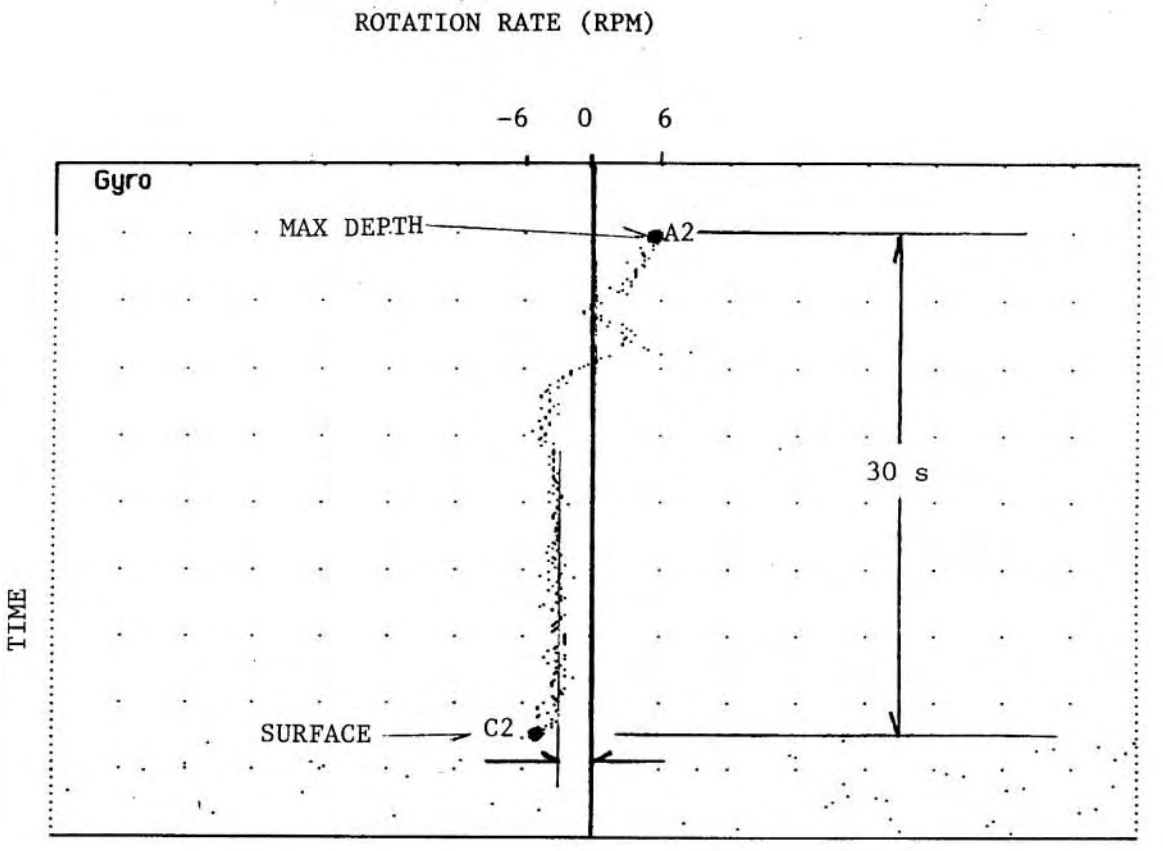

Figure 6.7b The Rate Gyro Record From Dive 2. Note the constant rate of rotation after the turn-around transient.

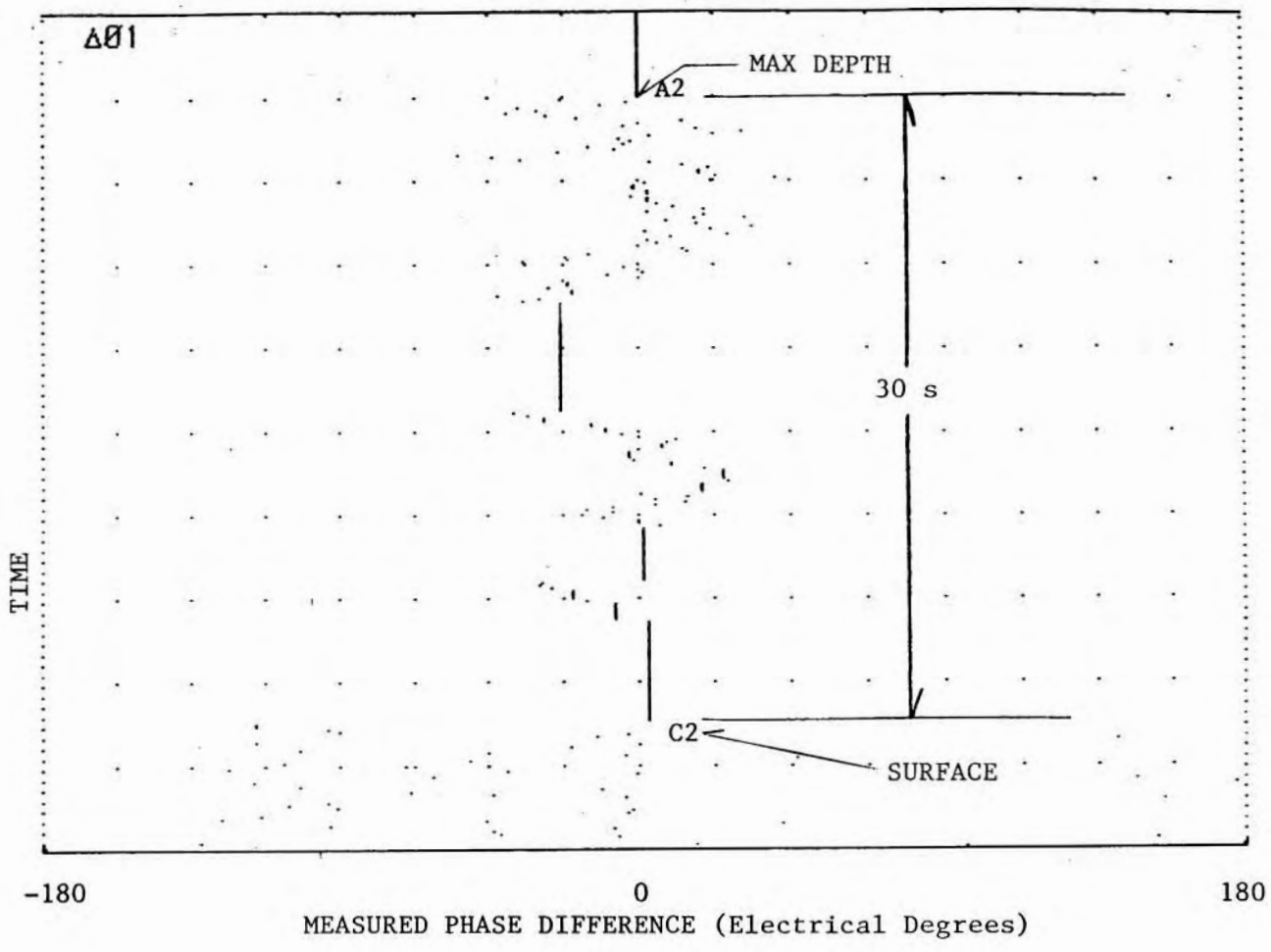

Figure 6.8a Phase Comparator 1 Responding to a Bad Acoustic Signal During Dive 2.

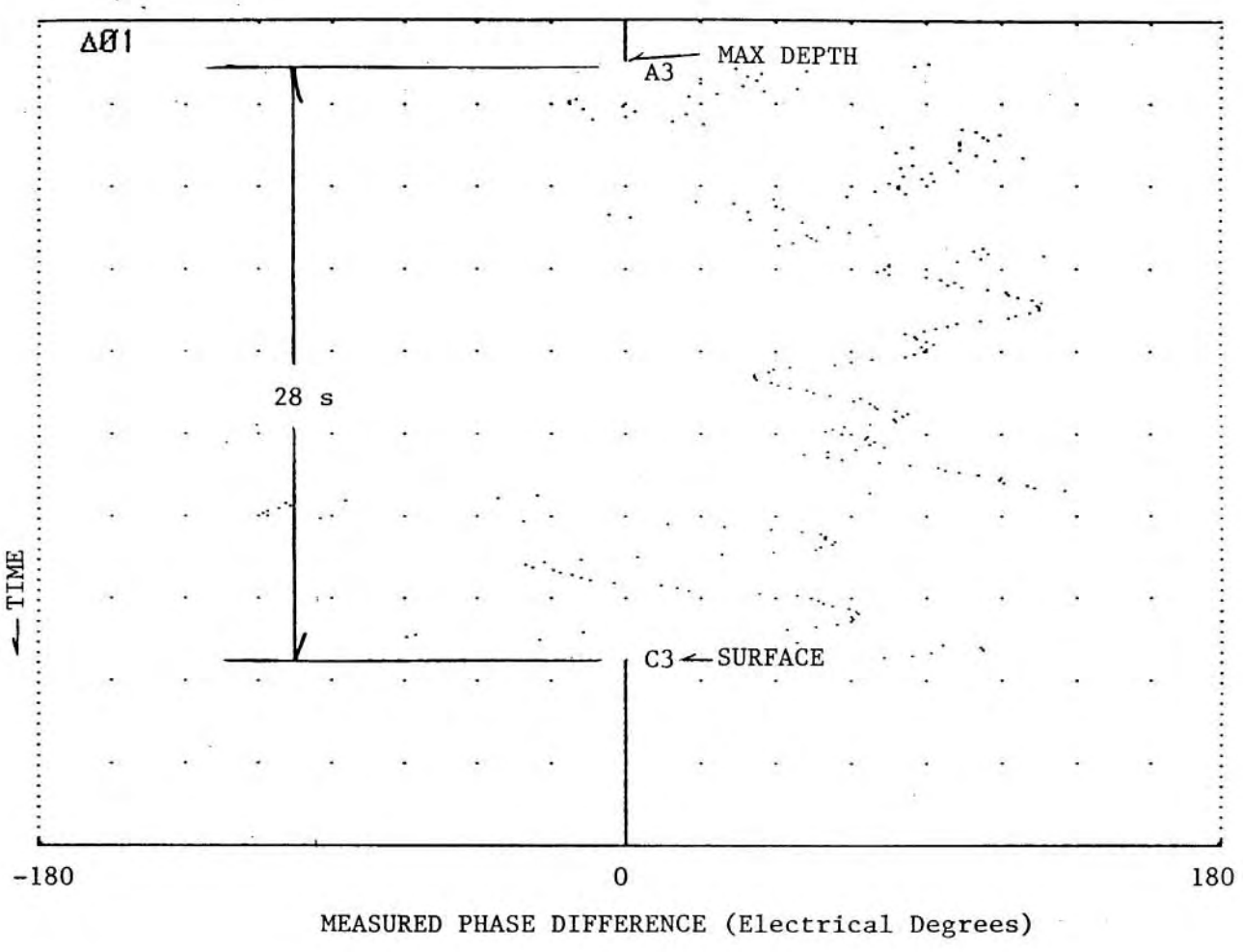

Figure 6.8b Phase Comparator 1 Successfully Locked onto the 15 KHz Beacon on Dive 3.

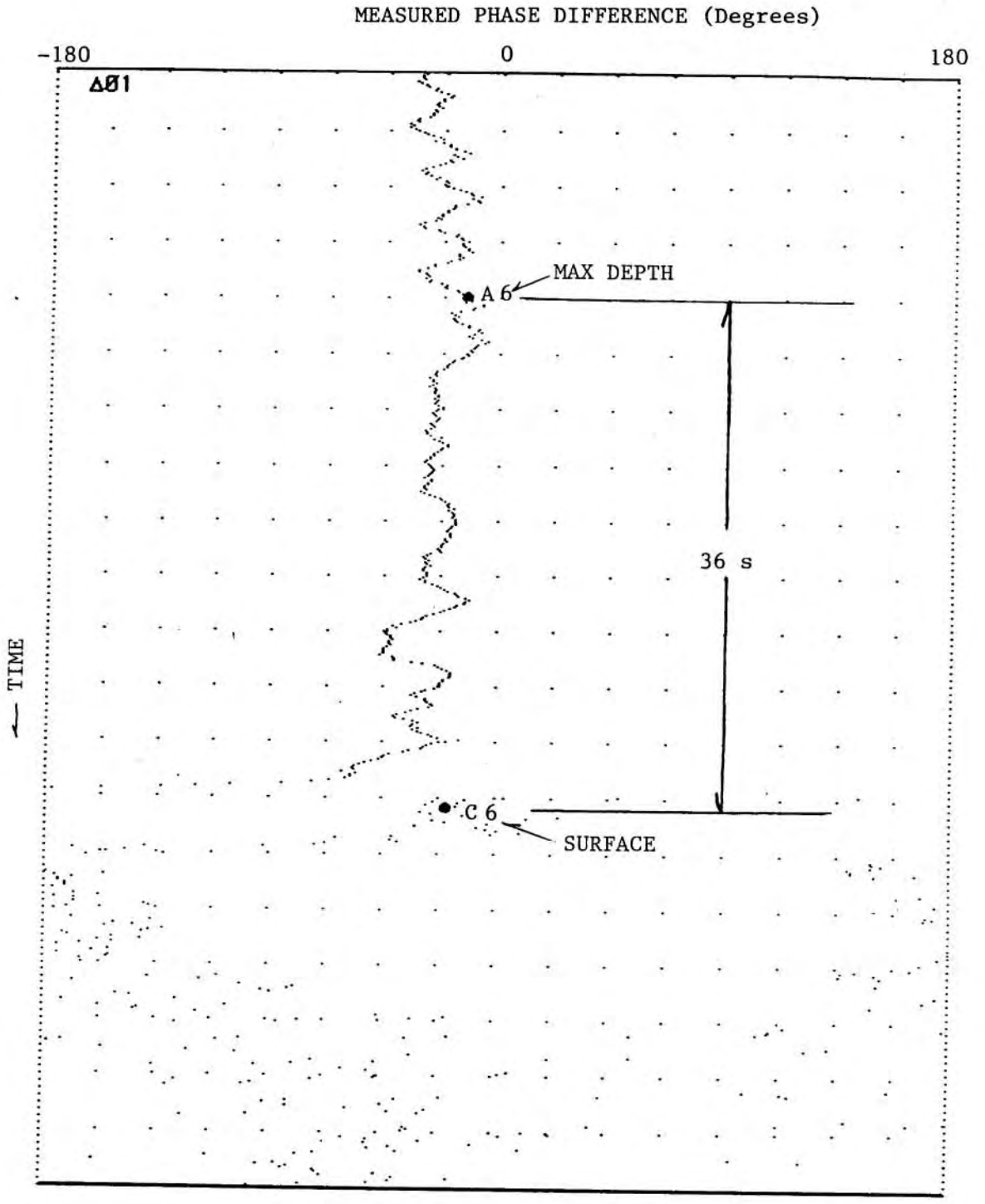

Figure 6.8c The Phase Comparator Record for Hydrophones 1 & 2. Note how the phase shoots dramatically off scale as the fish passes by the beacon.

transient, (2) fish rotation due to no differential inputs into the control loop, and (3) a faulty receiver channel.

Dive 6 shows good signal acquisition and correct overall operation. Very near the surface beacon, as the fish zooms past the beacon, one can expect a very rapid change in the measure phase difference (see Figure 6.8c). The high frequency fluctuations in the measured phase difference are not yet explained.

6.3.5 The Motor Set Point Record.

The motor set points are generated by the autopilot which uses the phase comparator and the rate gyro as inputs. There is provision to use the accelerometer inputs in the control algorithm but these were not tested at sea. For the purpose of these first trials, the motor set point was proportional to the phase difference measured by the hydrophone/receiver pairs. Electronic and mechanical stops prevented the control surfaces from exceeding a useful maximum excursion as determined by the stall characteristics of the control surface (about 15 degrees). Constant slamming into the stops would indicate excessive control effort. In the case where the acoustic signal is poor (eg Dive 2), the motor set point should default to zero deflection as shown in Figure 6.9. Figure 6.6 shows the motor set points for Motor 1 for Dive 6. Similar data exists for Motors 2 and 3. Dive 6 shows a well executed dive which resulted in accurate homing. The control effort increases slightly as the fish approaches the surface but only reaches maximum deflection as the fish brushes past the beacon.

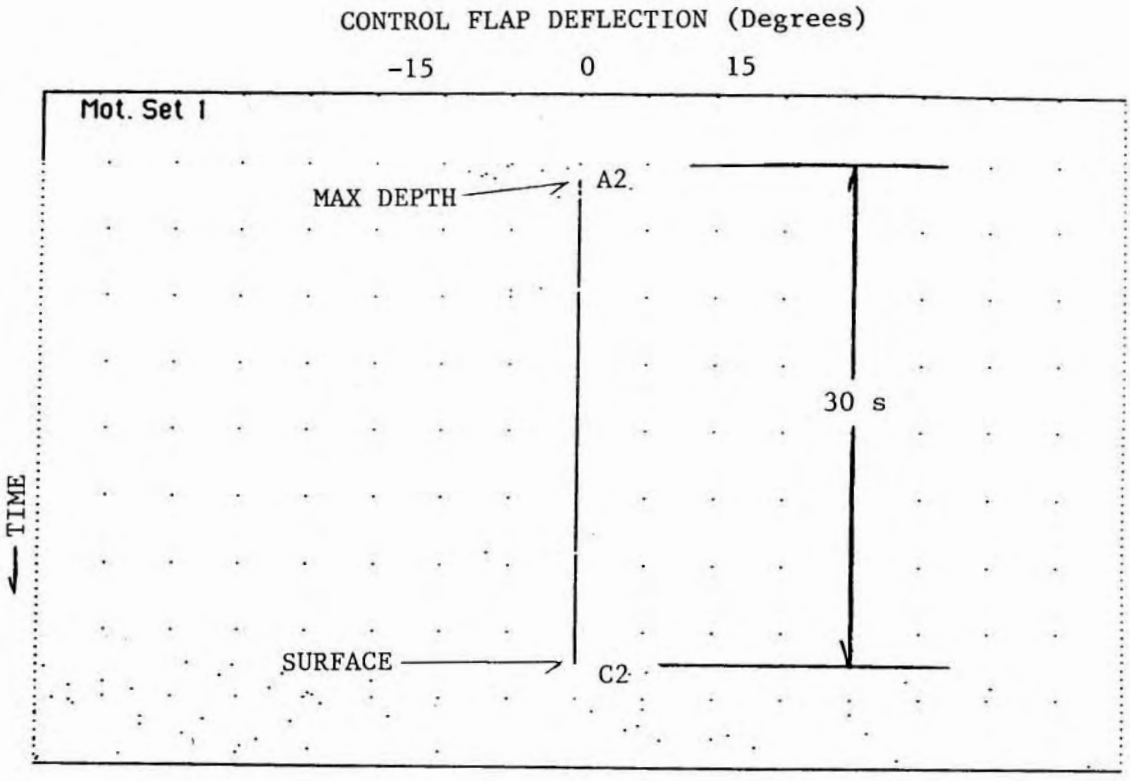

Figure 6.9 Motor 1 Correctly Defaulting to Zero Rudder Deflection as a Result of a Poor Acoustic Signal During Dive 2.

7 FUTURE DEVELOPMENT OF THE FLYING FISH CONCEPT

7.1 THE HYDROGRAPHIC SENSORS.

The Flying Fish was originally conceived as a platform for hydrographic sensors. This thesis focuses on the engineering development and proof-of-concept of a short baseline acoustic interferometer as the basis for a closed loop servo system to steer such a platform toward a monochromatic surface beacon. In parallel with this development effort, several manufacturers have been designing sensors which can be mechanically and electronically interfaced with the fish. These sensors will be incorporated in a second generation fish which is currently under development at the Woods Hole Oceanographic Institution. An extensive series of sea trails with these sensors is planned.

7.2 SYSTEM INTEGRATION: AUTOMATED TESTING AND FAULT ISOLATION AS A MEANS TO LOW MAINTENANCE.

Beyond the proof-of-concept prototype described in this thesis, are several key elements which must be available and working if the Flying Fish is to be more than a laboratory curiosity. Specifically, in an operational system, the automated testing and fault isolation capabilities need to be exploited to their full potential. Both the mechanical and electronic architecture of the fish are based on the need for low shipboard maintenance requirements. Any scientist/graduate student team should be able to use a personal computer of convenience to

control the measurement system and to collect data of known quality. The design philosophy was one of minimizing human involvement in order to reduce operating costs. Each system sub-assembly is built around a microprocessor that can be queried and excersised by the ship board computer. All sub-assemblies use a standard communications protocol. Such a modular architecture and standard interface promote automated testing. Figure 7.1 shows the major sea going system components. At present, the battery charger, air circulation pump, hydrophone test fixture, homing beacon, and tracking hydrophone exist as separate entities and have not been integrated with the shipboard fish controller. The launch and recovery fixtures exist in simplified form while the telemetry terminal and calibration fixture are hypothetical. All the hardware and the protocol exist for integrating this supplementary capability and the fault isolation diagnostics in the fish may be readily accessed manually. Automating this process will require additional software that should be written in response to experience gained in the field. This automated system check out could include:

-interrogating the shipboard bottom finding pinger to set the ballast release depth.

-setting the phase trim in the hydrophone receiver pairs.

7.3 MAINTENANCE AND QUALITY CONTROL

Beyond the simple questions of the technical feasibility of speeding up the data collection process are the questions of adaptability of the instrument to widespread use. These additional issues include (1) the required infrastructure (eg. the logistics of calibration, data handling,

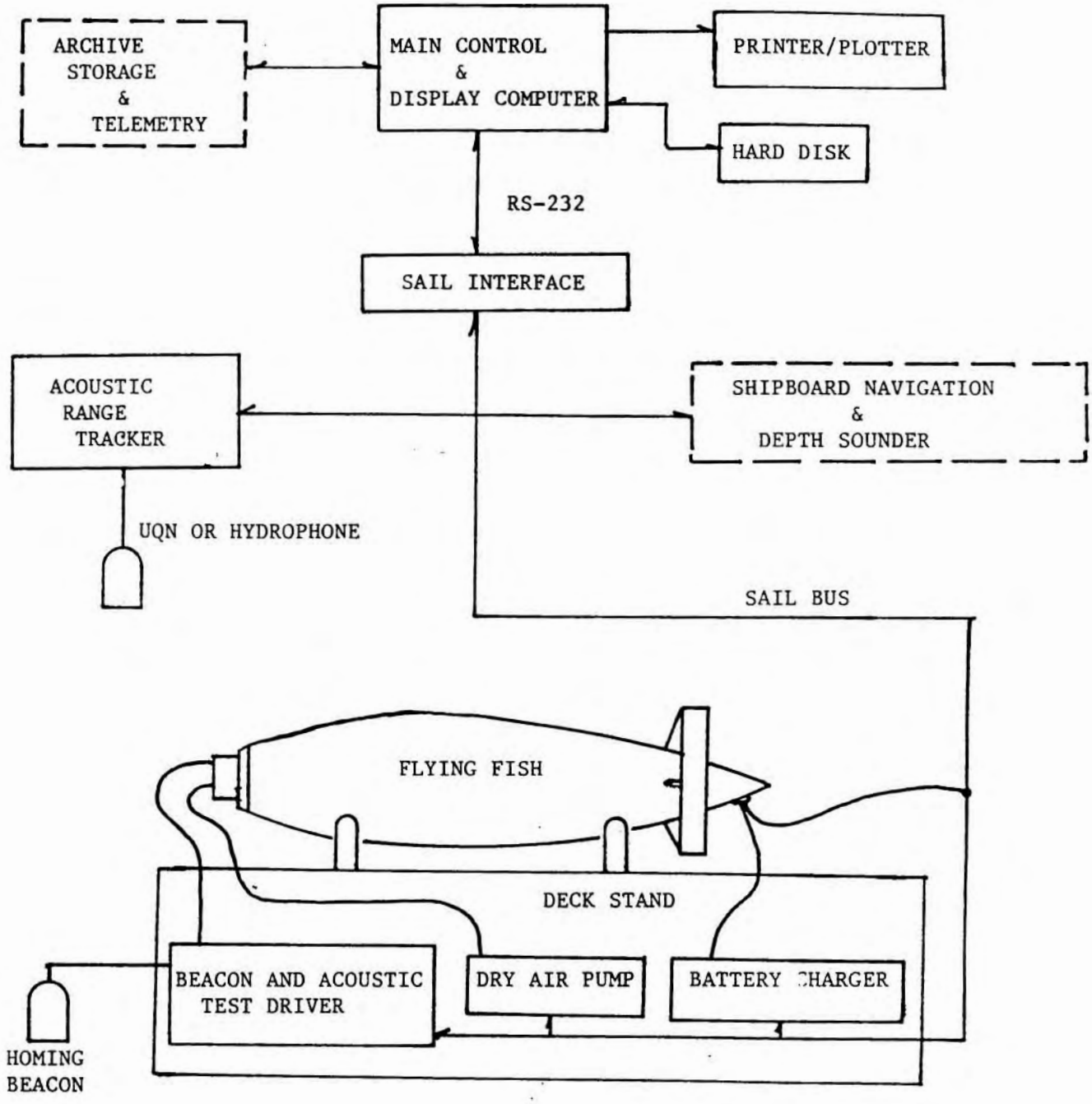

Figure 7.1 Schematic of major shipboard system components.

and quality control and (2) the cost (both initial outlay and ongoing maintenance).

7.3.1 Data Handling, Quality Control, and Satellite Telemetry.

Quality control is a serious issue when one is looking for 0.001°C variability in the deep ocean over time scales of ten years. During the International Geophysical Year (IGY 1957-58) "all data...were collected under the personal supervision of L. V. Worthington, W. G. Metcalf, A. R. Miller, and F. C. Fuglister" (Fuglister et al, 1970). This level of supervision aboard each vessel working in a global scale survey contradicts the initial premise that these measurments would be taken by operational groups with minimal training. One option is to have a centralized quality control center which, in near real time, could decide whether or not to re-survey an area where the data is suspect.

A second argument for telemetering the data to a central clearing house is based not on logistical arguments but on scientific need. For those interested in predicting oceanic weather patterns, it is important to collect, digest, and assimilate the hydrographic data on the same time scale as the meteorological and satellite data (i.e. near real time). Two types of data are collected by the fish and its support hardware: the first is the raw scientific data (including the sensor serial number, the deployment site--latitude and longitude, and the time; the second is engineering data used to monitor the health of the fish. The scientific data would consist of, typically, one meter averages of the conductivity, temperature, and depth, a total about 100 KBytes/deployment. At an average of six deployments per day, the scientific data set alone is over

0.5 MBytes/day. The engineering data would consist of pitch, yaw, control effort, and key battery and system voltages. This data may be collected between, as well as during, deployments but it may be sufficient to archive this data locally. This data may be accessed by the shipboard computer to plot the long term behaviour of the fish as (1) the flotation material degrades or (2)batteries cease to take a charge. The telemetry requirements are based, at a minimum, on the data that is required at a central location in near real time. Several commercial systems exist to implement this telemetry requirement but are not widely used in the oceanographic community. As data telemetry requirements grow, it is necessary to investigate the methods available. A detailed discussion of the various tradeoffs of existing telemetry systems is beyong the scope of this thesis. For the purposes of this document, it is sufficient to say that the issues of data telemetry and quality control must accompany any future development of the Flying Fish if large scale hydrographic surveys are to be undertaken.

7.3.2 Sensor Calibration.

Though the actual sensor suite to be carried aboard the fish has yet to be selected or tested, it is not premature to consider what sensor characteristics are conducive to routine hydrographic measurements. The precision, accuracy, temporal and spacial scales of the measurements are dictated by the science. The long and short term drift characteristics are dictated by the physics of the sensor.

Successful ocean surveys are characterized by careful and continuous attention to sensor accuracy and stability. This is especially true in

light of the high precision sought. Any questions in the data quality that cannot be answered by careful calibration records diminishes the scientific value of the data set. Historically, the art of reducing Nansen bottle samples to salinity and temperature measurements was a technique that required patience, care, and training. Few people were trusted to execute the procedure correctly and many data sets were summarily discarded due to suspect techniques. With present CTDs, the care must go into calibrating the sensors and monitoring the drift characteristics. At present, this calibration is very costly in terms of both money and man-hours.

If the Flying Fish CTD is to become the backbone of future large scale hydrographic surveys, and if the calibration costs are to be contained, an effective automated calibration program with strict quality controls must be designed as an integral system component. At a minimum, the sensor electronics should be self-calibrating, with any drift recorded by the shipboard computer. Each sensor should have an I.D. and a known history. This I.D. may be in the form of a bar code which is read and appended to the data from each profile. Further, the sensor pods should be designed to be replaced in the field without major disassembly of the fish.

Shipboard calibration may be the only way to maintain confidence in intercomparisons made between data sets collected by different instruments in different oceans several years apart.

7.4 CONCLUDING REMARKS

7.4.1 THE FLYING FISH IN THE CONTEXT OF AUTONOMOUS UNDERWATER VEHICLES.

The Flying Fish is a mission specific vehicle. As such, no attempt has been made to look for generic answers to the problems of

(1)Power. Because the basic mission is one of vertically profiling the ocean, gravitational potential was exploited to propel the vehicle.

(2)Navigation. For Navigation purposes, the fish has no knowledge of its position in three dimentional space, nor does it know the range to the surface beacon. The only information is two orthogonal bearings derived from two phase difference measurements. Once the vehicle is on the surface, it is no longer able to maneuver.

(3)Communication. Communication between vehicle and support vessel is minimal, essentially a one bit "I'm OK" or "Help" ping.

Instead of pushing the state of the art in any of these three fields, emphasis was made on matching present day technology and capabilities with an outstanding oceanographic need.

7.4.2 THE FLYING FISH IN THE CONTEXT OF OCEANOGRAPHIC INSTRUMENTS

The Flying Fish prototype has been shown to be a viable alternative to conventional deployment of oceanographic instruments. It's principal attributes, portability, speed, and acoustic homing, are unique. The modular construction permits the inclusion of any reasonable suite of sensors that takes advantage of these attributes. The mechanical and electronic architecture promote the use of automated diagnostics and data collection and have yet to be fully realized. How successfully this instrument changes our perception of the world's oceans will be based not

only on the engineering performance exhibited at sea but in the degree of trust the scientific community places in the data gathered by the instrument and by how easily this data can be collected, assimilated, and disseminated.

APPENDIX 1 THE DESIGN OF THE RELEASE MECHANISM

Four prototype release mechanisms showed sufficient potential to pursue preliminary designs and testing: (1)a solenoid latch, (2) an explosive wire, (3) a self charging squib, and (4) an electromagnet. Of these, the electromagnet proved to be the most practical and reliable in the field. The design of this electromagnet is summarized here. Details regarding the other designs is beyond the scope of this document.

Simplicity, reliability, and failsafe capability were the primary design criterion. Power dissipation up to 5 Watts, because of the short deployment times, was considered acceptable. By continually burning up a nominal amout of power in the electromagnet coil, a fail safe in the event of a power outage is automatically built into the release. The magnet was designed to handle the large dynamic loads that occur during deployment. Once safely away from the ship, the drive current to the magnet can be reduced to save system power.

The electromagnet consists of three parts: the magnet core, the coil, and the keeper. The maximum static load that can be supported by the magnet is a function of the flux in the magnetic circuit. This flux is in turn a function of:

-the magnetic properties of the core material

-the number of ampere turns

-the gap between the core and the keeper

-the contact area.

A1.1 The magnetic material

For this discussion, two magnetic properties of the core material are of fundamental importance: (1)the permeability and (2) the saturation flux density.

(1)the permeability describes the ease with which the magnetic domains align themselves with an externally imposed field (see Equation A1.1).

(2)the saturation flux density indicates the maximum number of field lines that can exist within a given cross-section of a material.

The total flux in the circuit, given by Equation A1.2, can easily be calculated by assuming that the gap is small and all the flux goes through the keeper.

$$B = \mu H \qquad \text{A1.1}$$

where B is the flux density
μ is the permeability
H is the imposed field

$$\phi = \oint_A B \cdot dA = B \cdot A \qquad \text{A1.2}$$

where ϕ is the total flux
B is the flux density
A is the cross-sectional area

A1.4.2 The Gap.

The field strength is proportional to the number of ampere-turns. For an electromagnet, the magnetic circuit can be broken down into two contributions to the reluctance: (1) the magnet/keeper and (2) the gap (see Equation A1.3). Note that, though the gap is small, it can have a dramatic effect on the total flux generated.

The load bearing capability of the magnet is derived in Equations A1.4. Note that the reluctance of the gap dominates. Because the effective permeability of the magnet is dominated by the gap reluctance, there is little advantage in this application in using an exotic material with a high permeability (eg. Supermalloy; see Figure A1.1).

$$\oint H \cdot dL = Ni = H_1 L_1 + H_2 \partial = B \left(\frac{L_1}{\mu_1} + \frac{\partial}{\mu_o} \right) \qquad \text{A1.3}$$

where L is the total length of the magnetic circuit
L_1 is the length of the magnetic circuit in iron
δ is the gap length
Ni is the number of Ampere-turns in the coil
μ_1 is the permeability of the iron
μ_o is the permeability of a vacuum

$$F = \frac{W}{X} \qquad \text{A1.4a}$$

where $W = 1/2 \iint H \cdot B \, dA \, dL$
$= 1/2 \, B \cdot A \, (H_1 L_1 + H_2 \delta)$
= the work required to move a distance dx in the presence of a force F

$$\text{Substituting} \quad B = \frac{Ni \, (\mu_1 \, \mu_o)}{L_1 \mu_o + \partial \mu_1} \qquad \text{A1.4b}$$

$$\text{gives } F = \frac{- \mu_1^2 \, \mu_o \quad A \, (Ni)^2}{(\mu_o \, L_1 + \mu_1 \partial)^2} = \text{const } A \, (Ni)^2 \sim \frac{\text{const}}{\partial^2} \qquad \text{A1.4c}$$

A1.3 The Contact Area.

The important material property which will affect load bearing capability of the magnet is the saturation flux density. From Figure A1.1 it is evident that the saturation flux density among magnetic materials does not

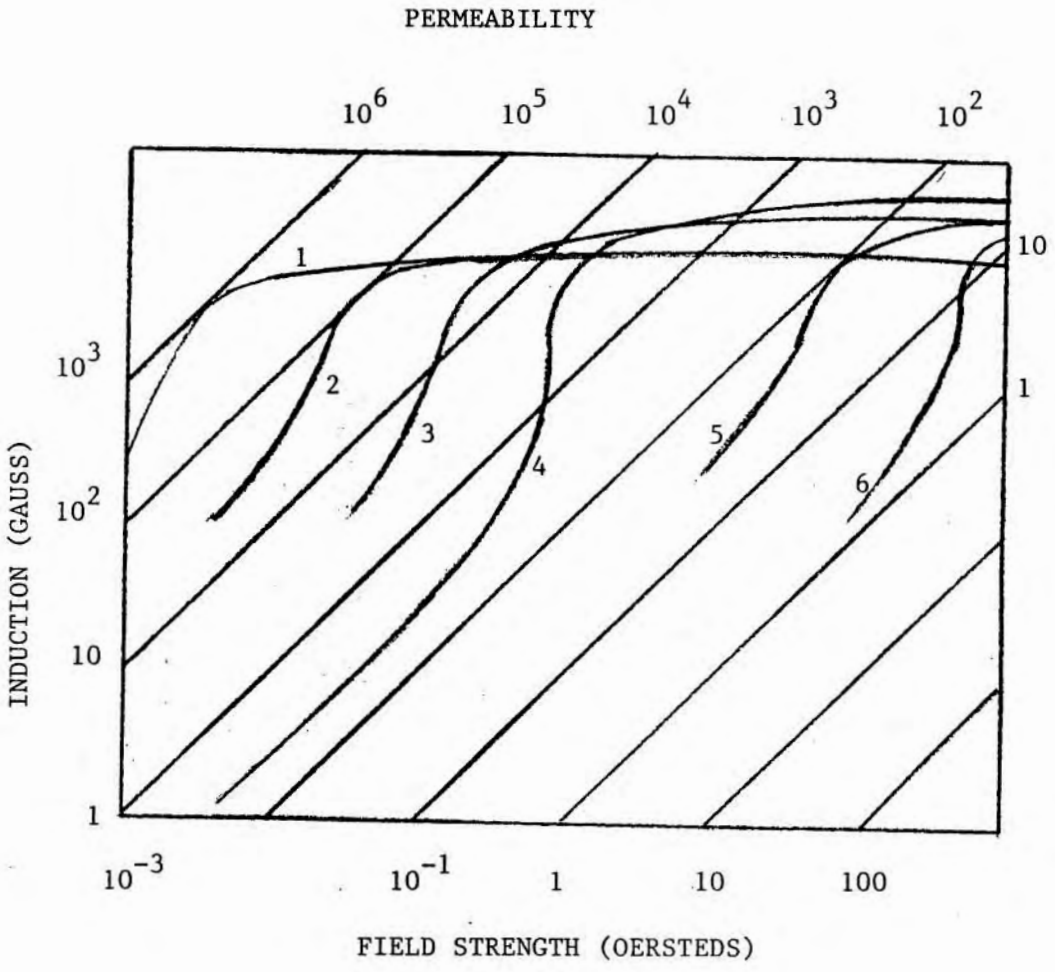

Figure A1.1 . Representative magnetization curves for some commercial materials (after

1. Supermalloy
2. Permalloy
3. 45 Permalloy
4. Magnetic Iron
5. 3 Cr Magnet Steel
6. Alnico 5

vary widely. Typical values are 15,000 to 20,000 Gauss.

Given a saturation flux density, a fixed gap, and a desired load, the overall geometry of the electromagnet can be specified. Equation A1.5 can be used to determine the number of ampere turns. Given the number of ampere-turns, one can use Equation A1.6 to calculate the required contact area as a function of static load.

$$Ni \sim B_{SAT} \frac{\partial}{\mu_o} \qquad \text{A1.5}$$

where B_{SAT} is the saturation flux density
μ_o is the permeability of a vacuum

$$F \sim \frac{\mu_o (Ni)^2}{\partial^2} A \qquad \text{A1.6}$$

A1.4.4 Sizing the Coil.

For a fixed voltage source and coil geometry, the power dissipated by the coil is independent of the number of turns. Another way to say the same thing: the load bearing capability of the magnet is a function of the total amount of copper and the contact area. Thus the wire gauge should be picked to operate at a convenient voltage and current supply such that the flux just reaches saturation at the limit of the expected dynamic load. At this limit, any increase in the drive current will have minimal effect on the holding power of the electromagnet.

Figure A1.2 shows the static release characteristics of the magnet designed for the Flying Fish.

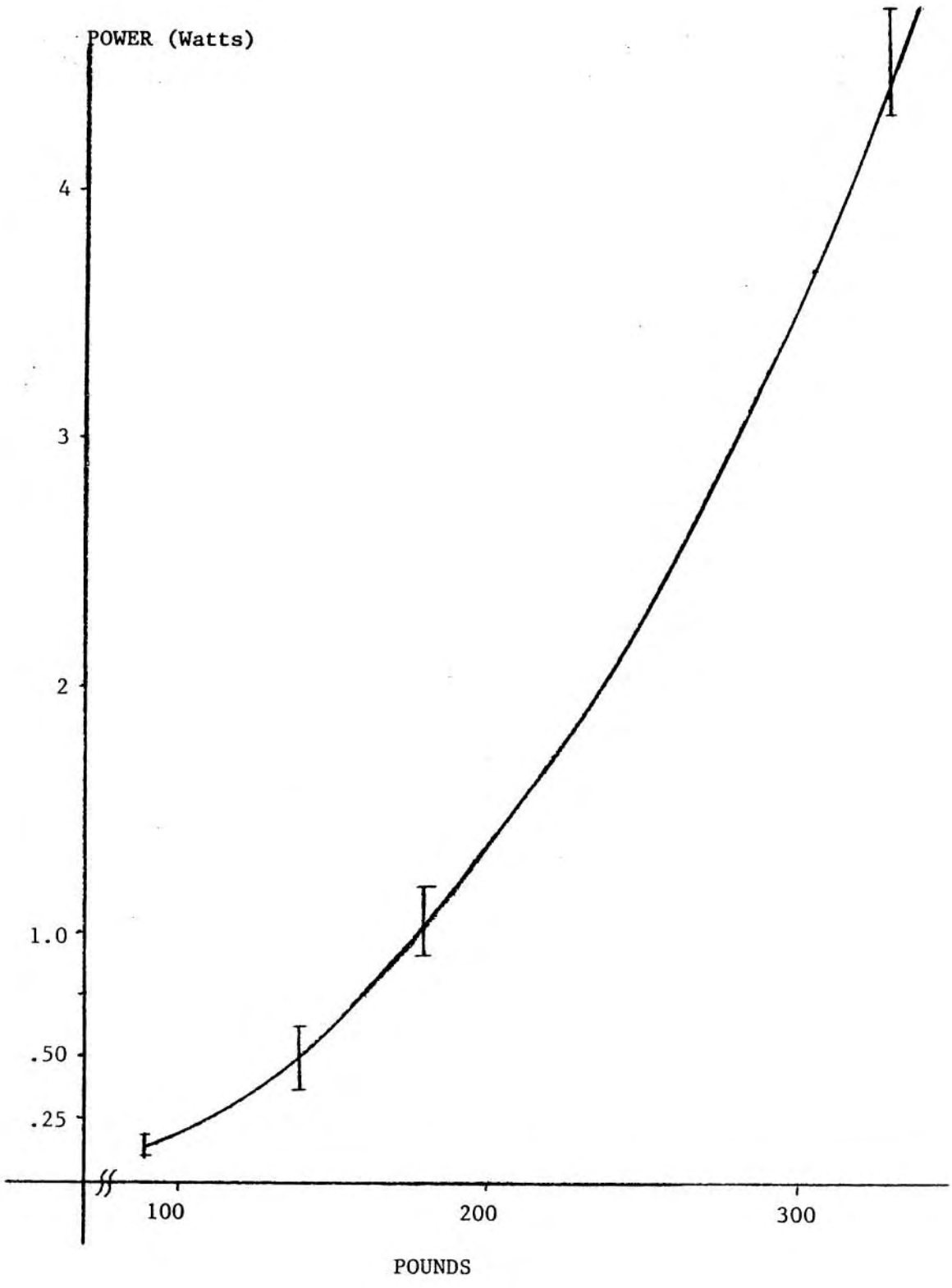

Figure A1.2 . Static load bearing capability of the electromagnetic release as a function of input power.

APPENDIX 2

COST BENEFIT ANALYSIS OF FISH SIZE

Assume that the drag force is proportional to a length squared term and a velocity squared term as shown in Equation A2.1a and use $(\text{Volume})^{2/3}$ as the length squared term. Now assume that the driving force is proportional to displacement (Equation A2.1b). This last assumption is reasonable since both the mechanism for propelling the vehicle and the complimentary energy reservoir are, as a rule, sized proportionally with the vehicle displacement.

$$F_{DRAG} = K_1 U^2 Vol^{2/3} \qquad \text{A2.1a}$$

where F_{DRAG} is the drag force
U is the vehicle velocity
Vol is the displace volume of the vehicle

$$F_{PROPULSION} = K_2 Vol \qquad \text{A2.1b}$$

At terminal velocity, the drag force and the driving force are equal. The resulting equation (A2.2) shows that the velocity can be increased indefinitely but only for very large increments in total displacement.

$$U = K_3 Vol^{1/6} \qquad \text{A2.2}$$

REFERENCES

STABILITY AND VEHICLE DYNAMICS

Abkowitz, M.A. "Stability and Motion Control of Ocean Vehicles." M.I.T. Press, Cambridge, Mass., 1969.

Albring, W. "Stability and Maneuverability of Bodies with Control Surfaces." Stevens Institute of Technology Translation, ETT Note 38, 1946.

Boltaccini, M.R. "The Stability Coefficients of Standard Torpedoes." NAVORD Report 3346, 18 July 1954,

Bryson, A.E. "Stability Derivatives for Slender Missiles." J.Aeronaut. Sci. Vol 20 No. 5 pp. 297-308, 1953.

Dempsey, "Static Stability Characteristics of a Series of Systematic Stern Control Surfaces on a Body of Revolution." David Taylor Naval Ship R & D Center Report 77-0085, Aug 1977.

Fidler, J.E. and Smith, C.A. "Methods for Predicting Submersible Hydrodynamic Characteristics." NCSC TM 238-78, July 1978.

Gertler, M. and Hagen, G.R. "Standard Equations of Motion for Submarine Simulation." Naval Ship R & D Center Report 2510, June 1967.

Humphreys, D.E. and Watkinson, K.W. "Prediction of Acceleration Hydrodynamic Coefficients for Underwater Vehicles from Geometric Parameters." NCSL Technical Report 327-78, Feb 1978.

Johnson, J.L. "The Static Stability Derivatives of a Series of Related Bodies of Revolution." DTMB Report C-383, 1951.

Lamb, H. "Hydrodynamics." Sixth Edition, Cambridge University Press, 1932.

Landweber, L. and Johnson, J.L. "Prediction of Dynamic Stability Derivatives of an Elongated Body of Revolution." DTMB Report C-359, May 1951.

Landweber, L. and Macagno, M. "Potential Flow About Series 58 Bodies in General Translational and Rotational Motion." Naval Ship R & D Center Report 2505 June 1967.

Lang, T. "Hydrodynamic Coefficients of Torpedo Bodies." NOTS 1107 NAVORD R3485 April 27 1955.

Multhopp, H. "Aerodynamics of the Fuselage." NACA Technical Memorandum No. 830, 1937.

Munk, M.M. "aerodynamic Theory of Airships." Aerodynamic Theory Vol 6, 1934.

"Nomenclature for Treating the Motion of a Submerged Body Through a Fluid." Society of Naval Architects and Marine Engineers, Technical and Research Bulletin No. 1-5, 1950.

Perkins, C.D. and Hage R.E. Airplane Performance, Stability and Control. John Wiley and Sons Inc., 1949.

Weinblum, G.P. "On Hydrodynamic Masses." DTMB Report 809, April 1952.

DRAG CHARACTERISTICS

Carmichael, B.H. and Niehuss, O. "Computer Study to Establish the Lower Limit of Length to Diameter Ratio Advisable for Low Drag Bodies." SID 64-1938.

Cebeci, T. "Laminar and Turbulent Incompressible Boundary Layers on Slender Bodies of Revolution in Axial Flow." Journal of Basic Engineering Vol 92 No. 3, 1970.

Hoerner, S.F. Fluid Dynamic Drag. 1958.

Myers, J.J. Ed. Handbook of Ocean and Underwater Engineering. McGraw-Hill, N.Y. 1969.

Parsons, J.S. and Goodson, R.E. "Shaping of Axisymmetric Bodies for Minimum Drag in Incompressible Flow." Journal of ;Hydronautics Vol 8.

Young, A.D. "The Calculation of the Total and Skin Friction Drags of Bodies of Revolution at Zero Incidence." British R & M 1874, April 1939.

LIFT CHARACTERISTICS

Abbott, I.H. and Von Doenhoff, A.E. Theory of Wing Sections. Dover Publications Inc., N.Y. 1959.

Jacobs, E.N., Ward, K.E., and Pinkerton,R.M. "The Characteristics of 78 Related Airfoil Sections from Tests in the Variable Density Wind Tunnel." NACA Report No. 460.

CONTROL SURFACE DESIGN

deYoung, J. "Theoretical Additional Span Loading Characteristics With Arbitrary Sweep, Aspect Ratio, and Taper Ratio." NACA TN 1491, Dec 1947.

Fehlner, L.F. "The Design of Control Surfaces for Hydronautic Applications." DTMB Report C-358, Jan 1951.

Garner, E.I. "Wing Tunnel Investigation of Control Surface Characteristics XX; Plain and Balanced Flaps on an NACA 0009 Rectangular Semi-span Tail Surface." NACA Wartime Report Oct 1944.

Sears, R.I. "Wind Tunnel Data on the Aerodynamic Characteristics of Airplane Control Surfaces." NACA Wartime Report L-663 Dec 1943.

Weinig, F. "Lift and Drag of Wings with Small Span." NACA TM 1151, August 1947.

STRUCTURES AND MATERIALS

Couch, W.P., Ward, G.P., and Blumerburg, W.F. "Investigation of Filament-Reinforced Plastic Deep Submergence Pressure Hulls." Naval Ship R & D Center Report 3071, June 1969.

ACTUATOR DESIGN

Barash, T. "A Disolvable Link Release Mechanism." Exposure Vol 8, No 5, Nov 1980.

Rosfelder, A.M. "Hydrostatic Actuation of Deep Sea Instruments." Journal of Ocean Technology Vol 1, No 1, 1966.

CONTROL SYSTEMS

Schick, G.B. Isaacs, J.D. and Sessions, M.H. "Autonomous Instruments in Oceanographic Research." Forth National ISA Marine Sciences Instrumentation Symposium. Cocoa Beach Florida Jan 1968.

Gardner, F.M. Phaselock Techniques. John Wiley and Sons, New York, 1966.

Ogata, K. Modern Control Engineering. Prentice-Hall Inc. Englewood Cliffs, N.J. 1970.

ELECTRONIC COMMUNICATION STANDARDS

Bradley, A.M. and Mellinger, E.C.

Bradley, A.M. and Terry, W.E. "A Coherent Approach to Instrument Intercommunication and Testing via SAIL." IEEE Proceedings, 3rd Symposium on Oceanographic Data Systems, pp. 51-54, 1983.

Mesecar, R. and Dillon, W. "Serial ASCII Instrumentation Loop for Marine Research Applications." IEEE Proceedings, Oceans, pp. 296-300, Sept 1981.

OCEANOGRAPHY

Fuglister, F.C. The Woods Hole Oceanographic Institution Atlas Series Vol 1, Woods Hole Oceanographic Institution, Woods Hole Mass, July 1970.

Marsh, H.W. "Underwater Sound and Instrumentation." Section 3, Handbook of Ocean and Underwater Engineering. Myers, J.J., Holm, C.H., and McAllister, R.F. Eds. McGraw-Hill Co. New York, 1969.

Wenz, G.M. "Acoustic Ambient Noise in the Ocean." J. Acoust. Soc. Am. Vol 34, pp. 1936, 1962.

BATTERIES

Senderak, K. and Beard, K. "Development of Sealed Lead Acid Batteries for Aircraft and Other Battery Applications." 30th Power Sources Symposium, Atlantic City, New Jersey, June 1982.